ENZYME AGING: STRUCTURAL INSIGHTS FROM NTE AND PATATIN

by

Sanjeeva Joseph Wijeyesakere

A dissertation submitted in partial fulfillment
of the requirements for the degree of
Doctor of Philosophy
(Toxicology)
in The University of Michigan
2009

Doctoral Committee:

Professor Rudy J. Richardson, Chair
Professor Ari Gafni
Professor Martin A. Philbert
Associate Professor Peter Mancuso
Research Assistant Professor Jeanne A. Stuckey

Neuropathy Target Esterase (NTE): Probing the Enigma.

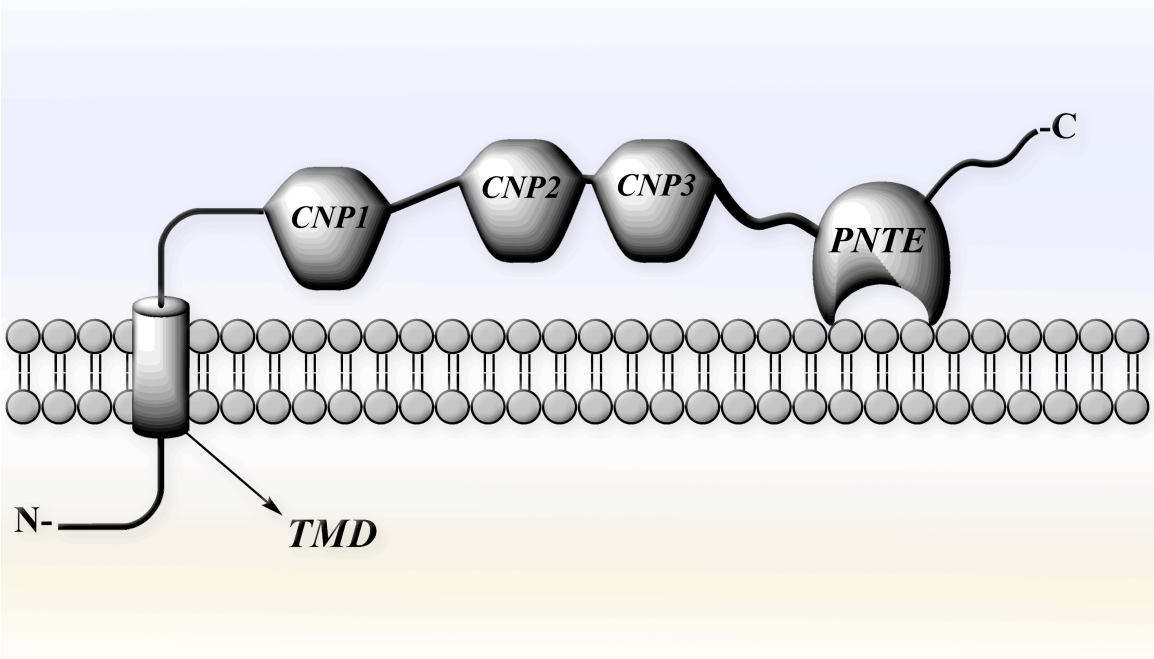

‘No man is an island, entire of itself; every man is a piece of the continent, a part of the main. If a clod be washed away by the sea, Europe is the less, as well as if a promontory were, as well as if a manor of thy friend's or of thine own were: any man's death diminishes me, because I am involved in mankind, and therefore never send to know for whom the bell tolls; it tolls for thee’.

- John Donne, Meditation XVII; From Devotions upon Emergent Occasions (1623)

To my parents & teachers

Acknowledgements

I would like to thank the following people and organizations for their advice, help and support:

Personnel:

Rudy Richardson, ScD, DABT.
Jeanne Stuckey, PhD.
Ari Gafni, PhD.
Peter Mancuso, PhD.
Martin Philbert, PhD.
Walter Piper, PhD.
Jennifer Meagher, PhD.
John (Ron) Rubin, PhD.
All the members (past and present) of the Richardson and Stuckey Laboratories.

Material Support from the Monsanto Company who provided the pat17 plasmid.

Funding Sources (Grants & Fellowships):

Army Research Organization (DAAD19-02-1-0388).
NIH Training Grant (T32 ES07062).
Dow Chemical Company.
Rackham Student Research Grant (University of Michigan).
Rackham Pre-doctoral Fellowship (University of Michigan).
Regents' Scholarship from the School of Public Health (University of Michigan).
University of Michigan LSI Center for Structural Biology.
Michigan Economic Development Corporation.

Table of Contents

List of Figures

List of Tables

Glossary

Aging:	Post-inhibitory reaction wherein the [inhibited] enzyme looses the ability to be reactivated by strong nucleophiles. This occurs when OP adduct gains a net negative charge (most often via loss of an alkyl side-chain).
Inhibition:	Loss of enzymatic activity due to the formation of an organophosphorus adduct on the catalytic nucleophile.
NTE:	Neuropathy target esterase; a neuronal lysophospholipase that interacts with organophosphorus compounds.
OP:	Organophosphorus compound. For the purposes of this thesis, there represent organic compounds derived from pent covalent phosphorus.
OPIDN:	A delayed axonopathy that occurs when certain OPs interact with NTE. Symptoms of OPIDN include paresthesias, ataxia, sensory loss and flaccid paralysis, which leads to spastic paralysis.
PNTE:	The catalytic domain of NTE that is homologous to patatin.
Patatin:	A plant serine hydrolase that is homologous to PNTE.

ABSTRACT

ENZYME AGING: STRUCTURAL INSIGHTS FROM NTE AND PATATIN

by

Sanjeeva Joseph Wijeyesakere

Chair: Rudy J. Richardson

Neuropathy target esterase (NTE) is an integral membrane protein whose covalent modification by organophosphorus compounds (OPs) results in a delayed axonopathy (called OP-induced delayed neuropathy (OPIDN)) whose mechanisms of initiation and progression are unknown. The current model for OPIDN states that inhibition of NTE by a neuropathic OP followed by a post-inhibitory aging reaction results in NTE gaining a new function that is detrimental to the survival of the axon. Thus, we hypothesized that if NTE gains a new function, it would also need to experience a change in its structure. To this end, we employed molecular modeling along with x-ray crystallography of NTE's plant homologue patatin-17 (pat17) to investigate conformational changes in tertiary structure associated with inhibition and aging of a neuropathic OP-pat17 conjugate. Analysis of NTE's catalytic (patatin-homology) domain (PNTE) revealed it to have 30% sequence homology and 18% identity to pat17, allowing us to build a homology model for PNTE using the crystal structure of pat17 as a template. This model revealed that contrary to previously published data, NTE has a Ser966-Asp1086 catalytic dyad with the Asp1086 acting as the general base during catalysis. Simulated inhibition (SI) and simulated aging (SA) work undertaken with this model using the neuropathic OP diisopropylphosphorofluoridate (DFP) indicated the absence of significant conformational changes following inhibition (Cα root mean square deviation (RMSD): 1.4Å) and aging (RMSD: 1.6Å), suggesting that the current model for

OPIDN's pathogenesis may be flawed. Furthermore, biochemical analysis of pat17 revealed that it could be inhibited and aged by OPs like DFP (IC_{50}: 181μM; $t_{1/2\ aging}$: 11.4 min). We also showed that pat17 could be inhibited by methyl arachidonyl fluorophosphonate (MAFP) (IC_{50}: 116nM). The crystal structures of pat17 aged with DFP along with that of pat17 inhibited with MAFP were solved via molecular replacement in space-group $P4_32_12$. Analysis of these crystal structures confirmed our SI and SA results, indicating no significant conformational change associated with inhibition by MAFP (RMSD: 1.07Å) and aging by DFP (0.98Å). In conclusion, a new model for the initiation and progression of OPIDN, based on disruption of membrane lipids is presented.

Chapter 1

Introduction

Organophosphorus compounds (OPs), in the context of this research endeavor, are a class of organic chemicals derived from pentacovalent phosphorus that find extensive industrial use as pesticides, fire retardants, lubricants, pharmaceuticals and plasticizers. OPs have also been used on the battlefield as chemical warfare agents and currently pose a threat with respect to their potential for use as chemical terrorism agents. Upon exposure, OPs are capable of eliciting acute cholinergic toxicity via the inhibition of acetylcholinesterase (AChE) in the central (CNS) and peripheral nervous systems (PNS). Neuropathic OPs, which include representatives of the phosphate, phosphonate and phosphoramidate classes (Fig 1.1), are capable of inducing a delayed axonopathy referred to as OP-induced delayed neurotoxicity (OPIDN) via a toxic gain-of-function model involving the integral membrane protein neuropathy target esterase (NTE). On the other hand, non-neuropathic NTE inhibitors (such as the phosphinates, sulfonates and carbamates) are incapable of inducing OPIDN and administration of these non-neuropathic inhibitors prior to dosing with neuropathic NTE inhibitors have been shown to be protective against the development of OPIDN (Richardson, 2005; Schwab and Richardson, 1986).

Currently, the causal factor in OPIDN is understood to be the inhibition of >70% of neuronal NTE by neuropathic OPs (such as diisopropyl phosphorofluoridate (DFP) and diisopropyldiamidophosphorofluoridate (Mipafox)), followed by 'aging' of the OP adduct. Aging is a post-inhibitory reaction that leads to the NTE-OP conjugate gaining a net negative charge. The most common mechanism for aging (as seen in the case of the phosphates and phosphonates) involves the net loss of an alkyl (R) group from NTE's OP adduct. Following the aging reaction, NTE remains permanently bound to the negatively charged OP moiety and consequently cannot be re-activated through the use of strong nucleophiles such as fluoride. As such, the crucial premise in the current model for OPIDN's pathogenesis is that it depends on a chemical modification of NTE and that inhibition, while being a necessary step in OPIDN, is not sufficient to elicit this condition in the absence of the aging reaction (Richardson, 2005; Johnson, 1982) (Fig 1.2). The exact mechanism through which the aged NTE-OP conjugate results in axonopathy is unclear, although it has been proposed that the process of organophosphorylation and aging of

NTE by a neuropathic OP could induce a functional change in the protein, leading to NTE gaining a new 'toxic' role that is ultimately detrimental to the well-being of the neuron (Glynn, 1999). Consequently, this 'toxic gain-of-function' model for the pathogenesis of OPIDN, in addition to providing a testable hypothesis for OPIDN's initiation and progression, presents an avenue of research that has not been investigated extensively.

While sporadic cases of delayed neuropathy following exposure to OPs had been reported since the nineteenth century, historically, the largest epidemic of OPIDN took place in the United States in the era of prohibition. During this period, the extract of Jamaican ginger (called 'Jake') was used widely as a means to obtain alcohol. Certain stocks of this illicit alcohol were adulterated with solvents that contained the neuropathic OP tri-ortho-cresyl-phosphate (TOCP). The resulting epidemic (colloquially termed 'Jake-leg') affected upwards of 20,000 people (Smith *et al.*, 1930). Subsequent outbreaks of OPIDN following exposure to TOCP have been reported in Morocco (1959) (Glynn, 2003; Smith and Spalding, 1959) and Sri Lanka (1977-1978) (Senanayake and Jeyaratnam, 1981). At present, due in part to more stringent regulation of OPs, most cases of OPIDN are sporadic and associated with failed attempts at committing suicide. However, given the commercial use of OPs along with the threat posed by possibility that neuropathic OPs could be used as agents in chemical terrorism, as well as the intriguing scientific questions surrounding the biochemical mechanism involved in the initiaion and progression of this 'chemical transection' of an axon, the need to further explore OPs and the delayed axonopathy they elicit is highlighted (Richardson, 2005).

OPIDN can be produced by a single exposure to a neuropathic OP following an asymptomatic period of 1-2 weeks (Davis and Richardson, 1980). Lipophilic OPs tend to be absorbed easily and are capable of readily crossing the blood-CNS and blood-PNS barriers. The pathogenesis of OPIDN involves progressive distal degeneration of sensory and motor axons in peripheral nerves and spinal cord tracts. The signs and symptoms of OPIDN become evident 1-2 weeks post exposure to a neuropathic OP and begin as paresthesias (abnormal feeling that may include tingling and numbness) in the distal extremities followed by sensory loss, ataxia (loss of coordination) and an advance to flaccid paralysis. Severe cases of OPIDN could result in quadriplegia (Lotti and Moretto, 2005; Richardson, 2005).

There is currently no cure or treatment for OPIDN other than general supportive therapy and once initiated, the progression of this condition cannot be halted. Physiologically, some regeneration of peripheral nerve axons is possible and reinnervation of muscle may occur over a time-span of several months. However, the injury to descending inhibitory pathways in the spinal cord is persistent and reinnervation of muscle only permits a progression from flaccid paralysis to

spastic paralysis due to the inability of central nervous system (CNS) neurons to regenerate (Richardson, 2005).

Thus far, research into NTE has shown it to be a biochemical enigma, a protein with no confirmed physiological role (although recent evidence has suggested that it may be a lysophospholipse) and, whose structure has hitherto eluded investigators. Molecular biochemical studies have shown that NTE is an integral membrane protein consisting of 1327 amino acids that is anchored to membrane of the endoplasmic reticulum (ER) and isolated in microsomal fractions of cell homogenates. It is found in neuronal cells as well as in some non-neuronal cell types such as lymphocytes (Schwab and Richardson, 1986)**.** NTE is classified as a serine esterase with an active site serine at position 966. Operationally, this is known from the fact that it catalyzes the hydrolysis of esters (Richardson, 2005) as well as the fact that its active site serine (Ser966) appears in the consensus sequence for an esterase/lipase motif (G-X-S-X-G; G-T-S-I-G in NTE) (Schrag and Cygler, 1997).

Previous reports have indicated that NTE may consist of a novel catalytic triad of ser-asp-asp compared to the more 'traditional' ser-his-asp/glu catalytic triad seen in other serine hydrolases such as AChE (Zhang *et al*., 2002). Moreover, based on its primary sequence, it has been shown that human NTE shares 41% sequence identity with the swiss cheese protein in Drosophila (Lush *et al*., 1998), which, like NTE, has been hypothesized to have an *N*-terminal signaling domain that could be capable of binding cyclic nucleotides (Li *et al*., 2003; Kretzschmar *et al.*, 1997). The catalytic center of NTE is known to have homology to patatin and calcium independent phospholipase A2 (iPLA-2) while the putative regulatory domains of NTE have homology to cyclic nucleotide (CNP) binding domains (Glynn, 2003).

Patatin is a 40 kDa protein that constitutes approximately 40% of the soluble protein in potato tubers (Pots *et al.*, 1999; Racusen and Foote, 1980) and is known to have lipid acyl hydrolase activity (Andrews et al., 1988). The crystal structure of patatin shows it has a catalytic center composed of a ser77-asp215 dyad (Rydel *et al*., 2003), compared to the ser-his-glu catalytic triad observed in AChE (Zhang *et al*., 2002) and NTE's proposed Ser-Asp-Asp triad (Atkins and Glynn, 2000). Although the studies did not quantify potency, previous research has revealed that patatin is inhibited by OPs such as DFP and methyl-p-nitrophenyl-octylphosphonate (Strickland *et al*., 1995; Hirschberg, *et al.*, 2001). Given this similarity between the patatin and NTE inhibitory profile, it would be prudent to further explore and characterize the inhibitory profile of patatin in the presence of neuropathic and non-neuropathic OPs in order to develop the use of patatin as an analogue of NTE in testing the neuropathic potential of compounds.

Structurally, it is known that the act of phosphorylating amino acids in proteins is capable of inducing conformational changes in their tertiary structures. Examples of such phosphorylation-induced conformational changes are seen in that phosphorylation of tyrosine residues 992, 1068, and 1086 in the C-terminus of human epidermal growth factor receptor has been reported to induce the necessary conformational change for its role intracellular signaling (Bishayee *et al*., 1999). Similarly, conformational changes are witnessed in the mitogen-activated protein kinase (MAP kinase) isoform, extracellular signal-regulated protein kinase-2 (ERK2), which, when phosphorylated at Thr-183 and Tyr-185 undergoes a large conformational change that results in refolding of the ERK2 'lip' (the activation loop which contains the phosphorylation sites) (Canagarajah *et al*., 1997). Based on these examples of large conformational changes in proteins following their phosphorylation, it would be reasonable to assume that the organophosphorylation of NTE could also result in a conformational change.

Currently, it has been postulated that organophosphorylation and aging of NTE by neuropathic OPs would induce a functional change in the protein, leading to it gaining a new 'toxic' role (Glynn, 1999). Given the maxim that 'form follows function', it is reasonable to infer that if NTE were to gain a new (albeit, a toxic) function, it would also have to undergo a change in its structure. Furthermore, such changes should be visible in NTE's catalytic (patatin-homology) domain (PNTE) (since this is the known region in which OPs interact with NTE), as well as in its plant homologue, patatin. In order to test this hypothesis, the presence of these changes could be elucidated by investigating the structures of PNTE and patatin following inhibition and aging by OPs and comparing them to their corresponding native states.

Given the widespread use of OPs, as well as the subtle onset and permanent incapacitating effects of OPIDN, it is essential to be able to predict the potential of a given OP to produce this disease as opposed to causing acute cholinergic toxicity (Richardson, 2005). Therefore, it is important to develop screening methods to identify the potential of OPs to inhibit NTE and age, thereby leading to the development of OPIDN. To accomplish these goals, it will be necessary to identify whether patatin can be utilized as a model of hen-brain NTE and thus open the possibility of using patatin as a potential screening tool in identifying the neuropathic potential of OPs.

Therefore, this research aims to study the similarities between patatin and the NTE catalytic domain. It is hoped that the results of this investigation would reveal the structural changes witnessed following inhibition by aging and non-aging inhibitors of NTE.

Hypothesis

Published information on patatin and neuropathy target esterase (NTE) indicates that these enzymes have similar selectivity for substrates and inhibitors with long alkyl chains. Moreover, among proteins of known 3D structure, fold recognition identified patatin-17 (pat17) as the best model for the tertiary structure of NTE's catalytic (patatin-homology) domain (PNTE). Therefore, it is hypothesized that the 3D structures of pat17 and PNTE are similar and that if conformational changes are seen in pat17 when its active site is adducted by aged and non-aged organophosphorus compounds (OPs), then these will be similar to the conformational changes seen in PNTE when it is adducted by the corresponding OPs.

Type A (Neuropathic) NTE Inhibitors

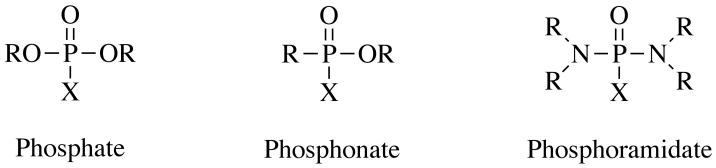

Type B (Non-neuropathic; Protective) NTE Inhibitors

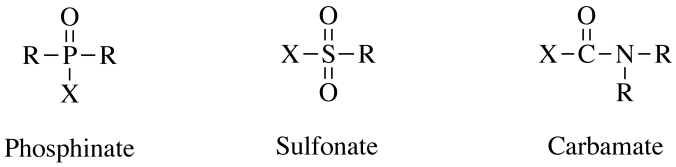

Figure 1.1: Classes of NTE inhibitors. Type A inhibitors are capable of undergoing the aging reaction, thereby being able to initiate OPIDN. Type B inhibitors cannot age and exposure to these inhibitors will not result in OPIDN. In addition to this, prior administration of type B inhibitors will protect against OPIDN from subsequent administration of type A compounds (Adapted from Richardson, 2005).

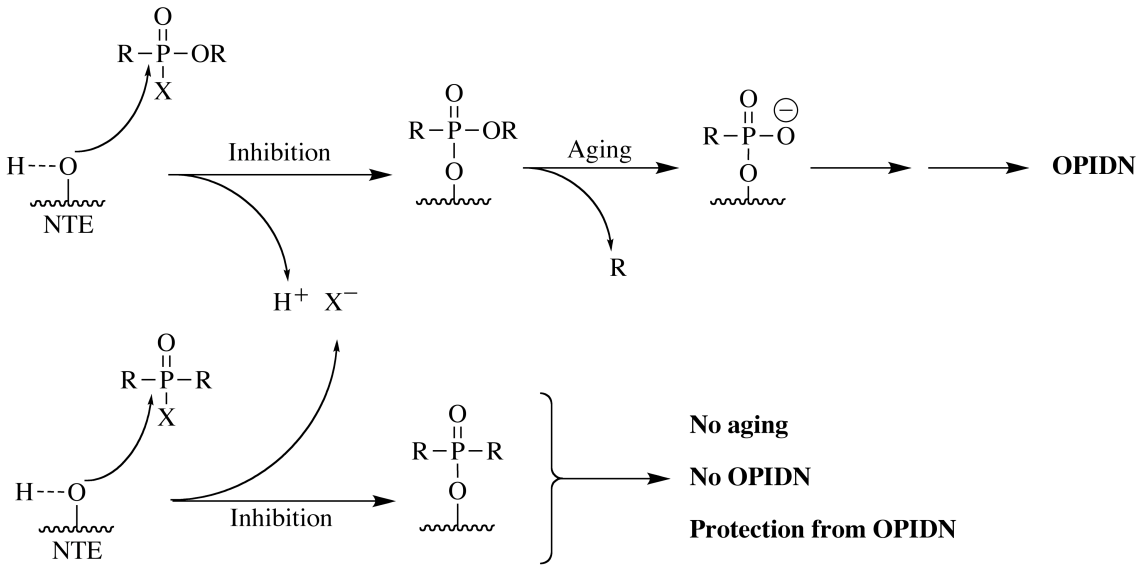

Figure 1.2: Inhibition and aging of NTE. Inhibition of NTE in the presence of a neuropathic (top row) and non-neuropathic (bottom row) OP. The aging process leads to a negatively charged phosphate adduct on NTE, which prevents reactivation of the enzyme by powerful nucleophiles and it is postulated that this results in the toxic gain-of-function of NTE, leading ultimately (through some unknown processes) to the development of OPIDN (adapted from Richardson, 2005).

References

Andrews, D.L., Beames, B., Summers, M.D., and Park, W.D. (1988). Characterization of the lipid acyl hydrolase activity of the major potato (Solanum tuberosum) tuber protein, patatin, by cloning and abundant expression in a baculovirus vector. *Biochem. J.* **252**, 199--206.

Atkins, J., and Glynn, P. (2000). Membrane association of and critical residues in the catalytic domain of human neuropathy target esterase. *J. Biol. Chem.* **275**, 24477--24483.

Bishayee, A., Beguinot, L. and Bishayee, S. (1999). Phosphorylation of tyrosine 992, 1068, and 1086 is required for conformational change of the human epidermal growth factor receptor c-terminal tail. *Mol. Biol. Cell.* **10**, 525--536.

Canagarajah, B.J., Khokhlatchev, A., Cobb, M.H., and Goldsmith, E.J. (1997). Activation mechanism of the MAP kinase ERK2 by dual phosphorylation. *Cell.* **90**, 859--69.

Davis, C.S., and Richardson, R.J. (1980). Organophosphorus compounds. In *Experimental and Clinical Neurotoxicology* (P.S. Spencer and H.H. Schaumburg, eds.), Williams and Wilkins, Baltimore, pp. 527--544.

DeLano Scientific LLC, San Carlos, CA, USA. *The PyMOL Molecular Graphics System*. http://www.pymol.org.

Glynn, P. (1999). Neuropathy target esterase. *Biochem. J.* **344**, 625--631.

Glynn, P. (2003). NTE: one target protein for different toxic syndromes with distinct mechanisms? *Bioessays*. **25**, 742--745.

Hirschberg, H.J.H.B., Simons, J.W.F.A., Dekker, N., and Egmond, M.R. (2001). Cloning, expression, purification and characterization of patatin, a novel phospholipase A. *Eur. J. Biochem.* **268**, 5037--5044.

Johnson, M.K. (1982). The target for initiation of delayed neurotoxicity by organophosphorus esters: Biochemical studies and toxicological applications. *Rev. Biochem. Toxicol.* **4**, 141--212.

Kretzschmar, D., Hasan, G., Sharma, S., Heisenberg, M., and Benzer, S. (1997). The swiss cheese mutant causes glial hyperwrapping of and brain degeneration in Drosophila. *J. Neuroscience.* **17**, 7425--7432.

Li, Y., Dinsdale, D., and Glynn, P. (2003). Protein domains, catalytic activity, and subcellular distribution of neuropathy target esterase in Mammalian cells. *J. Biol. Chem.* **278**, 8820--8825.

Lotti, M, and Moretto, A. (2005). Organophosphate-induced delayed polyneuropathy. *Toxicol. Rev.* **24**, 37--49.

Lush, M. J., Li, Y., Read, D. J., Willis, A. C., and Glynn, P. (1998). Neuropathy target esterase and a homologous Drosophila neurodegeneration mutant protein contain a domain conserved from bacteria to man. *Biochem. J.* **332**, 1--4.

Pots, A.M., Gruppen, H., Hessing, M., van Boekel, M.A., and Voragen, A.G. (1999). Isolation and characterization of patatin isoforms. *J. Agric. Food. Chem.* **47**. 4587--4582.

Racusen, D., and Foote, M. (1980). A major soluble glycoprotein of potato tubers. *J. Food. Biochem.* **4**, 43--52.

Richardson, R.J. (1984). Neurotoxic esterase: Normal and pathogenic roles. In *Cellular and Molecular Neurotoxicology* (T. Narahashi, Ed.), pp. 285-295, Raven Press, New York.

Richardson, R.J. (2005). Neurotoxicity, delayed. In *Encyclopedia of Toxicology 2nd ed., Vol. 2* (P. Wexler, ed.), Academic Press, New York, pp. 302--306.

Rydel, T.J., Williams, J.M., Krieger, E., Moshiri, F., Stallings, W.C., Brown, S.M., Pershing, J.C., Purcell, J.P., and Alibhai, M.F. (2003). The crystal structure, mutagenesis, and activity studies reveal that patatin is a lipid acyl hydrolase with a Ser-Asp catalytic dyad. *Biochemistry*. **42**, 6696--6708.

Schrag, J.D., and Cygler, M. (1997). Lipases and alpha/beta hydrolase fold. *Methods Enzymol.* **284**, 85--107.

Schwab, B.W., and Richardson, R.J. (1986). Lymphocyte and brain neurotoxic esterase: dose and time dependence of inhibition in the hen examined with three organophosphorus esters. *Toxicol. Appl. Pharmacol*. **83**, 1--9.

Senanayake, N., and Jeyaratnam, J. (1981). Toxic polyneuropathy due to gingili oil contaminated with tri-cresyl phosphate affecting adolescent girls in Sri Lanka. *Lancet*. **1**, 88--89.

Strickland, J.A., Orr, G.L., and Walsh, T.A. (1995). Inhibition of diabrotica larval growth by patatin, the lipid acyl hydrolase from potato tubers. *Plant Physiol*. **109**, 667--674.

Smith, H.V., and Spalding, J.M. (1959). Outbreak of paralysis in Morocco due to ortho-cresyl phosphate poisoning. *Lancet*. **2**, 1019--1021.

Smith, M.I., Elvove, E., and Frazier, W.H. (1930). The pharmacological action of certain phenol esters with special reference to the etiology of the so-called ginger paralysis. *Public Health Rep.* **45**, 2509--2524.

Zhang, Y., Kua, J., and McCammon, J.A. (2002). Role of the catalytic triad and oxyanion hole in acetylcholinesterase catalysis: an ab initio QM/MM study. *J. Am. Chem. Soc*. **124**, 10572--10577.

Chapter 2

Modeling the Tertiary Structure of the Patatin Domain of Neuropathy Target Esterase

Neuropathy target esterase (NTE) is an integral membrane protein of unknown physiological function whose chemical modification by certain organophosphorus (OP) compounds triggers a delayed distal axonopathy with concomitant paralysis and sensory loss (Richardson, 2005). While the primary pathology associated with organophosphorylation of NTE is seen in neurons, this protein is also expressed in non-neuronal cells, including lymphocytes and Leydig cells (Schwab and Richardson, 1986; Winrow *et al*., 2003)**.** Although the biological role of NTE remains unidentified, recent evidence indicates that it is vital for normal development, because NTE knockout mice are not viable beyond embryonic day 11 (Winrow *et al*., 2003).

Determining the tertiary structure of NTE would be expected to yield insight into its function. However, it has thus far eluded crystallization, owing in part to its size (1327 amino acid residues) and membrane anchorage to the endoplasmic reticulum (ER) (Richardson, 2005). Therefore, alternative strategies to structural elucidation could be considered, starting with computational modeling of discrete domains.

Preliminary bioinformatics analysis of the primary sequence of NTE has shown that its catalytic center resides within a domain that has homology to the plant protein, patatin (Winrow *et al*., 2003), a 40 kDa protein that constitutes as much as 40% (by weight) of the soluble protein in potato tubers (Pots *et al.*, 1999; Racusen and Foote, 1980). Like NTE (Glynn, 2005), patatin is known to have acyl hydrolase activity toward certain lipids (Andrews *et al*., 1988). The crystal structure of the patatin isoform pat17 (isolated from *Solanum cardiophyllum*) has been solved to a resolution of 2.2 Å and has shown this protein to have a catalytic center composed of a Ser77-Asp215 dyad whose residues (Ser77 Oγ and Asp215 Oδ2) are located 3.8 Å apart. This catalytic machinery is similar to that observed in mammalian cytosolic phospholipase A2 ($cPLA_2$), whose active site was originally thought to consist of a novel ser-asp-asp triad, but was revealed to consist of a ser-asp dyad, whose residues (Ser77 Oγ and Asp215 Oδ2) are located 2.9 Å apart (Dessen *et al*., 1999; Rydel *et al*., 2003). Such catalytic dyads are distinct from the classic ser-his-asp/glu catalytic triads observed in serine esterases and serine proteases (Zhang *et al*., 2002).

Patatin has sequence homology to cPLA2, and the crystal structure of pat17 has revealed it to have structural homology to $cPLA_2$, consisting of a modified α/β hydrolase fold (Ollis *et al*., 1992; Rydel *et al*., 2003).

Evidence for NTE being a serine esterase/lipase is known operationally from the fact that it catalyzes the hydrolysis of esters and that its esterase activity is inhibited by preincubation with Organophosphorus compounds like DFP and mipafox (Kropp *et al*., 2004) as well as the fact that its active site serine (Ser966) appears in the consensus sequence for an esterase/lipase motif (G-X-S-X-G; G-T-S-I-G in NTE) (Schrag and Cygler, 1997). In the case of NTE, Ser966 acts as the catalytic nucleophile and recent evidence has shown that NTE is able to hydrolyze 1-palmitoyl-lysophosphatidylcholine and deacylate phosphatidylcholine to glycerophosphocholine, thereby pointing to a potential role for NTE in the turnover of membrane lipids (van Tienhoven *et al*., 2002).

Despite certain similarities to classical serine esterases/lipases, site-directed mutagenesis studies have revealed that single mutations of histidines to alanines in the NTE esterase domain do not abrogate its esterase activity. Furthermore, these investigations suggested that the NTE active site consists of an unprecedented catalytic triad consisting of Ser966-Asp960-Asp1086, as opposed to the more traditional ser-his-asp/glu triads found in serine proteases and serine esterases (Zhang *et al*., 2002; Zhu *et al*., 2005).

Moreover, based on its primary sequence, it has been postulated that NTE may consist of 4 membrane spanning domains with the catalytic Ser966 residue located within the fourth transmembrane domain (TMD), thereby indicating that NTE may belong to a novel class of serine esterases (Atkins and Glynn, 2000). However, this prediction is problematic. If NTE were to possess a Ser966-Asp960-Asp1086 catalytic triad with the active site Ser966 residue located inside the last putative TMD (TMD4), it would be implausible for Asp1086, being 120 residues away from Ser966, to interact with the catalytic Ser966 residue, given that the typical length of a mammalian TMD is 17-25 residues (von Heijne, 1996). Furthermore, because serine hydrolase activity requires water as a reactant, it is difficult to envision, but it is not improbable, for a water molecule to penetrate the hydrophobic environment of the lipid bilayer to enter the NTE active site. Nevertheless recent findings in the field of intramembrane proteases, such as Site-2 protease and the rhomboids, indicate that these enzymes are able to hydrolyze peptide bonds within the lipid membrane (Kinch *et al*., 2006). Therefore, while it is possible that NTE could be an intramembrane esterase/lipase, the true nature of the interaction between NTE and the ER membrane is yet to be established.

The crystal structures of both patatin and cPLA2 have revealed that these proteins contain active sites composed of ser-asp dyads, in contrast to the ser-asp-asp catalytic triad that has been proposed for NTE. While the tertiary structure of NTE has yet to be elucidated, the sequence similarity between patatin and the catalytic domain of NTE prompted the hypothesis that, like patatin and cPLA2, the active site of NTE may consist of a ser-asp catalytic dyad. To test this hypothesis, a computationally derived model for the tertiary structure of the patatin (catalytic) domain of NTE (PNTE) has been constructed using the pat17 X-ray crystal structure as the template. The model serves to suggest hypotheses and provide insights about the catalytic machinery of NTE and provides a preliminary step toward understanding the putative structure of NTE's catalytic domain.

Materials and methods

Bioinformatics

The NTE sequence (accession number NP_006693) was obtained from the NCBI Entrez Protein database (http://www.ncbi.nlm.nih.gov/entrez/). The protein family database (PFAM; Bateman *et al*., 2004), an online database containing collections of protein domains and families, was used to identify domains in NTE from its primary sequence. Secondary structure predictions and analyses of the patatin and transmembrane domains were done using PredictProtein (Rost *et* al., 2003) and TMHMM (Krogh *et al*., 2001), which uses a hidden Markov model to identify membrane-spanning regions based on primary sequence. Hydropathy analyses of the PNTE and NTE TMD primary sequences were undertaken using the GREASE service on the University of Virginia FASTA server (http://fasta.bioch.virginia.edu/fasta_www/grease.htm). BoxShade 3.21 (http://www.ch.embnet.org/software/BOX_form.html), an on-line service for formatting multiple-sequence alignments, was employed to shade identical and homologous amino acid residues in the sequence alignment between PNTE and pat17.

NTE patatin domain model building

Secondary structure predictions for PNTE along with sequence alignments of PNTE against pat17 (PDB ID 1oxw) were obtained from the INUB server (Buffalo, NY; Fischer, 2000). Pymol (DeLano Scientific LLC, San Carlos, CA) and O (Jones *et al*., 1991) were utilized to build the PNTE structure based on the sequence alignments via virtual mutagenesis of the

corresponding residues on the template pat17 structure. Small chain breaks in the model were repaired using the lego-loop procedure in O. The resulting PNTE model was placed in a cubic shell of water molecules with a 4 Å depth. Energy minimization was undertaken using the Crystallography and NMR System (CNS; Brunger *et al.*, 1998) via simulated annealing to 500 K followed by cooling (step time of 0.5 fs per step) to room temperature (300 K) carried out in 25 K increments. Packing of residues in the active site of the resulting PNTE structure was evaluated visually. The refined model was analyzed in Pymol and Chem3D (CambridgeSoft, Cambridge, MA). Final images were rendered in Pymol.

NTE transmembrane domain model building

In order to verify the structure of the putative N-terminal NTE TMD predicted by PredictProtein and TMHMM, a computationally derived model was developed. Sequence alignments and secondary structure predictions of the NTE TMD against moricin (PDB ID 1kv4) were obtained from the INUB server (Buffalo, NY; Fischer, 2000). Pymol and O were utilized to build the NTE TMD model via virtual mutagenesis of the corresponding residues in the moricin structure. Due to the inherent hydrophobicity of the NTE TMD, the resulting structure was minimized *in vacuo* using the GROMOS implementation in Swiss PDB viewer (Guex and Peitsch, 1997). The refined model was analyzed in Pymol and MolMol (Koradi *et al*., 1996).

Results and Discussion

The NTE active site consists of a Ser966-Asp1086 catalytic dyad

Pfam analysis of the NTE primary sequence confirmed that the NTE active site resides within a patatin homology domain (residues 933-1099) (Fig 2.1). Alignment of PNTE and pat17 indicated 30% homology and 18% identity between the two sequences (Fig 2.2a). Analysis of the derived PNTE spatial model indicated that the overall structure of PNTE contains 7 α-helices (named α1- α 7) and 6 β-strands (named B1-B6) (Fig 2.2b). The β-strands are arranged in two β-sheets, one mixed β-sheet and one parallel β-sheet.

Analysis of the PNTE model shown in figure 2.2b showed that the NTE active site contains a catalytic dyad composed of Ser966 and Asp1086, instead of the previously hypothesized triad consisting of Ser966, Asp960, and Asp1086 presented by Atkins and Glynn (2000). In our model, Ser966 and Asp1086 are located on conserved loops with the Ser966 Oγ

located 2.93 Å from the Asp1086 Oδ2. This is similar to distances observed between ser-asp dyads in other serine esterases/lipases, such as the 3.8 Å distance between the Ser77 Oγ and Asp215 Oδ2 in the crystal structure of the patatin active site (Rydel *et al*., 2003) and the 2.9 Å distance between the Ser228 Oγ and Asp549 Oδ2 in the crystal structure of the mammalian $cPLA_2$ active site (Dessen *et al*., 1999). Moreover, the active site Ser966 residue of PNTE was found to be located in a 'nucleophilic elbow' formed by the loop between β2 and α2 (Fig 2.2b). Similar nucleophilic elbows have been found to contain the active site serine residues of both pat17 (Rydel *et al*., 2003) and cPLA2 (Dessen *et al*., 1999).

In marked contrast to the close proximity of Asp1086, the Oδ2 of Asp960 was found to be located 24.8 Å away from Ser966 Oγ, which is too far for Asp960 to play a direct role in catalysis (Fig. 2.2c). A possible explanation for discrepancies between the present model and the earlier site-directed mutagenesis results could be that mutation of Asp960 allosterically affects the structure of the NTE active site, thereby reducing the catalytic activity of the enzyme. Furthermore, given that our model indicates that Asp960 is exposed to solvent, mutating this residue may affect interactions between PNTE and other residues or domains in full-length NTE. However, these potential explanations will require experimental assessment.

In addition to identification of a probable catalytic dyad, it was observed that a conserved Gly938-Gly939-Ala940-Arg941 sequence, corresponding to the consensus sequence for an oxyanion hole (G-G-X-R) was present in close proximity to the NTE active site. Therefore, by analogy to pat17 and cPLA2, it is proposed that Gly938 and Gly939 define the oxyanion hole of NTE, with the backbone nitrogens of these residues located 4.8 Å and 5.7 Å, respectively, from the Ser966 Oγ. These dimensions from our model are somewhat larger than the corresponding 4.2 Å and 4.8 Å distances found between Ser288 Oγ and the backbone nitrogens of Gly197 and Gly198 in cPLA2 and the 3.4 Å and 3.8 Å distances observed between Ser77 Oγ the backbone nitrogens of Gly37 and Gly38 in pat17. However, despite the differences in these distances, the conservation of the G-G-X-R motif in NTE is indicative of these residues defining the putative oxyanion hole, and the exact measurements between its residues and the active site Ser966 need to be determined experimentally.

Therefore, based on the predictions arising from the present model, it is proposed that the catalytic dyad in NTE functions in a manner similar to catalytic dyads found in other serine hydrolases, such as patatin and $cPLA_2$. Consequently, it is proposed that Asp1086 acts as a general base and its Oδ2 activates the Ser966 Oγ by abstracting its proton, thereby turning Ser966 into a potent nucleophile, following which Ser966 would undertake its nucleophilic attack on the substrate (Dessen *et al*., 1999). Figure 2.3a depicts a comparison of the Ser-Asp catalytic dyad

model with the 'traditional' Ser-His-Asp/Glu catalytic triad model. In addition, figure 2.3a shows that the second aspartate residue in the formerly proposed Ser-Asp-Asp catalytic triad would be redundant and serve no function in the catalytic mechanism.

In the case of an organophosphorus ester (Fig 2.3b), the proposed catalytic mechanism would result in the formation of a trigonal bipyramidal intermediate, which would be stabilized by the oxyanion hole formed by Gly938, Gly939, Ala940, and Arg941. The collapse of the trigonal bipyramidal intermediate would yield an organophosphorylated-enzyme intermediate. The resulting organophosphorylated -enzyme intermediate would proceed to a second trigonal bipyramidal transition state via a transfer of a proton from Asp1086 to the leaving group. The subsequent replacement of the leaving group with a molecule of water would form a second trigonal bipyramidal intermediate, which would also be stabilized by the oxyanion hole. This second trigonal bipyramidal intermediate would be subsequently hydrolyzed by water, leaving behind the hydrolyzed substrate and the active enzyme (Fig 2.3b) (Dessen *et al*., 1999).

Because hydrolysis of the organophosphorylated enzyme would be expected to be slow in the case of organophosphorus esters, the organophosphorylated intermediate would be relatively stable, resulting in inhibition of the enzyme (Kropp *et al*., 2004). Moreover, the organophosphorylated intermediate has an additional potential pathway involving either S_N1- or S_N2-mediated displacement of a side chain, leaving a negatively charged phosphoryl moiety covalently attached to the active site, which could potentially be stabilized by the Nδ2 of Asn1092, located 5.8 Å away from the Oγ of Ser966. This displacement would be analogous to the 'aging' reaction of organophosphorylated AChE and NTE (Doorn *et al*., 2001; Kropp *et al*., 2004). Thus, the structure of the active site of the model suggests mechanisms of catalysis, inhibition, and aging reaction that need to be tested experimentally.

PNTE has a hydrophobic face and a hydrophilic face

Hydropathy analysis of the PNTE sequence indicated that approximately 50% of surface residues in PNTE are hydrophilic. Interestingly, mapping electrostatic potentials to the surface of the refined PNTE model revealed that one 'face' of PNTE was predominantly hydrophobic, while the other 'face' of PNTE was chiefly hydrophilic (Fig. 2.4). It was also found that the PNTE active site pocket is located in the hydrophobic face of PNTE. Therefore, while it is possible that PNTE is not a membrane-spanning domain, it might have points of membrane attachment or association, because NTE is known to hydrolyze lipids, and it has been shown to have lysophospholipase activity (Quistad *et al*., 2003). However, it is also important to consider the

possibility that the hydrophobic face of PNTE may represent an interior surface of the protein that is involved in interactions with other residues and domains in the structure of full-length NTE or other proteins that interact with NTE.

NTE has a single N-terminal transmembrane domain

Previously reported results by Atkins and Glynn (2000) suggested that NTE contains 4 putative membrane-spanning domains, with the active site Ser966 located within TMD4. However, PFAM analysis of the NTE primary sequence indicated that NTE contains a single N-terminal TMD (residues 9-31) (Fig. 2.1). Furthermore, TMHMM also predicted the presence of a single 23-residue N-terminal TMD (consisting of residues 9-31). Moreover, based on the 'positive inside' rule, TMHMM predicted a 95.7% probability that the N-terminus of the TMD is located in the lumen of the ER, thereby suggesting that the catalytic domain of NTE is located in the cytosol (Andersson and von Heijne, 1994).

Analysis of the NTE TMD and moricin primary sequences revealed 39% sequence homology and 22% sequence identity. Modeling the TMD structure using the moricin (PDB ID 1kv4) structure as a template indicated that the NTE TMD consists of a single right-handed α-helix. This is consistent with the expected structure for mammalian integral membrane protein domains (Ott and Lingappa, 2002). The α-helical nature of the NTE TMD was confirmed by examination of the Ramachandran plot for the NTE TMD model, which revealed that all residues in the NTE TMD were in the conformation expected of residues in a right-handed α-helix. In addition, hydropathy analysis of the NTE TMD primary sequence indicated that 100% of its residues are hydrophobic, thereby supporting the conclusion that NTE contains a single N-terminal TMD, and that the catalytic site of NTE is not contained within a membrane-spanning domain.

Therefore, based on the present modeling results and the literature, it is possible to propose a new representation for the overall structure of NTE, as depicted in Fig 2.5. As can be seen, instead of the four membrane spanning domains described by Atkins and Glynn (2000), it is proposed that NTE contains a single N-terminal integral membrane domain (residues 9-31). It is also proposed that the hydrophobic face of PNTE, which contains the NTE active site, is associated with the membrane (based on evidence that NTE hydrolyzes membrane lipids) (Zaccheo *et al*., 2004). However, the proposed model suggests that PNTE is not a true membrane-spanning domain, owing to the fact that the active site residues are seen on loops as opposed to α-helices, which are the expected secondary structures in mammalian transmembrane domains (Ott

and Lingappa, 2002). However, the details of the relative spatial arrangement of the TMD, putative cyclic nucleotide binding, and catalytic domains must await experimental determination.

The results obtained in the present study provide models for the putative tertiary structures of the catalytic and transmembrane domains of NTE, thereby affording preliminary insight into its structure. Experimental studies using X-ray crystallography and NMR spectroscopy are currently in progress to confirm or refute the predictions arising from the computational modeling results.

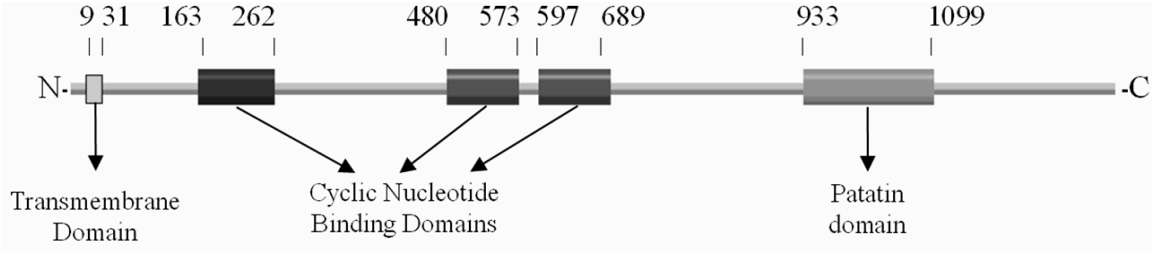

Figure 2.1: Domain organization in NTE. Results of the protein family analysis showing the domains in NTE. Numbering corresponds to amino acid residues at the N- and C- termini of each domain. As can be seen, NTE contains a single N-terminal transmembrane domain (TMD; residues 9-31), three cyclic nucleotide domains (CNP domains; residues 163-262, 480-573 and 597-689), and a patatin homology domain (PNTE, residues 933-1099) containing its active site.

Figure 2.2: Pat17-PNTE alignment and PNTE model. a) Sequence alignment of PNTE and pat17 sequence alignment of PNTE and pat17. Identical residues are identified by a black background, while homologous residues are identified by a grey background. Secondary structures of PNTE and pat17 are shown over their respective primary structures as arrows (representing β strands) and rectangles (representing α helices). α-helices and β strands in the PNTE sequence are numbered α1-α7 and β1- β6 respectively. Shading for homologous and identical residues in the aligned sequences was performed using BoxShade 3.21(http://www.ch.embnet.org/software/BOX_form.html). b) Putative tertiary structure for the NTE patatin domain. The PNTE structure consists of 7 α-helices (numbered α1-α7) and 6 β-strands (numbers B1-B6) arranged into one parallel and two anti-parallel β-sheets. Blue arrow denotes the location of nucleophilic Ser966 residue. Image was produced in PyMol (DeLano Scientific LLC, San Carlos, CA). c) Organization of the predicted active site of NTE. The Ser966 Oγ is located 2.96 Å from the Asp960 Oδ2. The 24.8 Å distance between the Ser966 Oγ and Asp960 Oδ2is too great for Asp960 to be directly involved in catalysis. Ser966, Asp960, and Asp1086 are depicted as sticks. Image was produced in PyMol.

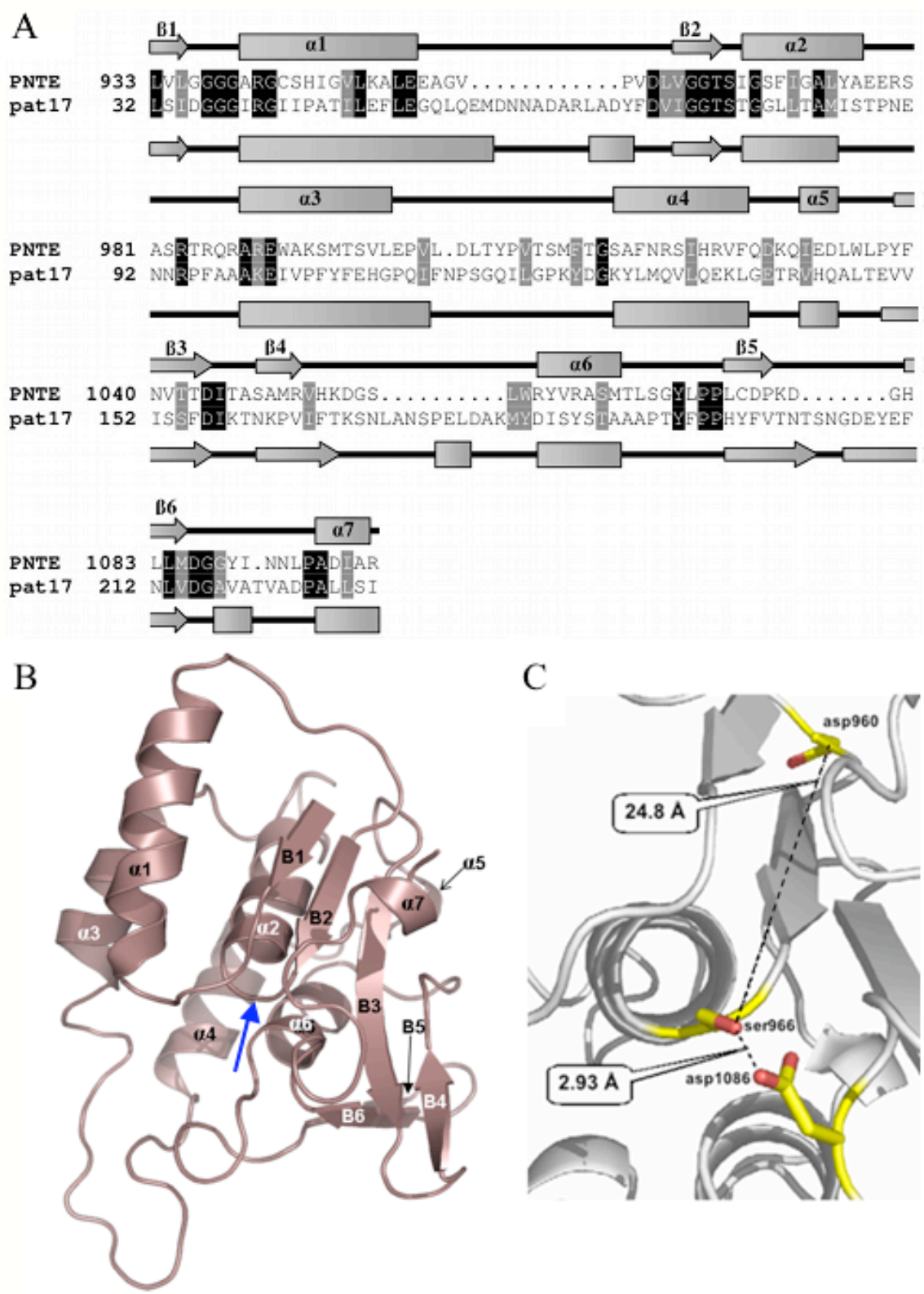
A
ß1
α1
ß2
α2
PNTE 933 LVLGGGGARGCSHIGVLKALEEAGV.....PVDLVGGTSIGSFIGALYAEERS
pat17 32 LSIDGGGIRGIIPATILEFLEGQLQEMDNNADARLADYFDVIGGTSTGGLLTAMISTPNE
α3
α4
α5
PNTE 981 ASRTRQRAREWAKSMTSVLEPVL.DLTYPVTSMGTGSAFNRSIHRVFQLKQIEDLWLPYF
pat17 92 NNRPFAAAKEIVPFYFEHGPQIFNPSGQILGPKYDGKYLMQVLQEKLGETRVHQALTEVV
ß3
ß4
α6
ß5
PNTE 1040 NVTTDITASAMRVHKDGS.....LWRYVRASMTLSGYLPPLCDPKD.....GH
pat17 152 ISSFDIKTNKPVIFTKSNLANSPELDAKMYDISYSTAAAPTYFPPHYFVTNTSNGDEYEF
ß6
α7
PNTE 1083 LLMDGGYI.NNLPADIAR
pat17 212 NLVDGNVATVADPALLSI
B
α1
B1
α5
α7
α3
α2
B2
B3
α4
α6
B5
B6
B4
C
asp960
24.8 Å
ser966
2.93 Å
asp1086

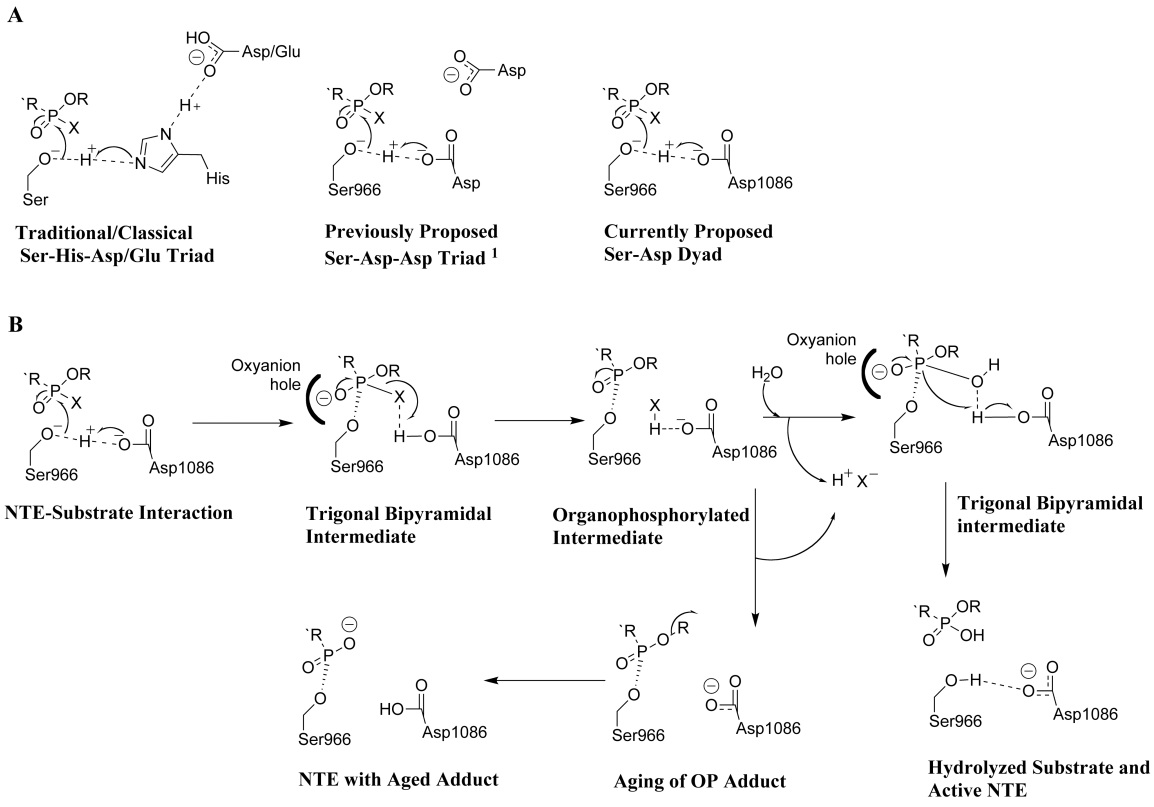

[1] Atkins and Glynn (2000).

Figure 2.3: NTE's catalytic dyad and mechanism of catalysis. a) Comparison of mechanisms of catalysis in a traditional Ser-His-Asp/Glu triad, Glynn's 'novel' Ser-Asp-Asp triad for NTE and our proposed Ser-Asp dyad for NTE. As can be seen, in Glynn's 'novel' triad, there is no role for the third aspartate residue, thereby lending support for our proposed Ser-Asp dyad for NTE's catalytic center. b) Proposed mechanism for hydrolysis of an organophosphorus (OP) ester by NTE's catalytic dyad. The aging reaction involving the loss of an alkyl group, thereby leaving behind a negatively charged OP adduct on the active site Ser966 residue is also depicted. It is currently postulated that aging of an OP adduct on NTE is the initiating step in the pathogenesis of OPIDN. Image was produced in ChemDraw (CambridgeSoft. Cambridge, MA).

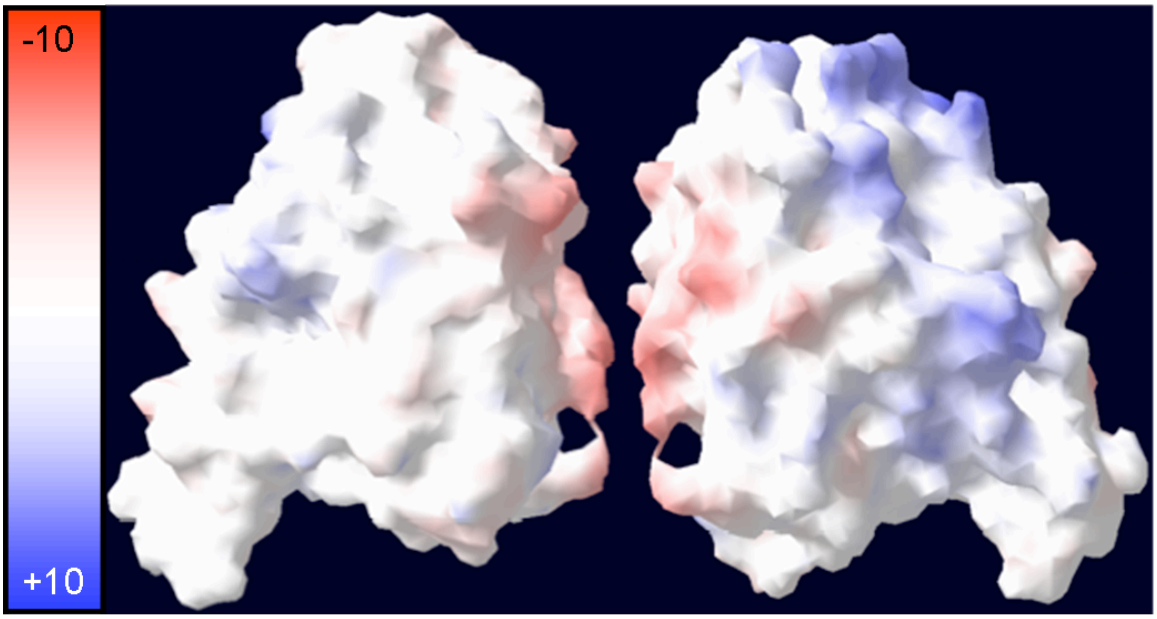

Figure 2.4: Surface maps of PNTE. Colors represent the degree of charge with red = negatively charged residue, white = uncharged residue, and blue =positively charged residue. Image was produced using the Swiss PDB Viewer (Guex and Peitsch, 1997).

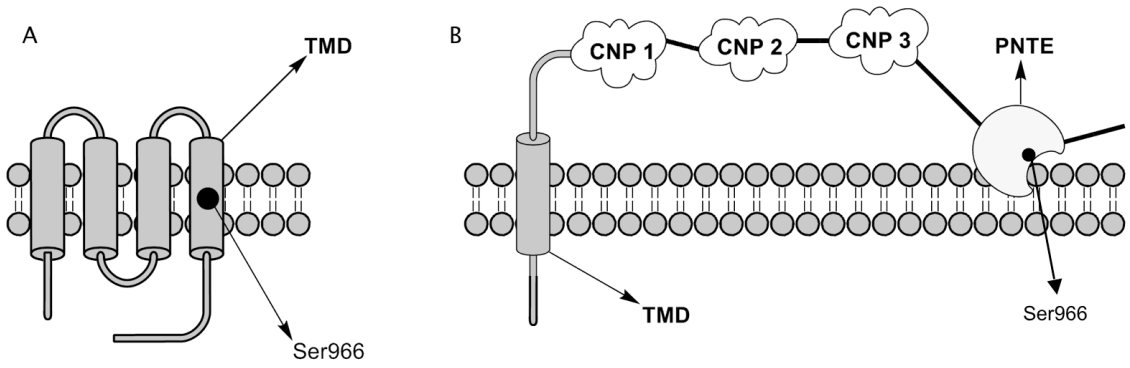

Figure 2.5: Models of NTE and its domains. a) Model proposed previously by Atkins and Glynn (2000) showing 4 transmembrane domains with the active site Ser966 residue located in the center of TMD4 (Ser966 is represented by a black dot), and b) Model proposed based on the present results depicting a single transmembrane domain, the PNTE domain containing the NTE active-site dyad, and previous results (Glynn, 2000; Nasser *et al*., 2006) showing the 3 putative cyclic nucleotide-binding (CNP) binding domains. Based on the data presented in this paper, it is proposed that PNTE could be associated with the membrane, but that it cannot be considered an integral membrane domain. Image was produced in ChemDraw (CambridgeSoft. Cambridge, MA).

References

Andersson, H., and von Heijne, G. (1994). Positively charged residues influence the degree of SecA dependence in protein translocation across the E. coli inner membrane. *EMBO. J.* **13**, 2267--2272.

Andrews, D.L., Beames, B., Summers, M.D., and Park, W.D. (1988). Characterization of the lipid acyl hydrolase activity of the major potato (Solanum tuberosum) tuber protein, patatin, by cloning and abundant expression in a baculovirus vector. *Biochem. J.* **252**, 199–206.

Atkins, J., and Glynn, P. (2000). Membrane association of and critical residues in the catalytic domain of human neuropathy target esterase. *J. Biol. Chem*. **275**, 24477--24483.

Brunger, A.T., Adams, P.D., Clore, G.M., DeLano, W.L., Gros, P., Grosse-Kunstleve, R.W., Jiang, J.S., Kuszewski, J., Nilges, M., Pannu, N.S., Read, R.J., Rice, L.M., Simonson, T., and Warren, G.L. (1998). Crystallography & NMR system: A new software suite for macromolecular structure determination. *Acta Crystallogr. D Biol. Crystallogr*. **54.** 905--921.

DeLano Scientific LLC, San Carlos, CA, USA. *The PyMOL Molecular Graphics System*. http://www.pymol.org.

Dessen, A., Tang, J., Schmidt, H., Stahl, M., Clark, J.D., Seehra, J., and Somers, W.S. (1999). Crystal structure of human cytosolic phospholipase A2 reveals a novel topology and catalytic mechanism. *Cell*. **97**, 349--360.

Doorn, J.A., Schall, M., Gage, D.A., Talley, T.T., Thompson, C.M., and Richardson, R.J. (2001). Identification of butyrylcholinesterase adducts after inhibition with isomalathion using mass spectrometry: Difference in mechanism between (1R)- and (1S)-stereoisomers. *Toxicol. Appl. Pharmacol.* **176**, 73--80.

Fischer, D. (2003). 3DS3 and 3DS5 3D-SHOTGUN meta-predictors in CAFASP3. *Proteins*. **51**, 434--441.

Glynn, P. (2000). Neural development and neurodegeneration: two faces of neuropathy target esterase. *Prog. Neurobiol.* **61**, 61--74.

Glynn, P. (2003). NTE: one target protein for different toxic syndromes with distinct mechanisms? *Bioessays*. **25**, 742--745.

Glynn, P. (2005). Neuropathy target esterase and phospholipid deacylation. *Biochim. Biophys. Acta*. **1736**, 87--93.

Guex, N., and Peitsch, M.C. (1997). SWISS-MODEL and the Swiss-PdbViewer: an environment for comparative protein modeling. *Electrophoresis*. **18**, 2714--2723.

Jones, T.A., Zou, J-Y., Cowan, S.W., and Kjeldgaard, M. (1991). Improved methods for building protein models in electron density maps and the location of errors in these models. *Acta Cryst*. **A47**, 110--119.

Kinch, L.N., Ginalski, K., and Grishin, N.V. (2006). Site-2 protease regulated intramembrane proteolysis: sequence homologs suggest an ancient signaling cascade. *Protein Sci*. **15**, 84--93.

Koradi, R., Billeter, M., and Wuthrich, K. (1996). *J. Mol. Graphics Modell*. MOLMOL: a program for display and analysis of macromolecular structures. **14**, 51--55.

Krogh, A., Larsson, B., von Heijne, G., and Sonnhammer, E.L. (2001). A combined transmembrane topology and signal peptide prediction method. *J. Mol. Biol*. **305**, 567--580.

Kropp, T.J., Glynn, P., and Richardson, R.J. (2004). The mipafox-inhibited catalytic domain of human neuropathy target esterase ages by reversible proton loss. *Biochemistry*. **43**, 3716--3722.

Lemberg, M.K., Menendez, J., Misik, A., Garcia, M., Koth, C.M., and Freeman, M. (2005). Mechanism of intramembrane proteolysis investigated with purified rhomboid proteases. *EMBO J.* **24**, 464--472.

Nasser, F.A., Wijeyesakere, S.J., Stuckey, J.A., and Richardson, R.J. (2006). Modeling the cyclic nucleotide binding domains of neuropathy target esterase. *The Toxicologist*. **90**, 299.

Ollis, D.L., Cheah, E., Cygler, M., Dijkstra, B., Frolow, F., Franken, S.M., Harel, M., Remington, S.J., Silman, I., Schrag, J., Sussman, J.L., Verschueren, K. H. G., and Goldman, A. (1992). The alpha/beta hydrolase fold. *Protein Eng*. **5**, 197--211.

Ott, C.M., and Lingappa, V.R. (2002). Integral membrane protein biosynthesis: why topology is hard to predict. *J. Cell. Sci*. **115**, 2003--2009.

Pots, A.M., Gruppen, H., Hessing, M., van Boekel, M.A., and Voragen, A.G. (1999). Isolation and characterization of patatin isoforms. *J. Agric. Food. Chem*. **47**. 4587--4582.

Quistad, G.B., Barlow, C., Winrow, C.J., Sparks, S.E., and Casida, J.E. (2003). Evidence that mouse brain neuropathy target esterase is a lysophospholipase. *Proc. Natl. Acad. Sci. U.S.A*. **100**, 7983--7987.

Racusen, D., and Foote, M. (1980). A major soluble glycoprotein of potato tubers. *J. Food. Biochem*. **4**, 43--52.

Richardson, R.J. (2005). Neurotoxicity, delayed. In *Encyclopedia of Toxicology 2nd ed., Vol. 2* (P. Wexler, ed.), Academic Press, New York, pp. 302--306.

Rost, B., Yachdav, G., and Liu, J, (2003). The PredictProtein server. *Nucleic Acids Res*. **32**, W321--W326.

Rydel, T.J., Williams, J.M., Krieger, E., Moshiri, F., Stallings, W.C., Brown, S.M., Pershing, J.C., Purcell, J.P., and Alibhai, M.F. (2003). The crystal structure, mutagenesis, and activity studies reveal that patatin is a lipid acyl hydrolase with a Ser-Asp catalytic dyad. *Biochemistry*. **42**, 6696--6708.

Schrag, J.D., and Cygler, M. (1997). Lipases and alpha/beta hydrolase fold. *Methods Enzymol*. **284**, 85--107.

Schwab, B.W., and Richardson, R.J. (1986). Lymphocyte and brain neurotoxic esterase: dose and time dependence of inhibition in the hen examined with three organophosphorus esters. *Toxicol. Appl. Pharmacol*. **83**, 1--9.

van Tienhoven, M., Atkins, J., Li, Y., and Glynn, P. (2002). Human neuropathy target esterase catalyzes hydrolysis of membrane lipids. *J. Biol. Chem*. **277**, 20942--20948.

von Heijne, G. (1996). Prediction of transmembrane protein topology. In *Protein structure prediction* (M.J.E. Sternberg, eds.), Oxford Univ. Press, Oxford, pp. 101--110.

Winrow, C.J., Hemming, M.L., Allen, D.M., Quistad, G.B., Casida, J.E., and Barlow, C. (2003). Loss of neuropathy target esterase in mice links organophosphate exposure to hyperactivity. *Nature Genetics*, **33**, 477--485.

Zaccheo, O., Dinsdale, D., Meacock, P.A., and Glynn, P. (2004). Neuropathy target esterase and its yeast homologue degrade phosphatidylcholine to glycerophosphocholine in living cells. *J. Biol. Chem*. **279**, 24024--24033.

Zhang, Y., Kua, J., and McCammon, J.A. (2002). Role of the catalytic triad and oxyanion hole in acetylcholinesterase catalysis: an ab initio QM/MM study. *J. Am. Chem. Soc*. **124**, 10572--10577.

Zhu, Y.C., Liu, X., Maddur, A.A., Oppert, B., and Chen, M.S. (2005). Cloning and characterization of chymotrypsin- and trypsin-like cDNAs from the gut of the Hessian fly [Mayetiola destructor (Say)]. *Insect Biochem. Mol. Biol.* **35**, 22--32.

Chapter 3

Conformational Changes in the Catalytic Domain of Neuropathy Target Esterase Following Inhibition and Aging

Since Anfinsen's groundbreaking research into determinants of protein folding (Anfinsen, 1973), predicting a protein's structure solely from its amino acid sequence has been considered the 'holy grail' of structural biology. Recent advances in computational techniques and computing power provide researchers with an opportunity to gain insight into the structures of proteins whose tertiary structures have yet to be determined experimentally. One such protein is neuropathy target esterase (NTE), a putative lysophospholipase (Quistad *et al.*, 2003; van Tienhoven *et al.*, 2002) whose structure is currently unknown. NTE is known to be a cellular target for the toxicity elicited by a subclass of organophosphorus compounds (OPs) termed neuropathic OPs. OPs represent a class of compounds, derived from pentacovalent phosphorus, that are used extensively in industry as pesticides, fire retardants, lubricants, pharmaceuticals and plasticizers. OPs have also been used in the battlefield as chemical warfare agents and currently pose a threat with respect to the potential for chemical terrorism (Richardson, 2005).

Chemical modification of NTE by certain OPs triggers a delayed distal axonopathy with simultaneous paralysis and sensory loss known as OP induced delayed neuropathy (OPIDN), a condition for which there is no cure. The signs and symptoms of OPIDN become evident 1-4 weeks post-exposure to a single dose of an OP. There are two broad classes of OPs; neuropathic OPs are capable of producing OPIDN, while non-neuropathic OPs are not (Richardson, 2005). During the Prohibition era in the United States, alcohol contaminated with the neuropathic OP tri-*ortho*-cresyl-phosphate (TOCP) was responsible for an epidemic of OPIDN where more than 20,000 people were affected. More recently, epidemics of OPIDN arising from exposure to TOCP have been reported from countries such as Sri Lanka and India (Senanayake and Jeyaratnam, 1981). Most modern cases of OPIDN arise from failed suicide attempts with OP insecticides (Lotti and Moretto, 2005).

OPIDN develops inexorably when >70% of neuronal NTE is organophosphorylated by a neuropathic OP and the resulting covalently-bound OP adduct undergoes an 'aging' reaction wherein it looses an alkyl side-chain, resulting in a negatively charged OP moiety covalently

bound to NTE's nucleophilic Ser966 residue (Glynn, 2003; Richardson, 2005). Very little is known about the manner in which axonal degeneration is initiated by NTE following its inhibition and aging. On the other hand, protein phosphorylation occurs frequently in nature as a means of controlling the biological functions of proteins through induced conformational changes (Bishayee *et al*., 1999; Canagarajah *et al*., 1997).

Thus, the gaps in knowledge about the physiological and pathogenic roles of NTE coupled with the biological precedent of protein phosphorylation prompted the hypothesis that the presence of the aged OP adduct may induce a functional change in NTE that is 'toxic' to the ultimate well-being of the neuron (Glynn, 1999). Consequently, given the addage that form follows function, if there is a true functional change, a structural change in NTE that is distinct from its native and inhibited states should also be present. This would be expected in the case of NTE, given that the current model for OPIDN postulates that interactions between neuropathic OPs and NTE results in NTE gaining a new function, as opposed to it ceasing its normal physiological role(s). Therefore, if the toxic-gain-of function model for OPIDN is correct and NTE does undergo a visbile conformational change following the aging reaction, this change in its tertiary structure would represent a unique chemical modification of the NTE that is ultimately detrimental to the survival of the axon.

However, NTE has thus far eluded crystallization, owing in part to its size (1327 amino acids in length) and membrane association (Richardson, 2005; Wijeyesakere *et al*., 2007). In lieu of an experimentally-derived 3-D structure of NTE, we have developed a homology model for its catalytic (patatin-homology) domain (PNTE) using the crystal structure of the plant protein patatin (PDB ID 1oxw) as a template. Using this model, we have shown that NTE's catalytic domain consists of a modified α/β hydrolase fold and contains a Ser966-Asp1086 catalytic dyad similar to that seen in mammalian cytosolic phospholipase A2 ($cPLA_2$) and patatin (Wijeyesakere *et al*., 2007).

Given the apparent importance of the aging reaction in the pathogenesis of OPIDN (Glynn, 2003; Richardson, 2005), it is prudent to investigate structural changes associated with inhibition and aging of NTE by a neuropathic OP. The significance of this research to the field of toxicology lies in that currently, there is very little known about NTE beyond its inhibition by OP compounds. Since it known in structural biology that form follows function, knowing the structure of NTE would yield insight into its possible physiological role in the cell. Thus, gaining an understanding of the structural changes in NTE associated with its organophosphorylation and aging would aid future research endeavors to solve the structure of NTE through experimental

techniques in order to determine how altered protein structure could lead to aberrations in function and produce disease.

Materials and methods

PNTE model

The PNTE model used in this investigation is the one described in Wijeyesakere *et al*. (2007). Briefly, this homology model was built based on the sequence alignment and secondary structure predictions for PNTE versus patatin-17 followed by the sue of the patatin-17 crystal structure (PDB ID 1oxw) as the template. Following this, the resulting model was refined via simulated annealing to 500 K using the crystallography and NMR system (Brunger *et al*., 1998).

Docking studies.

In order to better understand the nature of the initial interaction between DFP and PNTE prior to organophosphorylation, docking studies were undertaken with diisopropyl phosphorofluoridate (DFP) and its phosphorodiamidate analogue, *N*,*N*'-diisopropyldiamidophosphoryl fluoride (mipafox). The structures of DFP and mipafox were generated in Chem3D (CambridgeSoft, Cambridge, MA) and minimized using the MM2 protocol to a root mean square deviation (RMSD) gradient of 0.01 prior to their use in docking. Docking of DFP and Mipafox into the active site of PNTE was undertaken using the automated docking algorithm in Fujitsu CAChe (Fujitsu BioSciences, Sunnyvale, CA) employing a potential-mean-force technique with a Lamarckian genetic algorithm (run over 3,000 generations with a population size = 50, crossover rate = 0.8 and mutation rate = 0.3) (Morris *et al*., 1998). Flexibility was permitted in the ligands. The resulting models were analyzed in CAChe and PyMol (DeLano, 2002). Similar techniques were undertaken to dock mipafox into the active site of PNTE in order to compare its binding affinity to DFP. This technique was similar to that carried out in our laboratory on other serine hydrolases and stereoisomers of isomalathion (although flexibility was allowed in both, the ligand and a region of the macromolecule) (Doorn et al., 2001a,b, 2003).

Simulated inhibition (SI) and simulated aging (SA).

To gain a better understanding of the nature of the interactions of neuropathic OPs with PNTE, we undertook simulated organophosphorylation and inhibition (SI) and aging (SA) studies with aged and non-aged DFP (mipafox was excluded in this portion of the study due to its unusual mechanism of aging via de-protonation as opposed to the loss an alkyl side-chain (Kropp *et al*., 2004)). This allowed for testing *in silico* the hypothesis that aging results in a conformational change in PNTE that is distinct from the conformational change induced solely by inhibition. A similar computational procedure has been carried out recently through virtual mutation of a serine to phosphoserine (Groban et al., 2006).

SI was undertaken using the structure of diisopropylphosphoryl-serine (DPSer) that was built from the structure of monoisopropylphosphoryl-serine (MPSer) downloaded from the Hetero-compound Information Centre (http://alpha2.bmc.uu.se/hicup/; Kleywegt and Jones, 1998) using Chem3D. Ser966 in PNTE was replaced with DPSer using O 10.1 (Jones *et al*., 1991). The lego-loop procedure in O was employed to fix chain breaks arising from this substitution. Hydrogens were added to the DPSer-PNTE model at pH 7.0 followed by 300 rounds of minimization in Fujitsu CAChe using the MM3 protocol. SA of DPSer-PNTE was undertaken by deleting an isopropyl group from DPSer, thereby adding a negative charge to the resulting MPSer adduct. The MPSer-PNTE structure was minimized in Fujitsu CAChe using the MM3 protocol as described for SI. The resulting structures were analyzed in CAChe and PyMol. Packing of residues around the NTE active site in the minimized DPSer-PNTE and MPSer-PNTE models was undertaken via visual assessment.

The crystallography and NMR system (CNS; Brunger *et al.*, 1998) ver 1.2 was utilized to calculate the root-mean square deviation (RMSD) between the Cα backbones of native PNTE and DPSer-PNTE as well as the RMSD between the backbones of native PNTE and MPSer-PNTE. The calculated RMSD values were employed as a measure of the degree of overall conformational change arising from SI and SA of NTE by a neuropathic OP.

Results and discussion

DFP and mipafox can be accommodated in NTE's active site

Docking of DFP and mipafox into the active site of PNTE revealed that the phosphorus atom of DFP was located 4.7 Å from Ser966 OG and 3.7 Å from Asp1086 OD2 while the

phosphorus atom of mipafox was located 5.2 Å from Ser966 OG and 4.2 Å from Asp1086 OD2. These results indicated that these OPs could be accommodated in the active site of the PNTE model in an orientation suitable for organophosphorylation. The binding energies of DFP and mipafox to the active site of PNTE were calculated to be -36.1 kcal/mol and -30.77 kcal/mol respectively, thereby indicating favorable energetics for interactions between these ligands and NTE's active site Ser966 residue.

Arg941 makes polar contact with the OP ligand in NTE's active site

Analysis of PNTE's primary sequence had previously indicated that Arg941 would be a potential candidate residue in NTE's oxyanion hole formed by Gly938, Gly939, Ala940, and Arg941 (Wijeyesakere *et al*., 2007). Interestingly, the results of our docking studies revealed that Arg941's NH1 was located 3.0 Å from DFP's phosphoryl oxygen and 3.2 Å from the phosphoryl oxygen of mipafox (Fig 3.1). These results lend support Arg941's role in NTE's oxyanion hole and indicates a role for this residue in stabilizing the OP ligand as it enters NTE's active site in preparation for a nucleophilic attack on the OP ligand's phosphorus by NTE's Ser966 OG.

Conformational changes in PNTE after SI and SA

In order to gain an understanding of the association between covalent binding of an OP to the nucleophilic Ser966 residue of NTE and aging of the resulting OP adduct leading to OPIDN, we undertook simulated inhibition (SI) and simulated aging (SA) using our PNTE model with DFP. It has been hypothesized that inhibition of NTE with an OP results in a conformational change while aging results in a further conformational change, thereby leading to NTE's toxic gain-of-function (Glynn, 1999). It is currently thought that this second conformational change is distinct from that of the inhibited state and ultimately results in axonal degeneration, which manifests itself clinically as OPIDN.

Following energy minimization, it was evident that covalent binding of DFP to NTE's active site Ser966 residue did not result in any significant conformational change in its overall tertiary structure, as can be seen in Figure 3.2a. The calculated Cα backbone deviation of native PNTE versus its DFP-inhibited state was 1.4 Å. It was also found, however, that SI resulted in an expansion around PNTE's active site with the distance between Ser966 OG and Asp1086 OD2 increasing to 5.2 Å apart, compared to 2.9 Å in the native PNTE structure (Fig 3.3a).

In addition to this, SA of the inhibited PNTE structure did not show any significant conformational change relative to its native and inhibited states. The calculated backbone RMSD between native PNTE versus the its inhibited state was 1.6 Å (Fig 3.2b). The backbone Cα deviation between PNTE's inhibited and aged states was 0.2 Å. Aging of the covalently bound DFP adduct resulted in a slight expansion around the active site relative to the inhibited state with the Ser966 OG and Asp1086 OD2 located 5.5 Å apart (compared to the 2.9 Å distance seen in the native structure) (Fig 3.3b). This rotamer change is predumably due to charge repulsion betweent the negatively charged MIS moiety and the negatively charged aspartate. Interestingly, the negatively charged oxygen in the aged DFP adduct makes polar contact with Arg941 NH1 (2.7 Å), Gly938 N (3.4 Å) and Gly939 N (2.8 Å), which form NTE's oxyanion hole (Fig 3.4). Thus, it can be seen that the negative charge on the aged OP adduct is stabilized by the oxyanion hole in a manner similar to that seen in normal catalysis with a carbamate's tetrahedral intermediate (refer Fig 4.1a in chapter 4 and Fig 2.3b in chapter 2). This is also similar to the manner in which acetylcholinesterase's (AChE) oxyanion hole aids in the stabilization of the aged DFP adduct in the crystal structure of AChE (PDB ID 2dfp).

These findings can be compared to previous molecular dynamics research on acetylcholinesterase (AChE) undertaken by Hurley *et al*. (2005) that reported a net-RMSD of 1.2 Å associated with *in silico* inhibition (but not aging) of acetylcholinesterase (AChE) by the nerve agent VX. This RMSD is comparable to our result of 1.4 Å for SI of NTE's catalytic domain with DFP. With respect to aging of an OP adduct, the x-ray crystal structures of *Torpedo Calfornica* AChE inhibited and aged by DFP, sarin and soman (PDB IDs 2dfp, 1cfj and 1som respectively) reported no significant conformational changes in the overall structure of the enzyme, although some localized conformational changes were reported in AchE's acyl pocket (Millard et al., 1999). Similarly, analysis of the crystal structure of native human butyrylcholinesterase (BChE; PDB ID 1p0i) with its DFP- and echothiophate-aged forms (PDB ID 1xlu and 1xlv respectively) shows no evidence for a global conformational change associated with aging. The Cα RMSDs for the DFP- and echothiophate-aged forms of BChE relative to the native form of this enzyme are 0.51 Å (DFP-aged vs. native) and 0.55 Å (echothiophate-aged vs. native). This lack of a global conformational change following aging of an OP is consistent with the findings of our molecular modeling effort and serve to suggest that aging of an OP on a NTE is not expected to results in a significnat change in the structure of the enzyme relative to its native state.

Is there a conformational change in NTE leading to OPIDN? The need for a new model for OPIDN

The results of this investigation raise important questions about the putative function of a conformational change in NTE as the initiator of the progression to the delayed axonopathy that is characteristic of OPIDN. The lack of knowledge regarding the precise mechanism whereby the aged NTE molecule leads to the pathology seen in OPIDN prompted the hypothesis that the aged state of the enzyme may be functionally detrimental to axonal survivial, thereby suggesting that a conformational change may occur with aging that is distinct from the protein's native and inhibited states. Our results indicated that the overall degree of conformational change associated with inhibition of NTE was small and, contrary to our hypothesis, our investigation also revealed that the conformational change associated with aging of the DFP adduct is not significantly different from NTE's inhibited and native states.

Further evidence for a lack of a conformational change following inhibition and aging of an OP on a serine esterase can be found in the crystal structures of other α/β hydrolases such as acetylcholinesterase (AChE) from *T. calfornica* that have been solved in their native and aged variants. In addition to this, given the precedent in structural biology that form follows function, it would be logical to conclude that NTE's hypothesized toxic-gain-of-function in the absence of any structural changes would be unprecedented and highly unusual. These findings suggest that the association between aging and OPIDN may be correlative rather than causative and highlight the need for a new model to explain the pathogenesis of OPIDN.

However, a potential limitation of this study is that due to the lack of a model for the structure for the full-length NTE molecule, our modeling work was undertaken using its catalytic domain alone. Therefore, there is the remote possibility that, while PNTE undergoes a negligible overall conformational change with aging, a larger change is propagated though the entire molecule resulting in NTE's toxic gain-of-function, which leads to OPIDN. Another possibility is that aging affects interactions between NTE and its protein binding partners, thereby perturbing NTE's normal physiological function, presumably through a change in the surface electrostatic potentials of the complete NTE molecule (although no such change was visible with our PNTE model). Therefore, the results and conclusions of this investigation underscore the need for further experimental research into NTE's structure as well as its physiological and pathological functions.

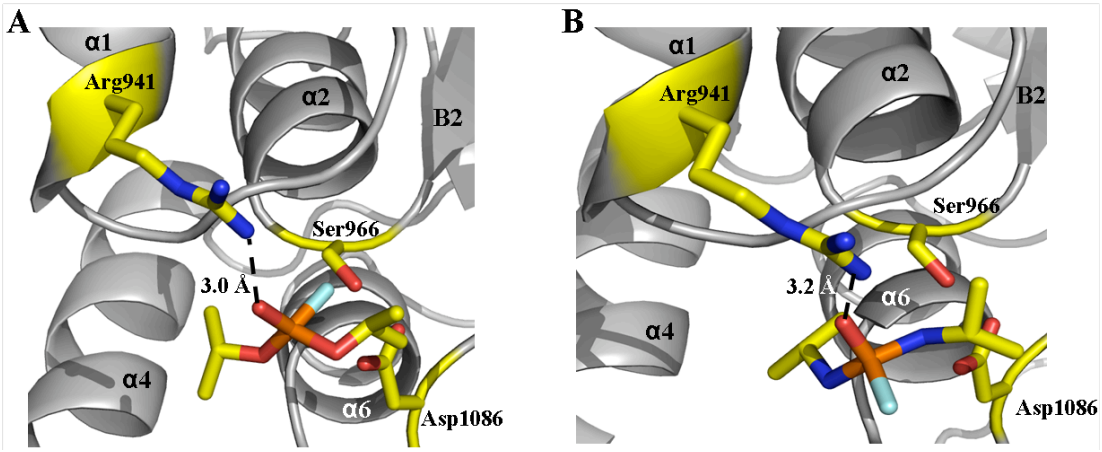

Figure 3.1: Docking DFP and mipafox into the PNTE model. Docking of a) DFP and b) mipafox into the active site of PNTE. As can be seen, the phosphoryl oxygens of the OPs make polar contact with Arg941 in NTE's oxyanion hole with the Arg941 NH1 being 3.0 Å from DFP's phosphoryl oxygen and 3.2 Å from mipafox's phosphoryl oxygen.

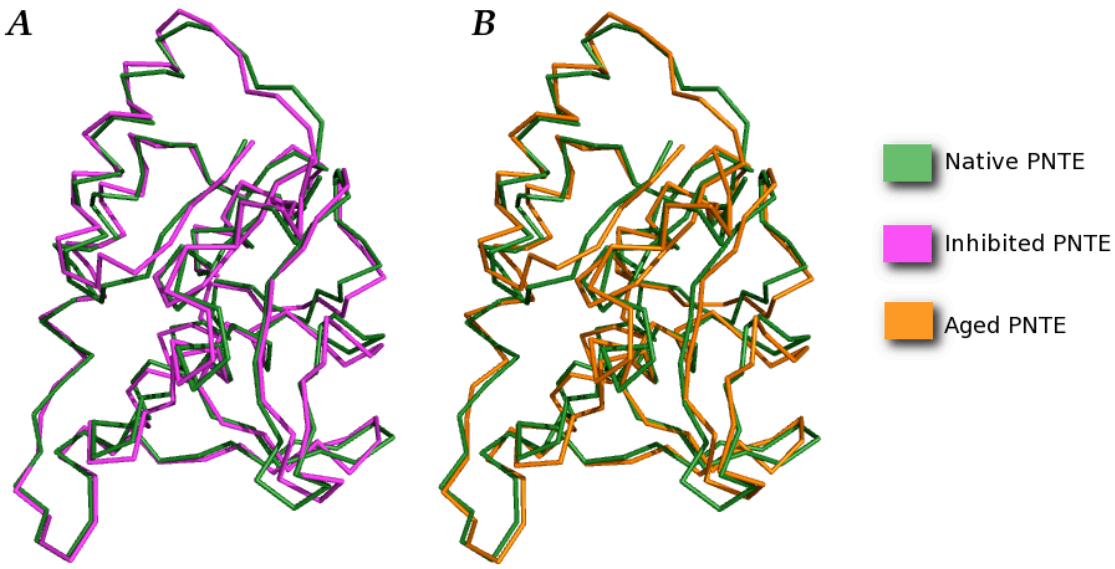

Figure 3.2: Structural changes in PNTE associated with inhibition and aging of DFP. The Cα backbone structures of native PNTE (green) is compared to the backbone structures of PNTE following (a) inhibition by DFP (purple), or (b) inhibition and aging of the DFP adduct (orange). As can be seen, inhibition of PNTE does not result in a significant conformational change relative to its native state (Cα backbone RMSD = 1.4 Å). Similarly, aging is not associated with a significant conformational change (Cα backbone RMSD = 1.6 Å (native versus inhibited and aged PNTE).

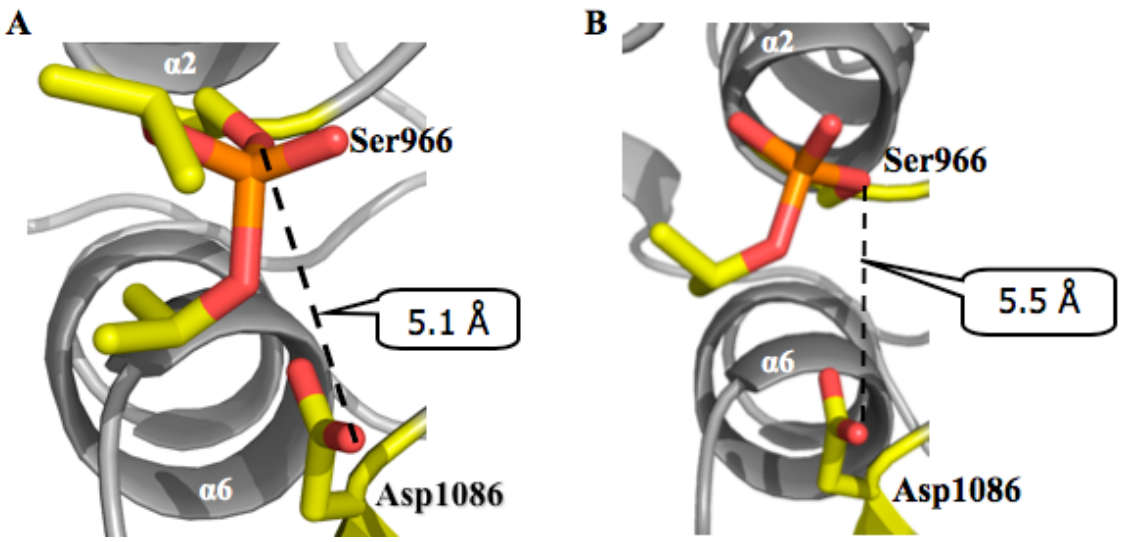

Figure 3.3: PNTE active site after inhibition and aging. Active site of PNTE after a) inhibition with DFP, and b) aging of the covalently bound DFP adduct. As can be seen, inhibition with DFP results in the active site Ser966 OG moving 5.1 Å away from Asp1086 OD2 (compared to 2.9 Å between these residues in the native PNTE structure). Aging results in a slight additional change, with the active site residues moving 5.5 Å apart (presumably due to charge repulsion by the negatively charged MIS and aspartate residues). However, these changes represent changes in rotamer conformations and are not the result of changes in the amino acid backbones of these residues.

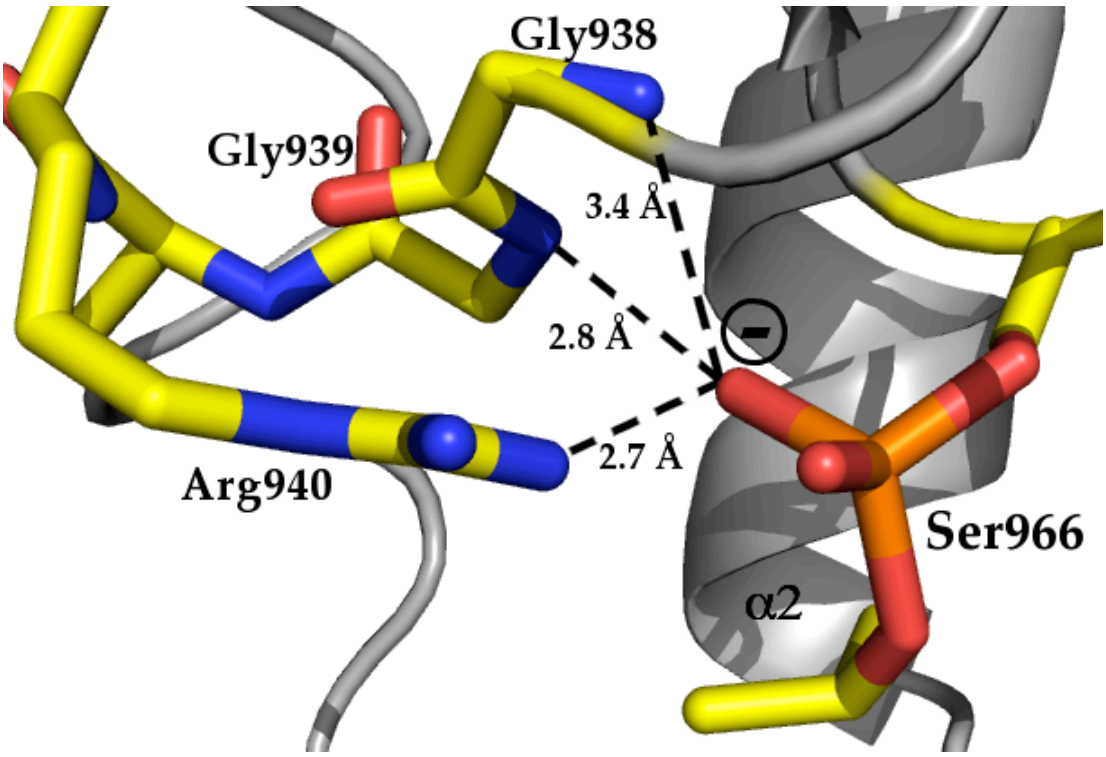

Figure 3.4: Aging of DFP on PNTE. As can be seen, the negative charge on the DFP-Ser966 adduct is stabilized by residues of the oxyanion hole (Gly938, Gly939 and Arg940), in a manner similar to what is expected for stabilization of the tetrahedral intermediate of an ester during normal catalysis and is similar to that seen the crystal structures of other aged OP-serine esterase conjugates. The negatively charged oxygen is indicated along with contact distances between it and Gly938 N (3.4Å), Gly939 N (2.8 Å) and Arg940 NH1 (2.7 Å).

References

Anfinsen, C.B. (1973). Principles that govern the folding of protein chains. *Science*. **181**, 223--230.

Bishayee, A., Beguinot, L. and Bishayee, S. (1999). Phosphorylation of tyrosine 992, 1068, and 1086 is required for conformational change of the human epidermal growth factor receptor c-terminal tail. *Mol. Biol. Cell*. **10**, 525--536.

Brunger, A.T., Adams, P.D., Clore, G.M., DeLano, W.L., Gros, P., Grosse-Kunstleve, R.W., Jiang, J.S., Kuszewski, J., Nilges, M., Pannu, N.S., Read, R.J., Rice, L.M., Simonson, T., and Warren, G.L. (1998). Crystallography & NMR system: A new software suite for macromolecular structure determination. *Acta Crystallogr. D Biol. Crystallogr*. **54.** 905--921.

Canagarajah, B.J., Khokhlatchev, A., Cobb, M.H., and Goldsmith, E.J. (1997). Activation mechanism of the MAP kinase ERK2 by dual phosphorylation. *Cell*. **90**, 859--69.

DeLano Scientific LLC, San Carlos, CA, USA. *The PyMOL Molecular Graphics System*. http://www.pymol.org.

Doorn, J.A., Talley, T.T., Thompson, C.M., and Richardson, R.J. (2001a). Probing the active sites of butyrylcholinesterase and cholesterol esterase with isomalathion: conserved stereoselective inactivation of serine hydrolases structurally related to acetylcholinesterase. *Chem. Res. Toxicol*. **14**, 807--813.

Doorn, J.A., Schall, M., Gage, D.A., Talley, T.T., Thompson, C.M., and Richardson, R.J. (2001b). Identification of butyrylcholinesterase adducts after inhibition with isomalathion using mass spectrometry: Difference in mechanism between (1R)- and (1S)-stereoisomers. *Toxicol. Appl. Pharmacol.* **176**, 73--80.

Doorn, J.A., Thompson, C.M., Christner, R.B., and Richardson, R.J. (2003). Stereoselective inactivation of Torpedo californica acetylcholinesterase by isomalathion: inhibitory reactions with (1R)- and (1S)-isomers proceed by different mechanisms. *Chem. Res. Toxicol*. **16**, 958--965.

Glynn, P. (1999). Neuropathy target esterase. *Biochem. J*. **344**, 625--631.

Glynn, P. (2003). NTE: one target protein for different toxic syndromes with distinct mechanisms? *Bioessays*. **25**, 742--745.

Groban, E.S., Narayanan, A., and Jacobson, M.P. (2006). Conformational changes in protein loops and helices induced by post-translational phosphorylation. *PLoS Comput. Biol*. **2**, e32.

Hurley, M.M., Balboa, A., Lushington, G.H., and Guo, J. (2005). Interactions of organophosphorus and related compounds with cholinesterases, a theoretical study. *Chem. Biol. Interact.* **157-158**. 321--325.

Jones, T.A., Zou, J-Y., Cowan, S.W., and Kjeldgaard, M. (1991). Improved methods for building protein models in electron density maps and the location of errors in these models. *Acta Cryst.* **A47**, 110--119.

Kleywegt, G.J., and Jones, T.A. (1998). Databases in protein crystallography. *Acta Cryst.* **D54**, 1119--1131.

Kropp, T.J., Glynn, P., and Richardson, R.J. (2004). The mipafox-inhibited catalytic domain of human neuropathy target esterase ages by reversible proton loss. *Biochemistry.* **43**, 3716--3722.

Lotti, M, and Moretto, A. (2005). Organophosphate-induced delayed polyneuropathy. *Toxicol. Rev.* **24**, 37--49.

Millard, C.B., Kryger, G., Ordentlich, A., Greenblatt, H.M., Harel, M., Raves, M.L., Segall, Y., Barak, D., Shafferman, A., Silman, I., and Sussman, J.L. (1999). Crystal structures of aged phosphonylated acetylcholinesterase: nerve agent reaction products at the atomic level. *Biochemistry.* **38**, 7032--7039.

Morris, G.M., Goodsell, D.S., Halliday, R.S., Huey, R., Hart, W.E., Belew, R.K., and Olson, A.J. (1998). Distributed automated docking of flexible ligands to proteins: Parallel applications of AutoDock 2.4. *J. Comput. Chem.* **19**, 1639--1662.

Quistad, G.B., Barlow, C., Winrow, C.J., Sparks, S.E., and Casida, J.E. (2003). Evidence that mouse brain neuropathy target esterase is a lysophospholipase. *Proc. Natl. Acad. Sci. U.S.A.* **100**, 7983--7987.

Richardson, R.J. (2005). Neurotoxicity, delayed. In *Encyclopedia of Toxicology 2nd ed., Vol. 2* (P. Wexler, ed.), Academic Press, New York, pp. 302--306.

Senanayake, N., and Jeyaratnam, J. (1981). Toxic polyneuropathy due to gingili oil contaminated with tri-cresyl phosphate affecting adolescent girls in Sri Lanka. *Lancet.* **1**, 88--89.

van Tienhoven, M., Atkins, J., Li, Y., and Glynn, P. (2002). Human neuropathy target esterase catalyzes hydrolysis of membrane lipids. *J. Biol. Chem.* **277**, 20942--20948.

Wijeyesakere, S.J., Richardson, R.J., and Stuckey, J.A. (2007). Modeling the tertiary structure of the patatin domain of neuropathy target esterase. *Protein J.* **26**, 165--172.

Chapter 4

Structural Insight into the Inhibition and Aging of NTE from X-Ray Crystal Studies of its Catalytic Domain Homologue, Patatin-17

As a protein, neuropathy target esterase (NTE) presents researchers with a mystery - a putative lysophospholipase (Tienhoven *et al.*, 2002 and Quistad *et al.*, 2003) whose structure is currently unknown, but is the target for a delayed axonopathy elicited by a subclass of organophosphorus compounds (OPs). Covalent interactions between these OPs (dubbed neuropathic NTE inhibitors) and NTE is known to trigger this axonopathy, termed OP-induced delayed neuropathy (OPIDN), which is characterized by a delayed onset of symptoms involving simultaneous paralysis and sensory loss. Currently there is no cure for OPIDN and once initiated, the progress to the final disease state (axonopathy of the long nerve fibers resulting in flaccid, followed by spastic paralysis of the outer extremities) is unavoidable. As denoted by its name, there is a delay between exposure and the onset of clinical symptoms, which become evident 1-4 weeks post-exposure to a sufficient dose of a neuropathic OP (Richardson, 2005; Richardson *et al*., 2009).

Overall, there are two broad classes of NTE inhibitors: neuropathic OPs whose members include phosphates, phosphonates, and phosphorodiamidates are capable of producing OPIDN, and non-neuropathic NTE inhibitors such as phosphinates, sulfonates and carbamates that are incapable of inducing OPIDN. It has been shown that pre-dosing an animal with a non-neuropathic NTE inhibitor has a protective effect with respect to a subsequently administered large dose of a neuropathic OP (Johnson, 1990). During the Prohibition era in the United States, alcohol contaminated with the neuropathic OP tri-*o*-cresyl-phosphate (TOCP) was responsible for an epidemic of OPIDN. While cases of OPIDN are now relatively rare, recent epidemics of OPIDN arising from exposure to TOCP have been reported from countries such as Sri Lanka and India (Richardson, 2005; Senanayake and Jeyaratnam, 1981). Most modern cases of OPIDN arise from failed suicide attempts with certain OP insecticides (Lotti and Moretto, 2005). Because OPs are used extensively in industry as pesticides, fire retardants, lubricants, pharmaceuticals and plasticizers, and given that they have also been used in the battlefield as chemical warfare agents, it is prudent to study the neuropathic potentials of these compounds, as they currently pose a

threat with respect to their potential for use as chemical terrorism agents (Richardson, 2005; Richardson *et al*., 2009). Furthermore, it has been suggested that OP exposure may be a contributing factor to some of the neurological disorders reported by those afflicted with Gulf War syndrome in the early and mid 1990s (Golomb, 2008; Haley *et al.*, 1997).

It is currently thought that the progression to OPIDN is inevitable when >70% of neuronal NTE is organophosphorylated by a neuropathic OP and the resulting covalently-bound OP adduct undergoes a secondary reaction known as 'aging'. Aging is a post-inhibitory reaction wherein the OP adduct typically undergoes net loss of an alkyl side-chain, resulting in a negatively charged OP moiety covalently bound to NTE's nucleophilic Ser966 residue (Glynn, 2003; Richardson, 2005). Very little is known about the manner in which axonal degeneration is initiated by NTE following its inhibition and aging (Figure 4.1). On the other hand, protein phosphorylation occurs frequently in nature as a means of controlling the biological functions of proteins through induced conformational changes (Bishayee *et al*., 1999; Canagarajah *et al*., 1997).

Thus, gaps in knowledge about the physiological and pathogenic roles of NTE coupled with the biological precedent of protein phosphorylation prompted the hypothesis that the presence of the aged OP adduct may induce a structural change in NTE that is distinct from the structures of native NTE and NTE in its inhibited (non-aged) state. It is possible that the conformational change associated with aging is responsible for NTE's 'toxic gain-of-function' which, through an unknown pathway, leads ultimately to axonal degradation and OPIDN (Glynn, 1999). However, attempts thus far to crystallyze NTE have yet to prove fruitful. This could be due to its size (1327 amino acids; 150 kDa) and membrane association (Li et al., 2003; Richardson, 2005). However, previous research by our lab has shown NTE's catalytic domain (termed the NTE patatin-homology domain (PNTE)) to be homologous (30% sequence homology and 18% sequence identity) to an isoform of the plant protein patatin, known as patatin-17 (pat-17; Wijeyesakere *et al.,* 2007), a soluble protein extracted from the tubers of heartleaf nightshade (*Solanum cardiophyllum*) and whose crystal structure has been solved (Rydel *et al*., 2003).

Patatin is a 40 kDa lipid acyl hydrolase (Hirayama *et al*., 1975; Andrews et al., 1988) expressed in potatoes and other members of the nightshade family (Ganal *et al*., 1991) and constitutes approximately 40% (by weight) of the soluble protein in potato tubers (Pots *et al.*, 1999; Racusen and Foote, 1980). The crystal structure of the patatin isoform, pat17, has shown this protein to have a catalytic center composed of a Ser77-Asp215 dyad (Rydel *et al*., 2003), compared to the Ser-His-Glu catalytic triad observed in AChE (Zhang *et al*., 2002) and is similar to the Ser966-Asp1086 dyad proposed for NTE (Wijeyesakere *et al*., 2007). While previous

research has suggested that patatin could be inhibited by OP compounds such as DFP and methyl-p-nitrophenyl-octylphosphonate (Strickland *et al*., 1995; Hirschberg, *et al.*, 2001), a detailed understanding of this inhibitory mechanism is unknown, since the inhibitory potencies of these compounds were not examined quantitatively.

Given the apparent importance of the aging reaction in the pathogenesis of OPIDN (Glynn, 2003), and the availability of a soluble PNTE homologue, it is prudent to investigate whether inhibition and aging of OPs on patatin result in a conformational change. Because it is posited in structural biology that form follows function, understanding conformational changes in NTE and its homologues following their interactions with OPs is expected yield insight into the pathogenesis of OPIDN. To this end, this paper presents the crystal structure of pat17 inhibited and aged by diisopropylphosphorofluoridate (DFP), a neuropathic OP, as well as the crystal structure of unaged pat17 inhibited by methyl arachidonyl fluorophosphonate (MAFP). These results serve to provide insight into the structural changes in patatin, as well as suggest hypotheses for the putative structural changes in NTE, associated with covalent modification by OPs.

Materials and methods

Supplies

Unless indicated, all reagents were purchased from Sigma-Aldrich (St. Louis, MO). DFP was purchased from Calbiochem (San Diego, CA). Racemic methyl arachidonyl fluorophosphonate (MAFP) was purchased from Cayman Chemical (Ann Arbor, MI).

Protein production

The pat17 plasmid was kindly supplied by the Monsanto Corporation (Chesterfield, MO). N-terminal hexa his-tagged Pat17 was purified via a modification of the procedure described by Rydel *et al*. (2003). The pat17 plasmid was transformed into competent *E. coli* (CD41 strain) and cells were selected on 2XYT plates containing 30 µg/L kanamycin. Colonies containing the pat17 plasmid were grown at 37 ºC (with shaking) in enriched (2XYT) media containing 30 µg/L kanamycin to an optical density (measured at 600 nm; OD_{600}) of 0.6, at which time production of pat17 was induced via the addition of 0.4 mM Isopropyl β-D-1-thiogalactopyranoside (IPTG). Following induction, the *E. coli* were allowed to grow overnight at 25 ºC (with shaking) after which the cells were harvested via centrifugation at 6000 × g for 10 min at 4 ºC. Bacterial cell pellets were stored at -80 ºC until needed.

His-tagged pat17 was purified via lysis in 50 mM Tris-HCl (pH 8.5 at 21 ºC) and 150 mM NaCl. Cells were lysed via sonication on ice for 3 min (6 × 30 sec cycles at 25 W with 30 sec pauses between cycles). Cell debris was removed via centrifugation at 20,000 ×g for 45 min at 4 ºC. Pat17 was recovered though affinity chromatography using a Ni-NTA column (Invitrogen, Carlsbad, CA) followed by elution in 50 mM Tris-HCl (pH 8.5), 150 mM NaCl and 300 mM imidazole at 4 ºC. The eluted protein was dialyzed overnight against 25 mM Tris-HCl (pH 7.5) at 4 ºC and purified to homogeneity via size exclusion chromatography at 4 ºC using a Sephadex-75 column equilibrated with 25 mM Tris (pH 7.5 at 21 ºC) and run at a rate of 1 ml/min at 4 ºC. The pat17-containing fractions were pooled and dialyzed overnight against 10 mM Tris-HCl (pH 7.4 at 21 ºC) at 4 ºC. Prior to its use in crystallography, pat17 was concentrated to 10 mg/ml using an Amicon ultra-15 concentrator with a 10,000 Da molecular weight cut-off (Millipore, Billerica, MA).

Protein crystallography

Initial screening of pat17 (at a concentration of 10 mg/ml in 10 mM Tris-HCl pH 7.4 (at 21 ºC)) in its native state was undertaken around conditions reported by Rydel *et al* (2003) (16%(w/v) polyethylene glycol-3350 and 0.24 M ammonium acetate). Crystal trays were setup by hand at 21 ºC via vapor diffusion using the hanging drop method. The conditions were monitored for a week and no crystal growth was observed. Since no crystal growth was observed under these conditions, spare-matrix screens were setup using commercially available screens (Crystal Screen (Hampton Research, Aliso Viejo, CA), Index (Hampton Research, Aliso Viejo, CA), Cryo (Emerald BioSystems, Bainbridge Island, WA), Wizard (Emerald BioSystems, Bainbridge Island, WA) and PEG (Qiagen, Valencia, CA)) using a Cartesian Honeybee crystallization robot (Genomic Solutions, Ann Arbor, MI). The crystal trays were observed over the course of a week and positive results (snowflake-like crystals) were obtained for the following conditions: (1) 30% (v/v) polyethylene glycol-200, Acetate (pH 4.5) and 0.1 M NaCl; (2) 40% (v/v) polyethylene glycol-300, Acetate (pH 4.5) and 0.2 M NaCl. Crystal trays were setup by hand around these conditions in order to obtain usable crystals of pat17.

Pat17 inhibited with 1 mM diisopropylfluorophosphate (DFP) was at a concentration of 10 mg/ml in 10 mM Tris-HCl. DFP-inhibited pat17 was crystallized via vapor diffusion at 4 ºC using the hanging-drop method with a precipitant solution of 0.1 M sodium acetate (pH 4.6), 46% (v/v) polyethylene glycol-400 and 75mM ammonium sulfate. A 2 µL drop of DFP-inhibited pat17 was placed on a silanized coverslip along with a 2 µL drop of the precipitant solution. The

protein-precipitant droplet was suspended over the grease-lined well of a Linbro plate (Hampton Research) containing 1 mL of precipitant solution.

Crystals of pat17 inhibited with DFP grew within two weeks to a maximum size of 0.1 mm x 0.1 mm x 0.1 mm prior to being harvested and flash-frozen in liquid nitrogen. Diffraction data were collected at the Advanced Photon Source (beamline 21-ID-D; Argonne, IL) using a Mar-300 CCD at -180 ºC with a crystal-detector distance of 600 mm. 360 degrees of data (1º step size; 1 sec exposure) were collected at a wavelength of 0.97626 Å to a resolution of 2.6 Å (see Table 1 for detailed data collection and refinement statistics). The resulting data were processed using the HKL2000 suite (Otwinowski *et al*., 1997). Analysis of the diffraction data revealed the crystals to be in space group $P4_32_12$ (a = b = 52.99 Å, c = 242.77 Å; $\alpha = \beta = \gamma = 90°$). The crystal's Matthew's coefficient and approximate solvent content were calculated in CCP4.

Crystals of pat17 inhibited with MAFP were obtained by soaking crystals of native pat17 in a precipitant solution containing 1.3 µM MAFP for 24 h. Crystals of native pat17 were grown via vapor diffusion at 21 ºC using the hanging-drop method with a precipitant solution of 0.1 M sodium acetate (pH 4.6), 49% (v/v) polyethylene glycol-400 and 225 mM cesium chloride. A 2 µL drop of native pat17 (at a concentration 10 mg/ml) was placed on a silanized coverslip along with a 2 µL drop of the precipitant solution. The protein-precipitant droplet was suspended over the grease-lined well of a Linbro plate (Hampton Research) containing 1 mL of precipitant solution.

Crystals of native pat17 grew within two weeks to a maximum size of 0.1 mm x 0.1 mm x 0.05 mm and once grown, were soaked for 24 h in a solution containing 1.3 µM MAFP, 0.1M sodium acetate (pH 4.6), 49% (v/v) polyethylene glycol-400 and 225 mM cesium chloride prior to being harvested and flash-froozen in liquid nitrogen. Diffraction data were collected at the Advanced Photon Source (beamline 21-ID-G; Argonne, IL) using a Mar-300 CCD at -180 ºC with a crystal-detector distance of 250 mm. 200 degrees of data (0.5º step size; 1 sec exposure) were collected at a wavelength of 0.97856 Å to a resolution of 2.09 Å (see table 1 for detailed data collection and refinement statistics). The resulting data were processed using the HKL2000 suite (Otwinowski *et al*., 1997). Analysis of the diffraction data revealed the crystals to be in space group $P4_32_12$ (a = b = 53.24 Å, c = 245.01 Å; $\alpha = \beta = \gamma = 90°$). The crystal's Matthew's coefficient and approximate solvent content were calculated in CCP4.

The structures of DFP and MAFP-inhibited pat17 were phased via molecular replacement with Phaser (McCoy *et* al., 2007) using the structure of native patatin (PDB ID 1OXW) as the search model. The resulting structures were refined further in the Crystallography and NMR System (CNS) (Brunger *et al*., 1998) via an initial round of rigid body refinement followed by

subsequent rounds of simulated annealing to 2500 K (step time of 0.5 fs per step) followed by cooling to room temperature (300 K) in 25 K steps. Following the initial round of rigid-body refinement, each of the structures was analyzed in O ver 12 (Jones *et al*., 1991) to verify the existence of adducts on the active site Ser77 residues.

The structure (along with their associated CNS parameter and topology files) for monoisopropylphosphoryl-serine (MIS) was downloaded from the Hetero-compound Information Centre (HIC-UP; Kleywegt and Jones, 1998). The structure of MAFP-bound serine (MAY) was taken from the structure of fatty acid amide hydrolase adducted to unaged MAFP (PDB ID 1MT5). The Dundee PRODRG2 server (Schuettelkopf and van Aalten, 2004) was used to generate the CNS parameter and topology files for MAY. These OP-bound serines were used to build the DFP and MAFP adducts into the visible adduct electron densities following three initial rounds of simulated annealing followed by fitting of the protein structures. Following further rounds of refinement and fitting, the DFP-inhibited and aged pat17 structure was refined to a maximum resolution of 2.6 Å while the MAFP-inhibited structure was refined to a resolution of 2.09 Å (Table 1).

Each of the refined structures was analyzed using PROCHECK (Laskowski *et al*., 1993). Analysis of each structure's Ramanchandran plot revealed that all residues were in the allowed conformations (Figure 4.6). The final pat17 structures were visualized in PyMOL (Delano Scientific, San Carlos, CA).

Pat17 Inhibition

The inhibitory potencies of DFP and MAFP against pat17 were assessed spectrophotometrically as the rate of phenyl valerate hydrolase activity. The rate of phenyl valerate hydrolysis by pat17 was verified to be linear with time and enzyme concentration prior to undertaking the inhibition assays. The spectrophotometric assays were performed as described previously for NTE by Randall *et al*. (1997). Following dilution of pat17 in 10 mM Tris-HCl (pH 7.4 at 21 °C) to a dilution where the uninhibited pat17 activity yields a reading of less than 1 absorbance unit at 37 °C, 40 µL of the diluted pat17 was titrated with varying concentrations of inhibitor (DFP or MAFP; 10 µL inhibitor dissolved in DMSO with total DMSO < 1% (v/v). Following an incubation period of 20 min at 37 °C, 100 µL of the substrate (5.26 mM PV/DMF/0.03% (v/v) Triton X-100) was added to the homogenate and allowed to incubate for 20 min at 37 °C. The reaction was stopped by the addition of 100 µL 1.23 mM 4-aminoantipyrine (4-AAP) in 9.5 mg/mL sodium dodecyl sulfate (SDS) after which the color was developed via the addition of 50 µL 2.1 mM potassium ferricyanide. The chromophore was allowed to develop for

5 min and read at 486 nm on a SpectraMax plate reader (Molecular devices, Sunnyvale, CA). The IC_{50}s of MAFP and DFP against pat17 were determined via linear regression; -log([inhibitor]) was plotted against % inhibition. The resulting linear regression equation was used to calculate the [DFP] and [MAFP] at which 50% inhibition was obtained. All inhibition studies were repeated three times.

Aging

Aging of patatin in the presence of DFP and MAFP was assessed in 50 mM Tris-HCl buffer (pH 7.4 at 21 ºC) as described earlier by Kropp *et al.* (2004). Pat17 was inhibited with either 4 mM DFP or 4 μM MAFP for 3 min at 37 °C after which each aliquot was diluted 1:2000 (v/v) with 50 mM Tris-HCl buffer (pH 7.4) to stop the inhibition reaction. The inhibited enzyme was allowed to age for timed intervals ranging from 0 to 20 min. Aliquots of inhibited enzyme solution were incubated with 2-PAM (final concentration 100 μM) for 20 min at 37 °C at the end of each time point. Following incubation with 2-PAM, the residual enzyme activity (*AR*) was measured. The residual activity of the enzyme in the absence of 2-PAM (*AI*) was assessed as the control (Kropp *et al.*, 2004). % Reactivation was calculated using the formula % reactivation = $[(AR_t - AI_t)/(AR_0 - AI_0)] \times 100$; where AR_T is the activity of reactivated enzyme at time = t; AI_T is the activity of the inhibited enzyme (without reactivation) at time = t. AR_0 is the activity of reactivated enzyme at time = 0 and AI_0 is the activity of the inhibited enzyme (without reactivation) at time = 0 (Richardson *et al*., 2009). All aging studies were repeated three times.

The apparent first-order rate constants of aging (k_4) for DFP and MAFP against pat17 were assessed via linear regression. % Reactivation versus time was plotted using linear regression such that $\ln(100/\%\text{ reactivation}) = k_4 \times t_{aging}$. The slope ($\beta_1$) of the linear regression was equal to the k_4 with the half-life of aging ($t_{1/2}$) being equal to $\ln(2)/k_4$ (Clothier *et al*., 1981; Jianmongkol *et al*., 1999).

Mass spectrometry of DFP-treated pat17

In order to verify the presence of an aged DFP adduct on pat17, surface-enhanced laser desorption/ionization-time of flight (SELDI-TOF) mass spectrometry (MS) was performed on pat17 treated with 1 mM DFP. Undiluted pat17 in 10 mM Tris-HCl (pH 7.4) was incubated for 20 min at 37 °C with 1 mM DFP while a control sample of undiluted pat17 was incubated with buffer alone. Following inhibition, the DFP-treated and control samples were diluted 1:1000 (v/v) in 50 mM ammonium bicarbonate (pH 8.0) to stop the inhibition. The DFP-inhibited pat17 was allowed to age for 20 min at 37 °C while the control sample was incubated at 37 °C for the same

time period. Following this, each sample underwent a buffer-exchange step using protein-desalting spin-columns (size-exclusion limit: 7,000 Da; Thermo Fisher Scientific, Rockford, IL) to remove any residual traces of DFP, which, if present, would inhibit the subsequent tryptic-digestion step.

Tryptic digestions of the protein samples were performed as described earlier by Doorn *et al*. (2001a). Acetonitrile was added to each sample to a final concentration of 10% (v/v). Subsequently, trypsin in 50 mM acetic acid (0.4 μg/μl) was added to each sample (1 μg trypsin per 40 μg protein), following which, the samples were incubated for 14 hours at 37°C to allow the tryptic digestion to proceed (Doorn *et al*., 2001a; Kropp *et al.*, 2004).

Prediction of the active site peptide's mass was performed using pat17's primary sequence obtained from the PDB (PDB ID 1oxw). The average mass of pat17's tryptic digest fragments was predicted using the MS-Digest feature in ProteinProspector ver. 5.2.2 (http://prospector.ucsf.edu/) (ProteinProspector, 2009) as described earlier by Kropp *et al*. (2004). Adduction of the active site serine with DFP was expected to result in positive average *m/z* (for the MH+ ions) shifts in the active site-containing fragment (LADYFDVIGGTSTGGLLTAMISTPNENNRPFAAAK; *m/z* (unoxidized methionine)=3615.08; *m/z* (oxidized methionine)=3631.08) corresponding to the average mass of the DFP adduct, taking into account the loss of a proton from the serine hydroxyl group.

SELDI-TOF MS was utilized to analyze adduction of DFP to pat17's active site Ser77. SELDI analysis was undertaken as described earlier by Doorn *et* al. (2001a) wherein 1 μL of each peptide mixture (DFP-treated and control) was mixed on a H4 Protein Chip® (Ciphergen Biosystems, Inc., Fremont, CA) with 1 μL of a 50% (v/v) acetonitrile/50% (v/v) 1% trifluoroacetic acid (w/v) solution saturated with α-cyano-4-hydroxycinnamic acid. The samples were air dried and permitted to crystallize on the chip following which the chip was inserted into the SELDI instrument.

Mass spectra were collected using a PBS-IIc SELDI-TOF-MS instrument (Ciphergen Biosystems, Inc., Fremont, CA). Data from approximately 100-150 laser shots were collected and averaged to yield the final spectrum. A seven-point external calibration of the MS instrument was undertaken prior to each run using commercially available protein standards (Ciphergen Biosystems, Inc., Fremont, CA). Peaks corresponding to the predicted *m/z* MH^+ values of active site peptide fragment and adducts were identified. The spectra analyzed using the Ciphergen ProteinChip software (ver. 3.2.1) (Ciphergen Biosystems, Inc., Fremont, CA). Peak coverage, defined as: 100 x (Number of observed peaks that were predicted) / (Number of predicted peaks) was determined manually using the *m/z* values list of predicted tryptic digest fragments obtained

from Protein Prospector. Peaks corresponding to modified variants of the same peptide fragment (e.g. peptide fragments with an oxidized methionine vs. its reduced counterpart) were counted as a single entity.

Results and discussion

Patatin is inhibited by DFP and MAFP

Currently, very little is known about the inhibitory potential of OPs such as DFP and MAFP against patatin. As seen in figure 4.2, our investigations with DFP (Figure 4.2a) and MAFP (Figure 4.2c) revealed that DFP is capable of inhibiting pat17 with a 20-minute IC_{50} of 181 μM (Figure 4.2a). In addition to this, the first order rate constant of aging (k_4) was determined to be 0.061 min^{-1} with the half-life of aging ($t_{1/2\ aging}$) equal to 11.4 min (Figure 4.2b). With respect to MAFP, it was found that the 20-minute IC_{50} of MAFP against pat17 is 116 nM (Figure 4.2c). Analysis of the potential of MAFP to age on patatin revealed complete reactivation at the highest time point (20 min), thereby indicating that unlike DFP, MAFP does not age on patatin (Figure 4.2d). The inability of MAFP to age on pat17 is an interesting finding since, being a phosphonate, it would be expected to age. The results from our enzymology work, when taken along with the findings from x-ray crystallography suggests that aging of MAFP's O-methyl alkyl moiety does not take place. One possible explanation for this apparent lack of aging could be due to the fact that we used a racemic mixture of MAFP. It is possible that the MAFP enantiomers possess different inhibitory potencies and the one with a higher inhibitory potency is less likely to undergo aging (presumably due to steric hindrances). This finding represents an area where further research is needed before a conclusive statement can be made regarding the potential of MAFP to age on patatin.

The potential for DFP to age in pat17 was confirmed via the use of SELDI-TOF MS (Figure 4.3). Based on identification of visible peaks, peak coverage was calculated to be 72%. Analysis of the control (uninhibited) and DFP-treated samples revealed the presence of the active site-Ser77 containing fragment at 3616.5 Da, thereby indicating the presence of an unoxidized methionine in this tryptic-digest fragment. Furthermore, two additional peaks, at 3738.9 Da and 3781.3 Da were visible on the DFP-treated sample. These peaks correspond to the expected mass-shifts associated with the presence of the unaged (observed, 3781.3 Da; expected, 3781.7 Da) and aged (observed, 3738.9 Da; expected, 3738.6 Da) DFP adducts. Therefore, these results confirm the findings from the enzymology work, which indicated that the neuropathic OP DFP could undergo aging following its inhibition of pat17.

The overall structure of patatin is a modified α/β hydrolase fold with a Ser77-Asp215 catalytic dyad

As seen in figure 4.4, the overall patatin structure consists of 8 β-strands and 13 α-helices arranged, as described earlier by Rydel *et al.* (2003), in a modified α/β hydrolase fold with a central 6-stranded β-sheet (consisting of five parallel strands and one anti-parallel strand) sandwiched in the front and back by α-helices. This is in contrast to the canonical α/β hydrolase fold that contains a central 8-stranded β-sheet sandwiched between α-helices.

Analysis of patatin's active site revealed that it to contain a Ser77 and Asp215 dyad as described earlier by Rydel *et al*. (2003). This catalytic dyad is located in a 153.6 $Å^3$ chamber at the end of a 9 Å gorge formed by Ala190, Pro191, Ala 217, Val218, Gln288, Thr291 and Asp292. A second 15 Å gorge is formed by Gly37, Arg40, Gly261, Thr262, Lys 289, Asp 292, Ala293 and Met331 was also visible in the structure. The catalytic Ser77 residue is found within the classic G-X-S-X-G lipase motif (Schrag and Cygler, 1997). Pat17's catalytic dyad is expected to function with Asp215 acting as a general base whose Oδ2 activates the Ser77 Oγ by abstracting its proton, thereby turning Ser77 into a potent nucleophile prior to its attack on the substrate (see Figure 4.1a for a detailed explanation of this process). This is a similar mechanism to those that have been proposed for functioning of $CPLA_2$'s active site dyad (PDB ID 1cjy) (Dessen *et al.,* 1999) and the predicted Ser966-Asp1086 dyad in NTE (Wijeyesakere *et al*., 2007). In contrast, the 'traditional' serine proteases (such as chymotrypsin) and serine esterases (such as acetylcholinesterase) possess ser-his-asp/glu triads (Zhang *et al*., 2002; Zhu *et al*., 2005). In a manner characteristic of serine hydrolases, the catalytic Ser77 nucleophile is located on a loop (termed the 'nucleophilic elbow') formed by β2 and α3.

Analysis of the OP adducts seen on pat17

As detailed in Table 1, crystals of DFP-inhibited pat17 grew within two weeks and diffracted to a maximum resolution of 2.6 Å at a wavelength of 0.97626 Å with an overall $\langle I/\sigma(I)\rangle$ of 20. The structure of pat17 inhibited and aged with DFP was solved in space-group $P4_32_12$ (a = b = 52.99Å, c = 242.77Å; α = β = γ = 90°) with a Matthew's coefficient of 2.1 indicating a solvent content of 41.6%. The data revealed the presence of a single pat17 molecule in the asymmetric unit along with 52 water molecules.

Similarly, as detailed in Table 1, crystals of pat17 soaked with MAFP diffracted to a maximum resolution of 2.09 Å at a wavelength of 0.97856 Å with an overall $\langle I/\sigma(I)\rangle$ of 20. The structure of MAFP-inhibited pat17 was solved in space-group $P4_32_12$ (a = b = 53.24 Å, c =

245.01 Å; α = β = γ = 90°) with a Matthew's coefficient of 2.12, indicating the presence of a single pa17 molecule in the asymmetric unit and a solvent content of 41.9%.

Initial analysis of the difference (F_o-F_c) maps of the DFP- and MAFP-inhibited structures indicated the presence of adducts (visible at 3σ) on the Ser77 nucleophile (Figure 4.5a and 4.5b). These were visible to a contour level of 6σ. Following further rounds of refinement of the pat17 structures via simulated annealing, these adducts were seen to be the aged DFP (Figure 4.5c) and unaged MAFP (Figure. 4.5d) moieties bound to pat17's catalytic Ser77 residue. The final R-factor for our DFP-inhibited and aged pat17 structure (90% of the data) was 21.09% with a free-R factor (10% of the data) of 28.47%, while the final R-factor for our MAFP-inhibited pat17 structure (90% of the data) was 19.88% with a free R-factor (10% of the data) of 23.66%.

Analysis of the Ramachandran plots for our final DFP and MAFP-treated crystal structures revealed that none of the residues possessed dihedral angles in a disallowed conformation (Figure 4.6). Analysis of the final DFP-pat17 structure revealed that 99.1% of residues were in the most favored and allowed regions (84.1% in the most favored regions with 15% in the allowed regions) while 0.9 % of residues were in the generously allowed region (Figure 4.6a). Analysis of the MAFP-pat17 structure also revealed that 99.1% of residues were in the most favored and allowed regions (88.7% in the most favored regions with 10.4% in the allowed regions) while 0.9 % of residues were in the generously allowed region (Figure 4.6b).

Our DFP-aged structure revealed that DFP's negatively charged phosphoryl oxygen moiety was stabilized by the oxyanion hole with the negatively charged oxygen located 3.3 Å from Gly37's backbone nitrogen. In addition to this, a water molecule is seen in close proximity to the aged DFP adduct (Figure 4.7). This water molecule is located 2.2 Å from Gly37's backbone nitrogen, 2.1 Å from DFP's negatively charged oxygen and 2.7 Å from the its phosphorus atom. This water appears to assist in the stabilization of the DFP adduct and may have a role in catalyzing the aging reaction, wherein the DFP adduct loses one of its alkyl side chains, thereby gaining its net negative charge. While this distance may appear to be small for a hydrogen bond, hydrogen bond lengths as short as 2 Å have been reported in the active site of the serine protease trypsin (Katz *et al*., 2002). However, due to the resolution of the DFP-aged pat17 structure (2.6 Å), it would be unwise to read too much into the location of this water molecule until a higher resolution structure is available.

Analysis of our MAFP-inhibited pat17 structure showed that MAFP's phosphoryl oxygen is stabilized by the backbone nitrogens in Gly37 and Gly38, which form a part of the protein's oxyanion hole (Figure 4.8). In addition to this, Asp215's Oδ2 was located 3.2 Å away from Ser77's Oγ. It was also found that MAFP's acyl side chain is contained within pat17's active site

chamber that is formed by Phe114, Ala188, Ala189, Ala190, Tyr193, Phe194, Ala217, Ala222, Thr260, Thr262, Gln288, Lys289, Thr329, Glu330 and Met331.

Interestingly, regions of density for MAFP's acyl chain were seen within pat17's 15 Å gorge that is relatively hydrophilic as it contains one amino acid (Met331) that is hydrophobic, 3 neutral residues (Gly37, Gly261 and Ala293) and 4 hydrophilic residues (Arg40, Thr262, Lys 289 and Asp 292). Contact distances between the twenty carbon atoms in MAFP's acyl side chain and their neighbor atoms in the greater pat17 structure are listed in Table 2. As can be seen, of the 47 contact distances listed in Table 2, 20 (43%) are made to hydrophobic atoms while the remaining 27 (57%) contacts are to hydrophilic atoms, thereby suggesting that it is possible for this hydrophobic acyl chain could be accommodated in this gorge. However, given that the electron density was not visible for certain regions of MAFP's acyl side chain (Figure 4.5d), as well as the fact that the MAFP enantiomers used in this study were unresolved, there is always the possibility that MAFP's acyl side-chain could take on different conformations within the active site chamber. Moreover, the increased hydrophobicity of MAFP (due to the presence of a 20-carbon atom acyl chain), could explain its increased potency against pat17. This is because patatin, as a lipid acyl hydrolase (Hirayama *et al*., 1975), would be expected to have an affinity for hydrophobic fatty acid chains. This suggests that OPs with increasingly hydrophobic side chains would have an increased inhibitory potency against patatin. This finding is similar to results reported by Paul Glynn and colleagues on inhibition of NTE's esterase domain (NEST) by MAFP wherein a 20-minute IC_{50} of 2 nM was reported (van Tienhoven *et al*., 2002). This can be compared to DFP's 20-minute IC_{50} (calculated from its bimolecular rate constant of 17,200 $M^{-1}min^{-1}$) against NEST of 2 μM (Kropp *et al*., 2004). Further to this, given's patatin's role as a lipid acyl hydrolase (Hirayama *et al*., 1975), the ability to accommodate long acyl chains within the active site chamber would be of potential value during the catalysis of phospholipids, as it would allow for the accommodation of one of the phospholipid substrate's fatty acid chains while the active site dyad catalyzes the hydrolysis of the second fatty acid chain.

There are no significantly visible global conformational changes associated with either inhibition or aging

Comparison of our DFP inhibited and aged structure of pat17; along with our MAFP inhibited pat17 structure to the previously published native pat17 structure (PDB ID 1OXW) showed Cα backbone root mean square deviations of 0.98 Å (DFP-inhibited and aged vs. native) and 1.07 Å (MAFP-inhibited vs. native) (Figure 4.8). These findings revealed that there are no significant global conformational changes associated with inhibition and aging of OPs on pat17.

When compared to published research on acetylcholinesterase (AChE) by Hurley *et al*. (2004), who reported a net-RMSD of 1.2 Å associated with *in silico* inhibition (but not aging) of AChE by the nerve-agent VX, these results support the notion that interactions between serine hydrolases and OPs do not results in large conformational changes. With respect to aging, results published by Millard and colleagues on the x-ray crystal structures of *Torpedo Calfornica* AChE inhibited and aged by DFP, sarin and soman (PDB IDs 2dfp, 1cfj and 1som respectively) reported no significant global conformational changes in the overall structure of the enzyme (although localized conformational changes in AChE's acyl pocket were reported) (Millard *et al*., 1999), a result consistent with our findings (in that no global conformational changes were visible in pat17).

Similarly, analysis of the crystal structure of native human butyrylcholinesterase (BChE; PDB ID 1p0i) with its DFP- and echothiophate-aged forms (PDB ID 1xlu and 1xlv respectively) shows no evidence for a global conformational change associated with aging of an OP. The Cα RMSDs for the DFP- and echothiophate-aged forms of BChE relative to the native form of this enzyme are 0.51 Å (DFP-aged vs. native) and 0.55 Å (echothiophate-aged vs. native). These findings, when taken together with the lack of global conformational changes in AChE (Millard *et al*., 1999) and pat17 following aging of an OP, serve to strengthen the argument against the presence of a global conformational change in the tertiary structure of NTE following its inhibition and aging by a neuropathic OP.

When considering our initial hypothesis and the 'toxic gain-of-function model' for the pathogenesis of OPIDN, our results were found to not support such a mechanism. These results also serves to cast doubt upon the association between a hypothesized conformational change in NTE and the progression to the delayed axonopathy that is characteristic of OPIDN. While lack of knowledge regarding the mechanism whereby the aged NTE molecule and the progression to OPIDN had initially prompted the hypothesis that a conformational change may occur with aging of the OP adduct that is distinct from the inhibited state, our work with patatin, a protein homologous to NTE's catalytic domain, has shown that the degree of conformational change due to inhibition and aging was non-significant and similar to published results for other α/β hydrolases such as AChE (Millard *et al.*, 1999). Therefore, because it is postulated that form follows function (and vice versa), it would be logical to conclude that NTE's hypothesized toxic-gain-of-function, in the absence of any structural changes, would be unprecedented and highly unlikely. These findings highlight the need for a new model to explain the pathogenesis of OPIDN.

One possible mechanism for the progression from inhibition and aging to disease could be that once aged, the NTE molecule is inhibited permanently. Therefore, perturbation of NTE's normal physiological role as a lysophospholipase could lead to cellular dysfunction and damage. However, a conclusive mechanism for the pathogenesis of OPIDN at a molecular level is an area for future research, as it requires a more complete understanding of NTE's true physiological role within the cell.

A potential limitation of this study, at least with respect top extrapolating these findings to NTE and OPIDN, is that this work was undertaken on a NTE-homologue and not full-length NTE. Therefore, there is the remote possibility that, while patatin undergoes a negligible conformational change with aging, a larger change could potentially be seen in NTE, leading to OPIDN. Another possibility is that inhibition and aging perturbs NTE's normal physiological function, a possibility that is explored in more detail in chapter 5. Therefore, the results and conclusions of this investigation highlight the need for further experimental research into NTE's structure and physiological function.

Table 1: Crystallographic data collection and refinement statistics.

Crystallography Data Collection and Refinement Statistics		
Data Collection Statistics		
Data Set	Patatin 17 + DFP (aged)	Patatin 17 + MAFP (inhibited)
Space group	$P4_32_12$	$P4_32_12$
Unit Cell (Å, °)	a = b = 52.99; c = 242.77 $\alpha = \beta = \gamma = 90$	a = b = 53.24; c = 245.01 $\alpha = \beta = \gamma = 90$
Wavelength (Å)	0.97626	0.97856
Resolution (Å)	50.0 - 2.6	50.0 - 2.09
R_{sym} (%) [1,2]	5.3 (41.7)	5.6 (10.4)
$\langle I/\sigma I \rangle$ [3]	20 (3)	20(20)
Completeness (%) [4]	95.3 (87.8)	99.0 (99.7)
Redundancy	6.4 (5.6)	4.6 (5.0)
Refinement Statistics		
Resolution (Å)	2.60	2.09
R-Factor (%) [5]	21.09	19.88
R_{free} (%) [6]	28.47	23.66
Water Molecules	52	138
Unique Reflections	10474	21756
R.m.s.d. [7]		
Bonds	0.65	0.01
Angles	1.33	1.15

[1] Statistics for highest resolution bin of reflections in parentheses.
[2] $R_{sym} = \Sigma_h \Sigma_j | I_{hj} - \langle I_h \rangle | / \Sigma_h \Sigma_j I_{hj}$, where I_{hj} is the intensity of observation j of reflection h and $\langle I_h \rangle$ is the mean intensity for multiply recorded reflections.
[3] Intensity signal-to-noise ratio.
[4] Completeness of the unique diffraction data.
[5] R-factor = $\Sigma_h | |F_o| - |F_c| | / \Sigma_h |F_o|$, where F_o and F_c are the observed and calculated structure factor amplitudes for reflection h.
[6] R_{free} is calculated against a 10% random sampling of the reflections that were removed before structure refinement.
[7] Root mean square deviation of bond lengths and bond angles.

Table 2: Contact distances between MAFP's acyl (AA) side chain and atoms in Pat17's tunnel.

Contact Distances Between MAFP's Acyl Chain and Neighbor Atoms in Pat17's Tunnel

MAFP AA side chain atom [1]	Neighbor atom	Distance (Å)	Hydrophobic (+/-) [2]
C1	Asp215OD2	2.7	-
	Asp215CG	3.2	-
	Met331CE	3.2	+
C2	Asp215OD1	3.0	-
	Asp215OD2	3.0	-
	Asp215CG	3.3	-
C3	Gly37N	3.2	-
C4	Asp292CG	3.5	-
	Asp292OD1	3.0	-
C5	Gly36CA	3.4	+
	Gly36C	3.1	+
	Gly36O	3.2	-
	Asp292OD1	3.3	-
	Ala222CB	3.3	+
C6	Gly36C	3.2	+
	Gly36O	3.1	-
	Gly37N	3.4	-
	Gly37CA	3.4	+
	Asp292OD1	3.3	-
C7	Gly37CA	3.4	+
	Asp292OD1	2.8	-
C8	Asp292OD1	2.9	-
	Asp292CG	3.4	-
	Asp292CB	3.2	+
C9	Arg40NH1	3.1	-
C10	Arg40NH2	3.3	-
	Lys289CA	3.5	+
	Lys289CB	3.5	+
	Lys289CG	3.3	+
C11	Arg40NH1	3.1	-
	Arg40NH2	3.3	-
C12	Lys289O	2.9	-
C13	Lys289O	3.5	-
C14	Ala293CB	3.5	+
C15	Thr262CA	3.1	+
	Thr262C	3.4	+
	Thr263N	2.9	-
C16	Thr263N	3.3	-
	Thr263CG2	3.2	+
C17	Leu324CD1	3.4	+
C18	Thr329O	3.0	-
	Arg40NH1	2.9	-
	Arg40CZ	3.3	+
C19	Thr329O	2.7	-
C20	Lys289CB	2.9	+
	Lys289CG	2.9	+
	Lys289CD	2.7	+

[1] Name of atom in MAFP's 20-carbon atom acyl side-chain.
[2] A plus (+) sign designates a contact made to a hydrophobic atom, while a minus (-) sign represents a contact made to a hydrophilic atoms.

Figure 4.1: Analysis of NTE's catalytic mechanism. The interaction between NTE and a carboxylic acid ester (such as phenyl valerate, the substrate used to measure NTE's activity) is contrasted with its interactions with a neuropathic and non-neuropathic OP. (a) Interaction between NTE and a carboxylic acid ester. Asp1086 (not shown) acts as a general base and activates the Ser966 nucleophile by abstracting its hydrogen. The activated Ser966 (shown as -OH) undertakes a nucleophilic attack on the substrate's acyl carbon forming a tetrahedral intermediate whose negative charge is stabilized by NTE's oxyanion hole (not shown). The net loss of the R-group results in acylation of the enzyme and the formation of an acyl-enzyme intermediate at which stage the enzyme is effectively inhibited and cannot attack another substrate molecule. In the case of a carboxylic acid ester, the acyl-enzyme intermediate is deacylated rapidly via hydrolysis (passing through another tetrahedral intermediate state) to release the carboxylic acid moiety and regenerate the enzyme, allowing it to attack another substrate molecule. While this portion of the figure depicts the mechanism of hydrolysis for NTE, it is important to note that this is the expected mechanism for catalysis of a carboxylic acid ester by any serine hydrolase that has employs a Ser-Asp catalytic dyad. (b) In the case of a neuropathic OP (such as a phosphonate (shown as R-P(O)-OR)), the process of formation of the organophosphorylated intermediate (at which time the enzyme is inhibited) is nearly identical to that seen with a carboxylic acid ester except for the fact that the rate of hydrolysis of the organophosphorylated intermediate is very slow. Once organophosphorylated with a neuropathic OP, the OP adduct can undergo a secondary reaction called aging involving the net loss of an alkyl side chain (via either an S_N1 or S_N2 mechanism) and becomes irreversibly bound to the enzyme. It is currently thought that this aged NTE state, through some unknown process, is the initiating factor in developing OPIDN. (c) On the other hand, a non-neuropathic NTE inhibitor such as a phosphinate (shown as R-P(O)-R) also inhibits NTE in a manner identical to a neuropathic OP but is unable to undergo the aging reaction. Therefore, these compounds are unable to initiate OPIDN and pre-dosing animals with non-neuropathic NTE inhibitors has been shown to have a protective effect against a subsequent exposure to a dose of a neuropathic OP that would produce OPIDN in naïve animals (Johnson, 1990). Further to this, it is important to state that in the even in the case of a non-neuropathic NTE inhibitor, the rate of hydrolysis of the organophosphorylated enzyme, while measurable, is extremely slow except in the presence of strong nucleophiles such as KF.

A.

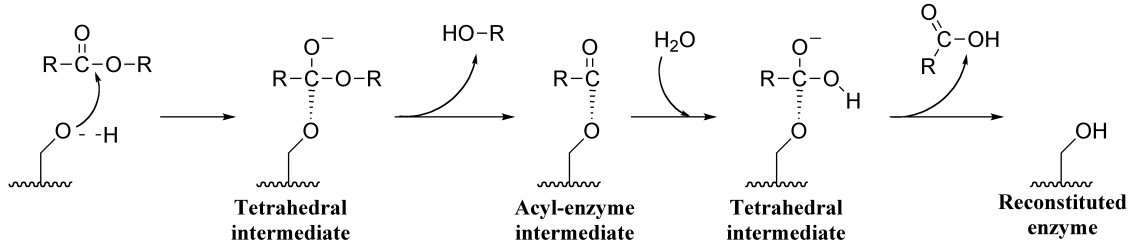
HO–R
H2O
Tetrahedral intermediate
Acyl-enzyme intermediate
Tetrahedral intermediate
Reconstituted enzyme

B.

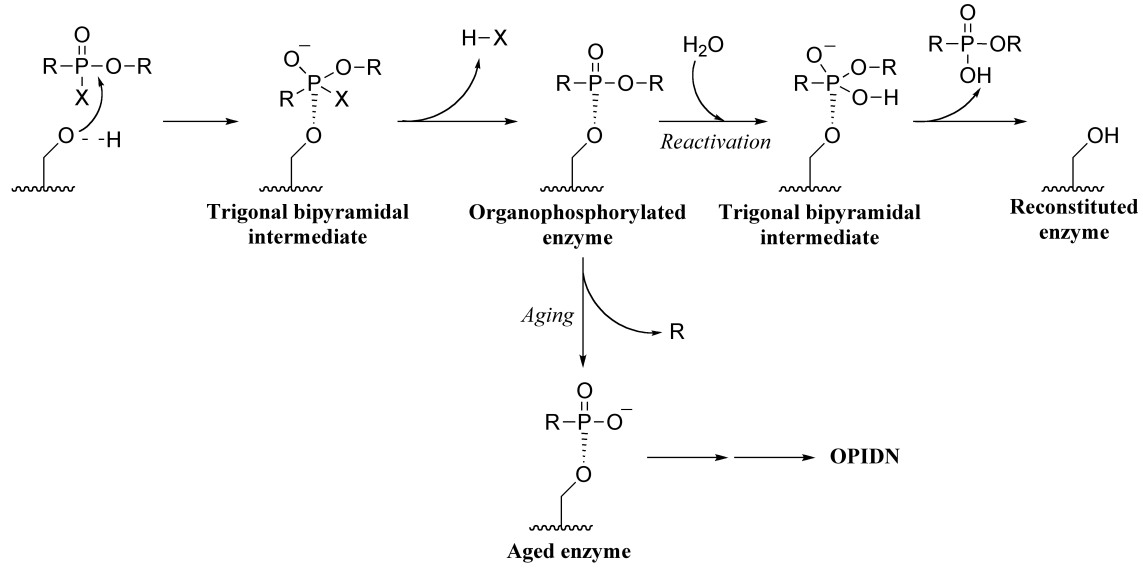
H–X
H2O
Reactivation
Trigonal bipyramidal intermediate
Organophosphorylated enzyme
Trigonal bipyramidal intermediate
Reconstituted enzyme
Aging
R
OPIDN
Aged enzyme

C.

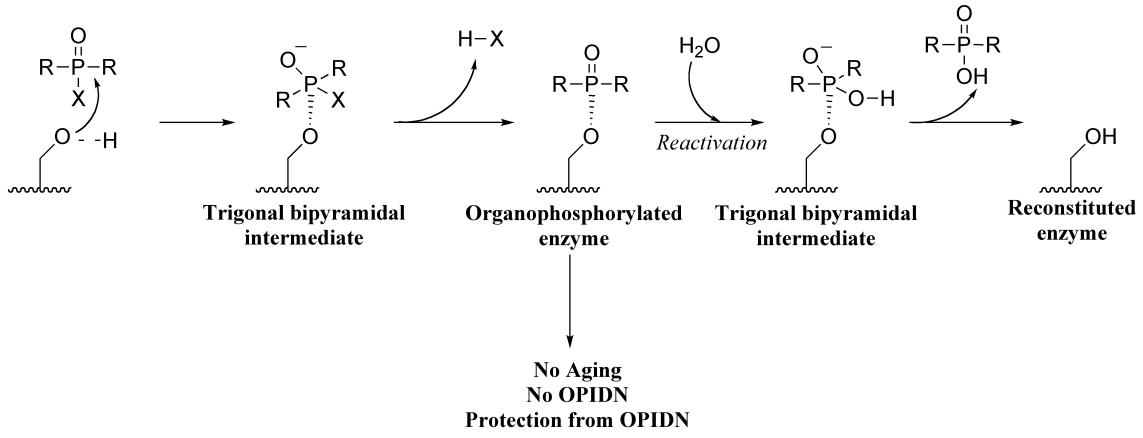
H–X
H2O
Reactivation
Trigonal bipyramidal intermediate
Organophosphorylated enzyme
Trigonal bipyramidal intermediate
Reconstituted enzyme
No Aging
No OPIDN
Protection from OPIDN

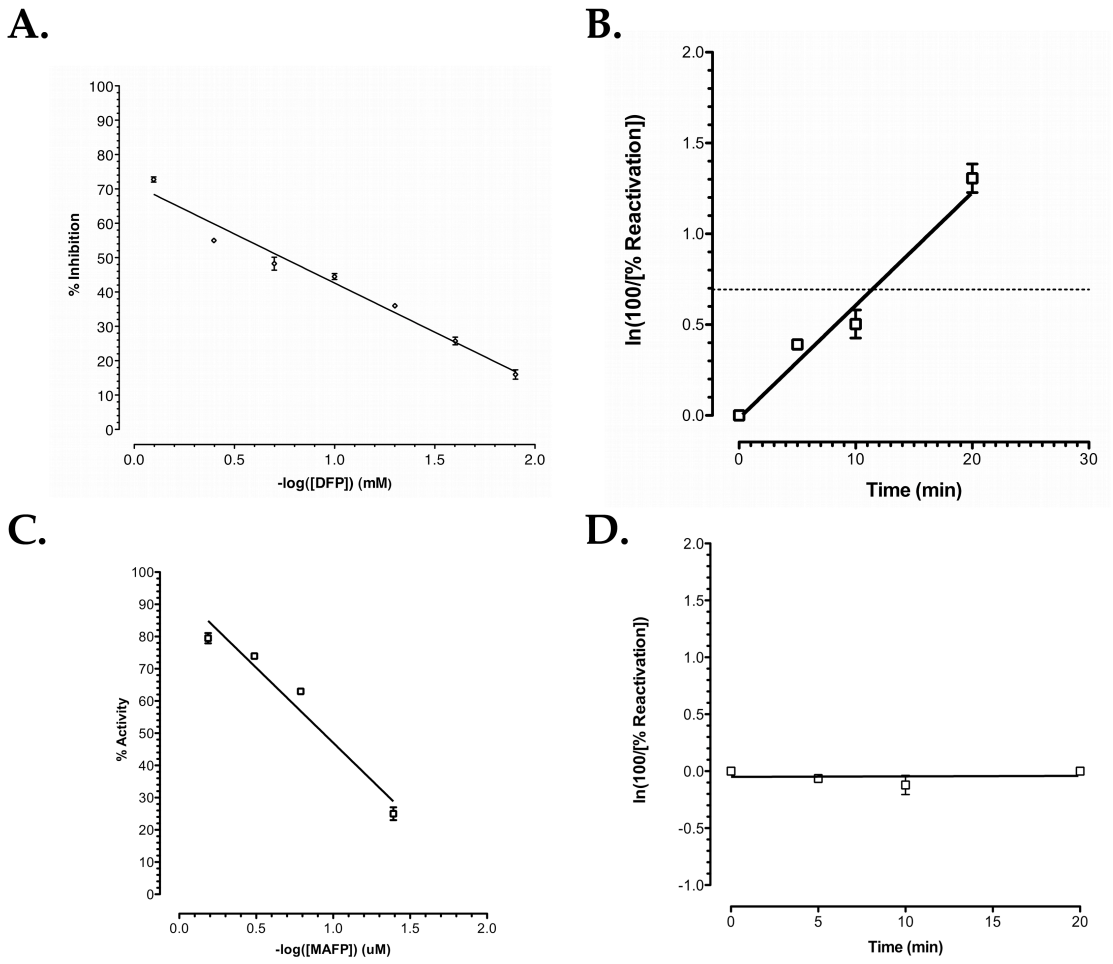

Figure 4.2: Pat17 enzymology. (a) Pat17-DFP 20-minute IC_{50} curve. As can be seen, the 20-minute IC_{50} for DFP against pat17 is 181 µM. (b) Aging of DFP on patatin. The k_4 for the aging of DFP on patatin was calculated to be 0.061 min^{-1} with a half-life of aging ($t_{1/2\ aging}$) equal to 11.4 min. (c) Inhibition and aging of pat17 by MAFP. The Pat17-MAFP 20-minute IC_{50} curve indicates that the 20-minute IC_{50} for MAFP against pat17 is 116 nM. (d) Unlike DFP, reactivation studies of MAFP against pat17 indicated complete reactivation at the highest time point (20 min); thereby indicating that MAFP is not able to undergo the aging reaction during this time period.

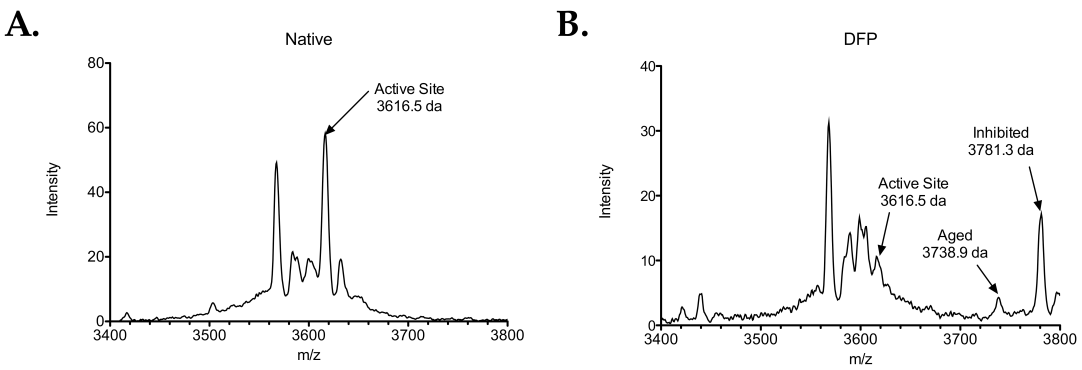

Figure 4.3: SELDI-TOF MS of pat17. Peaks correspond to the average masses of MH+ species. (a) Tryptic digest of native pat17. The active site peak can be seen at 3616.5 Da (expected, 3615.1 Da). (b) Tryptic digest of DFP-treated pat17. The intensity scales very between the native and DFP-treated spectra due to the fact that DFP is a potent inhibitor of the serine protease trypsin. Once again, the active site containing fragment can be seen at 3616.5 Da. Two additional peaks corresponding to the presence of unaged (3781.3 Da) and aged (3738.9 Da) DFP adducts are also visible.

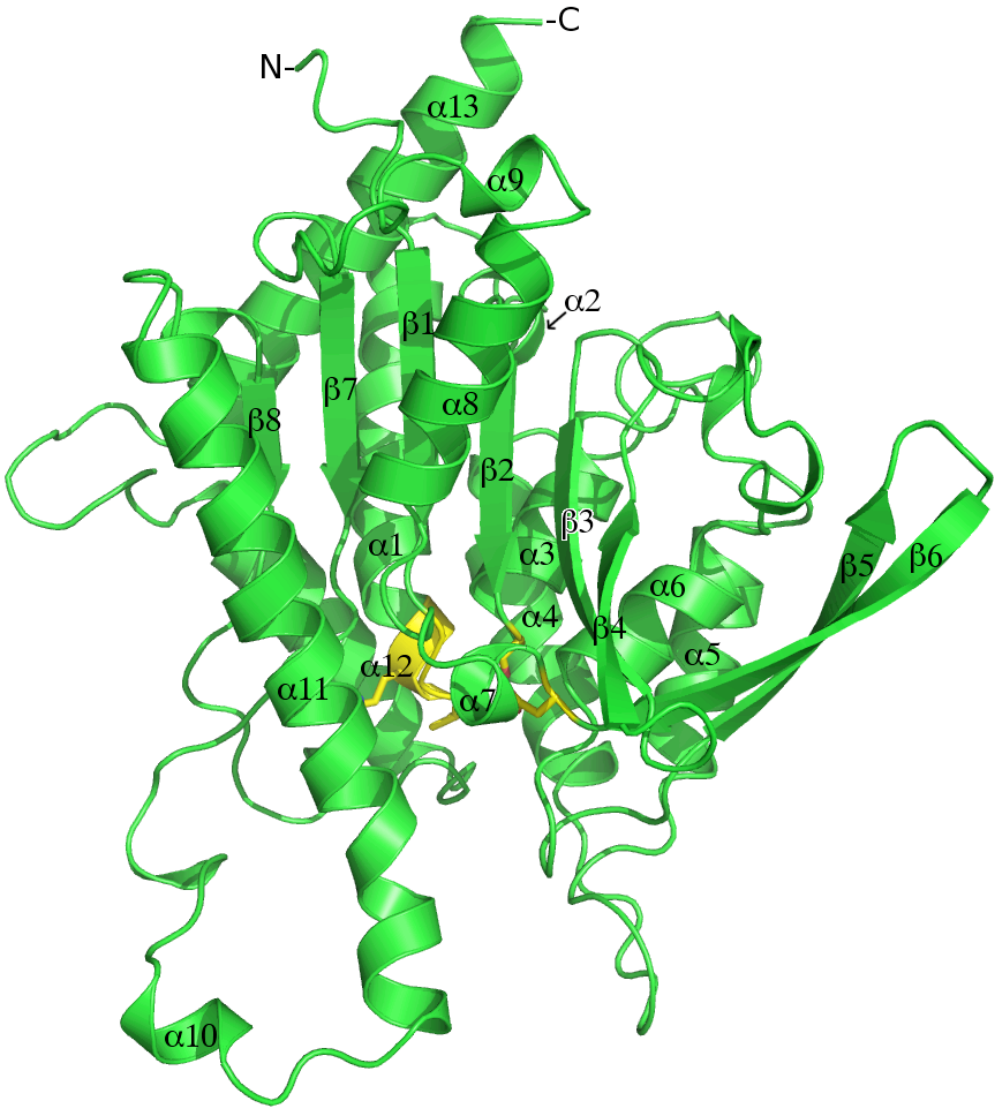

Figure 4.4: Overall view of pat17. As can be seen, pat17 consists of 8 β-strands and 13 α-helices. The protein belongs to a modified α/β hydrolase fold with a central β-sheet sandwiched by α-helices. The residues that form the oxyanion hole and active site dyad are shown in yellow.

Figure 4.5: Pat17 electron density maps. (Top row) Initial difference (F_o-F_c) maps contoured at 3σ (shown as a black mesh) showing the positive densities around (a) the DFP and (b) the MAFP adducts on pat17's catalytic Ser77. (Middle and bottom row) Electron density ($2F_o$-F_c) maps contoured at 1σ (shown as a black mesh) showing the visible electron densities around. Analysis of the initial difference maps revealed that the adduct densities were visible to 6σ (c) the aged DFP and (d) the unaged MAFP adducts on pat17's catalytic Ser77. The inability of MAFP to age was verified using kinetic measurements (see Figure 4.2d). The active site Ser77 and Asp215 residues are rendered as sticks with the following color scheme: yellow = carbon, blue = nitrogen and red = oxygen.

A.

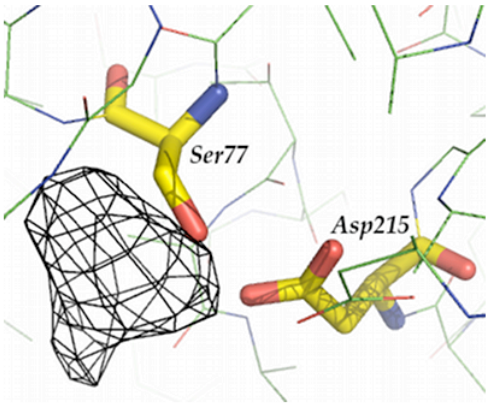

B.

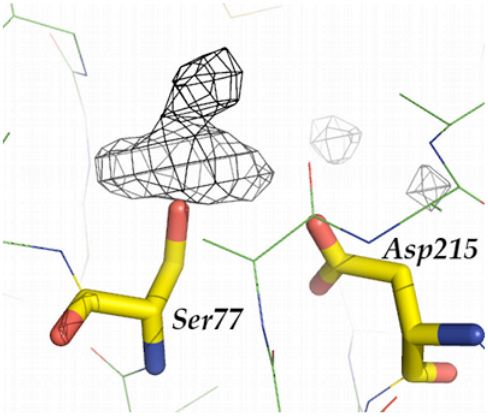

C.

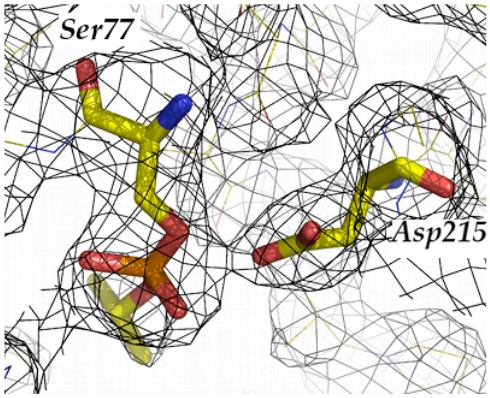

D.

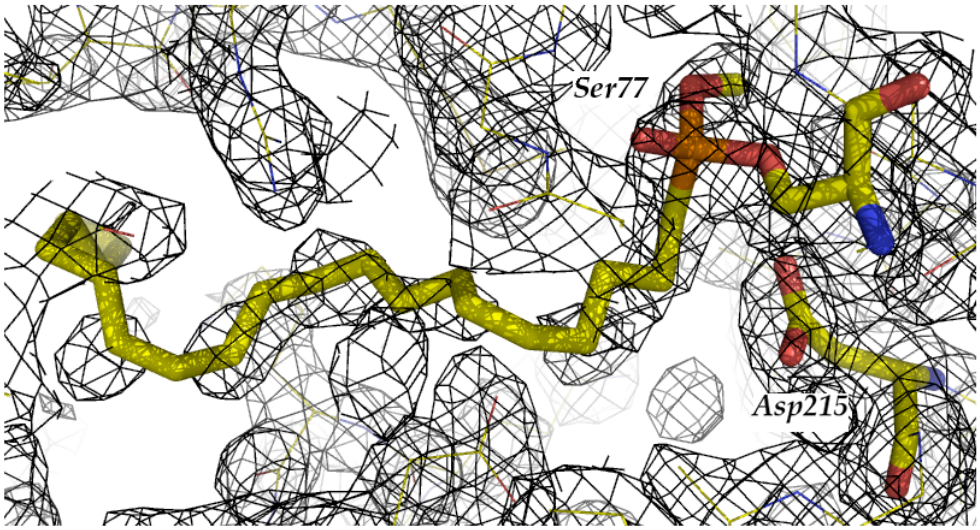

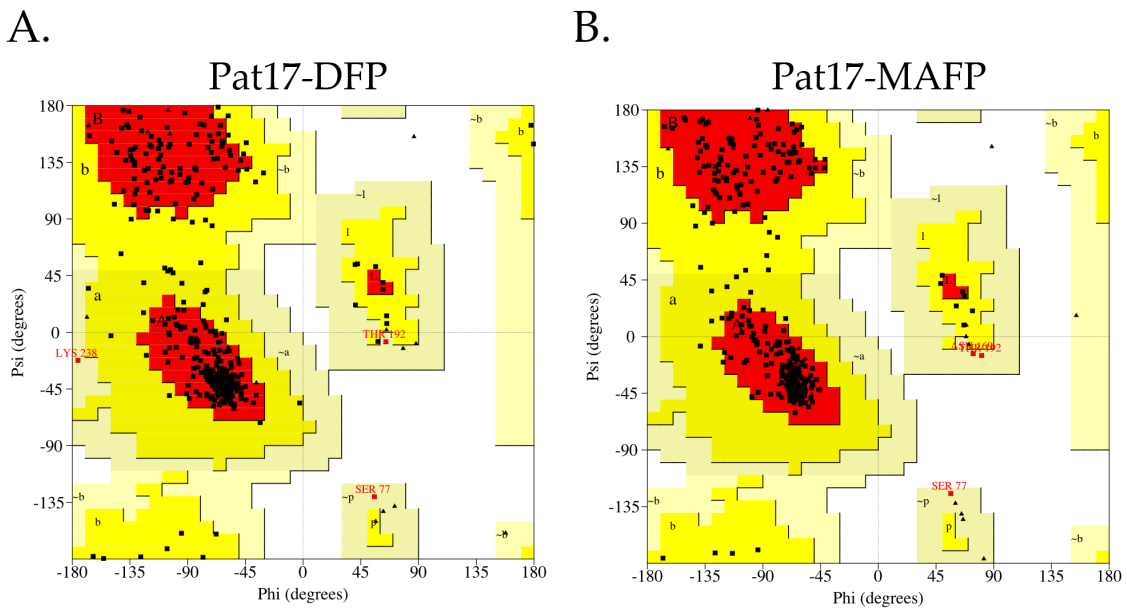

Figure 4.6: Pat17 Ramachandran plots. The plots depict the dihedral phi and psi angles for the final (a) DFP and (b) MAFP-treated pat17 crystal structures. Glycines are depicted as triangles (▲). Analysis of the final DFP-aged structure revealed that 99.1% of residues were in the most favored and allowed regions (84.1% in the most favored regions with 15% in the allowed regions) while 0.9 % of residues were in the generously allowed regions. Analysis of the MAFP-inhibited structure revealed that 99.1% of residues were in the most favored and allowed regions (88.7% in the most favored regions with 10.4% in the allowed regions) while 0.9 % of residues were in the generously allowed regions. No residues were seen to possess disallowed dihedral angles in either structure.

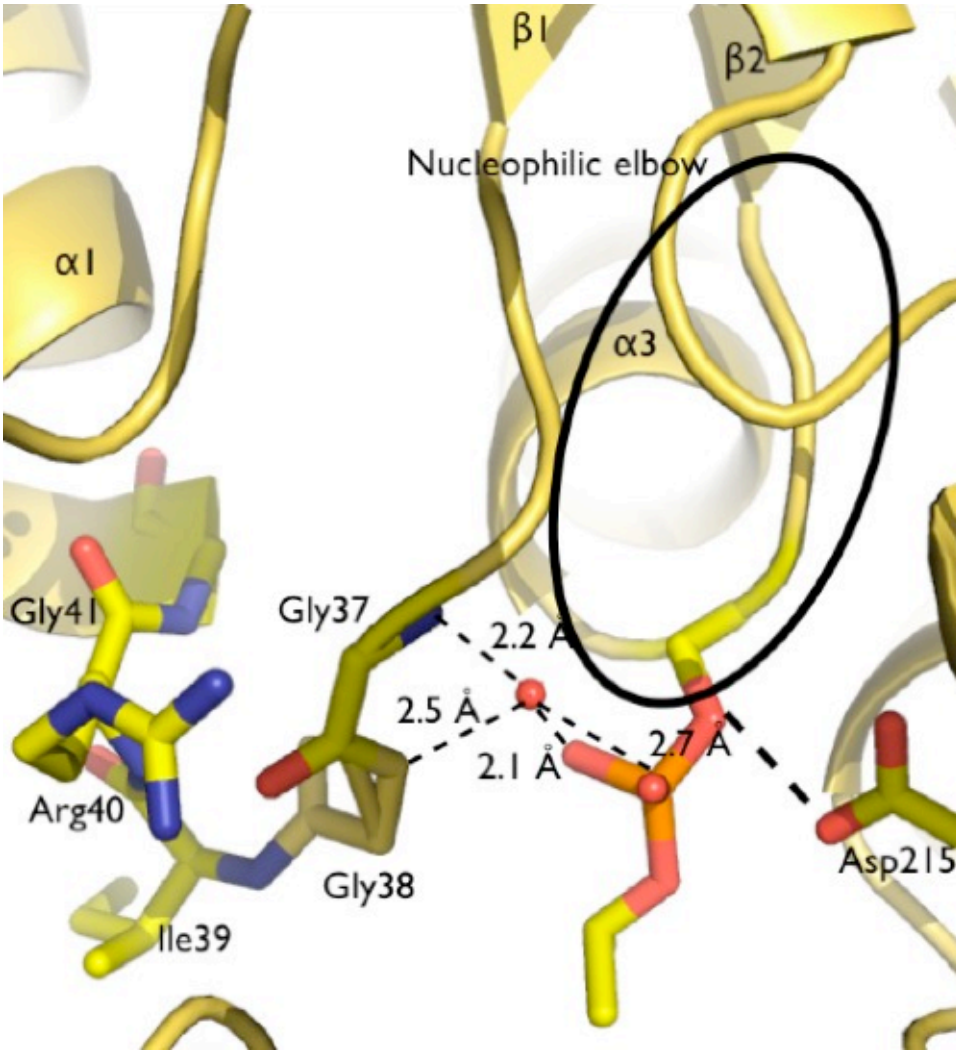

Figure 4.7: The active site of pat17 with the aged DFP adduct. Residues that comprise patatin's catalytic dyad (Ser77 and Asp215) as well as the oxyanion hole (Gly37, Gly38, Ile39, Arg40 and Gly41) are labeled and rendered as sticks with the following color scheme: yellow = carbon, blue = nitrogen and red = oxygen. Contact distances between the DFP-aged structure's visible water molecule and the aged DFP adduct along with pat17's oxyanion hole are shown.

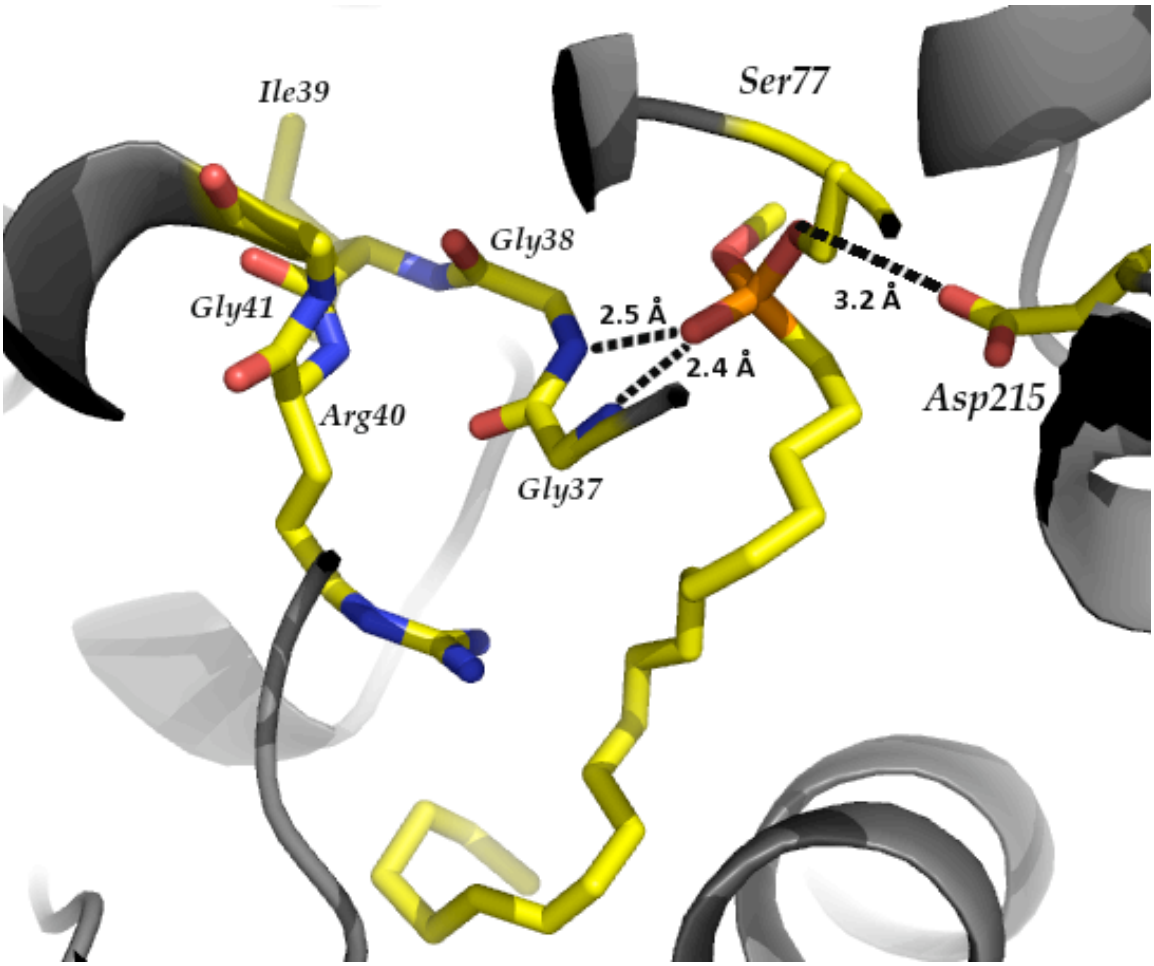

Figure 4.8: Patatin's active site covalently bound to the unaged MAFP moiety. Residues that comprise patatin's catalytic dyad (Ser77 and Asp215) as well as the oxyanion hole (Gly37, Gly38, Ile39, Arg40 and Gly41) are labeled and rendered as sticks with the following color scheme: yellow = carbon, blue = nitrogen and red = oxygen. Contact distances between the MAFP adduct's phosphoryl moiety and pat17's oxyanion hole are shown. As can be seen, pat17's Ser77 Oγ is located 3.2 Å from Asp215's Oδ2.

References

Andrews, D.L., Beames, B., Summers, M.D., and Park, W.D. (1988). Characterization of the lipid acyl hydrolase activity of the major potato (Solanum tuberosum) tuber protein, patatin, by cloning and abundant expression in a baculovirus vector. *Biochem. J.* **252**, 199--206.

Bishayee, A., Beguinot, L. and Bishayee, S. (1999). Phosphorylation of tyrosine 992, 1068, and 1086 is required for conformational change of the human epidermal growth factor receptor c-terminal tail. *Mol. Biol. Cell.* **10**, 525--536.

Brunger, A.T., Adams, P.D., Clore, G.M., DeLano, W.L., Gros, P., Grosse-Kunstleve, R.W., Jiang, J.S., Kuszewski, J., Nilges, M., Pannu, N.S., Read, R.J., Rice, L.M., Simonson, T., and Warren, G.L. (1998). Crystallography & NMR system: A new software suite for macromolecular structure determination. *Acta Crystallogr. D Biol. Crystallogr.* **54.** 905--921.

Canagarajah, B.J., Khokhlatchev, A., Cobb, M.H., and Goldsmith, E.J. (1997). Activation mechanism of the MAP kinase ERK2 by dual phosphorylation. *Cell*. **90**, 859--69.

Clothier, B., Johnson, M.K., and Reiner, E. (1981). Interaction of some trialkyl phosphorothiolates with acetylcholinesterase: Characterization of inhibition, aging and reactivation. *Biochim. Biophys. Acta* **660**, 306--316.

DeLano Scientific LLC, San Carlos, CA, USA. *The PyMOL Molecular Graphics System*. http://www.pymol.org.

Dessen, A., Tang, J., Schmidt, H., Stahl, M., Clark, J.D., Seehra, J., and Somers, W.S. (1999). Crystal structure of human cytosolic phospholipase A2 reveals a novel topology and catalytic mechanism. *Cell*. **97**, 349--360.

Doorn, J.A., Talley, T.T., Thompson, C.M., and Richardson, R.J. (2001a). Probing the active sites of butyrylcholinesterase and cholesterol esterase with isomalathion: conserved stereoselective inactivation of serine hydrolases structurally related to acetylcholinesterase. *Chem. Res. Toxicol*. **14**, 807--813.

Doorn, J.A., Schall, M., Gage, D.A., Talley, T.T., Thompson, C.M., and Richardson, R.J. (2001b). Identification of butyrylcholinesterase adducts after inhibition with isomalathion using mass spectrometry: Difference in mechanism between (1R)- and (1S)-stereoisomers. *Toxicol. Appl. Pharmacol.* **176**, 73--80.

Doorn, J.A., Thompson, C.M., Christner, R.B., and Richardson, R.J. (2003). Stereoselective inactivation of Torpedo californica acetylcholinesterase by isomalathion: inhibitory

reactions with (1R)- and (1S)-isomers proceed by different mechanisms. *Chem. Res. Toxicol.* **16**, 958--965.

Ganal, M. W., Roeder, M., Park, W., and Tanksley, S. (1991). Genetic and physical mapping of the patatin genes in potato and tomato. *Mol. Gen. Genet.* **225**, 501--509.

Glynn, P. (1999). Neuropathy target esterase. *Biochem. J.* **344**, 625--631.

Glynn, P. (2003). NTE: one target protein for different toxic syndromes with distinct mechanisms? *Bioessays.* **25**, 742--745.

Golomb, B.A. (2008). Acetylcholinesterase inhibitors and Gulf War illnesses. *Proc. Natl. Acad. Sci .U.S.A.* **105**, 4295--4300.

Groban, E.S., Narayanan, A., and Jacobson, M.P. (2006). Conformational changes in protein loops and helices induced by post-translational phosphorylation. *PLoS Comput. Biol.* **2**, e32.

Hirschberg, H.J.H.B., Simons, J.W.F.A., Dekker, N., and Egmond, M.R. (2001). Cloning, expression, purification and characterization of patatin, a novel phospholipase A. *Eur. J. Biochem.* **268**, 5037--5044.

Haley, R.W., Horn, J., Roland, P.S., Bryan, W.W., Van Ness, P.C., Bonte, F.J., Devous, M.D., Mathews, D., Fleckenstein, J.L., Wians, F.H., Wolfe, G.I., and Kurt, T.L. (1997). Evaluation of neurologic function in Gulf War veterans. A blinded case-control study. *J. Am. Med. Assoc.* **277**, 223--230.

Hirayama, O., Matsuda, H., Takeda, H., Maenaka, K., and Takatsuka, H. (1975). Purification and properties of a lipid acyl-hydrolase from potato tubers. *Biochim. Biophys. Acta.* **384**, 127--137.

Hurley, M.M., Balboa, A., Lushington, G.H., and Guo, J. (2005). Interactions of organophosphorus and related compounds with cholinesterases, a theoretical study. *Chem. Biol. Interact.* **157-158**. 321--325.

Jones, T.A., Zou, J-Y., Cowan, S.W., and Kjeldgaard, M. (1991). Improved methods for building protein models in electron density maps and the location of errors in these models. *Acta Cryst.* **A47**, 110--119.

Jianmongkol, S., Marable, B.R., Berkman, C.W., Talley, T.T., Thompson, C.M., and Richardson, R.J. (1999). Kinetic evidence for different mechanisms of acetylcholinesterase inhibition by (1R)- and (1S)-stereoisomers of isomalathion. *Toxicol. Appl. Pharmacol.* **155**, 43-53.

Johnson, M.K. (1990). Organophosphates and delayed neuropathy--is NTE alive and well? *Toxicol. Appl. Pharmacol.* **102,** 385--399.

Katz, B.A., Spencer, J.R., Elrod, K., Luong, C., Mackman, R.L., Rice, M., Sprengeler, P.A., Allen, D., and Janc, J. (2002). Contribution of multicentered short hydrogen bond arrays to potency of active site-directed serine protease inhibitors. *J. Am. Chem. Soc*. **124**, 11657--11668.

Kleywegt, G.J., and Jones, T.A. (1998). Databases in protein crystallography. *Acta Cryst*. **D54**, 1119--1131.

Kropp, T.J., Glynn, P., and Richardson, R.J. (2004). The mipafox-inhibited catalytic domain of human neuropathy target esterase ages by reversible proton loss. *Biochemistry*. **43**, 3716--3722.

Laskowski, R., MacArthur, M., Moss, D., and Thornton, J. (1993). PROCHECK - a program to check the stereochemical quality of protein structures. *J. Appl. Crystallogr.* **26**, 91--97.

Li, Y., Dinsdale, D., and Glynn, P. (2003). Protein domains, catalytic activity, and subcellular distribution of neuropathy target esterase in Mammalian cells. *J. Biol. Chem*. **278**, 8820--8825.

Lotti, M, and Moretto, A. (2005). Organophosphate-induced delayed polyneuropathy. *Toxicol. Rev*. **24**, 37--49.

McCoy, A.J., Grosse-Kunstleve, R.W., Adams, P.D., Winn, P.D., Storoni, L.C., and Read, R.J. (2007). Phaser crystallographic software. *J. Appl. Cryst.* **40**, 658--674

Millard, C.B., Kryger, G., Ordentlich, A., Greenblatt, H.M., Harel, M., Raves, M.L., Segall, Y., Barak, D., Shafferman, A., Silman, I., and Sussman, J.L. (1999). Crystal structures of aged phosphonylated acetylcholinesterase: nerve agent reaction products at the atomic level. *Biochemistry*. **38**, 7032--7039.

Otwinowski, Z., and Minor, W. (1997) Processing of x-ray diffraction data collected in oscillation mode. In *Methods in Enzymology: Macromolecular Crystallography, Part A* (Carter, C. W., Jr., and Sweet, R. M., Eds.), Academic Press, New York, pp. 307--326.

Pots, A.M., Gruppen, H., Hessing, M., van Boekel, M.A., and Voragen, A.G. (1999). Isolation and characterization of patatin isoforms. *J. Agric. Food. Chem*. **47**. 4587--4582.

ProteinProspector. (2009). http://prospector.ucsf.edu/.

Quistad, G.B., Barlow, C., Winrow, C.J., Sparks, S.E., and Casida, J.E. (2003). Evidence that mouse brain neuropathy target esterase is a lysophospholipase. *Proc. Natl. Acad. Sci. U.S.A*. **100**, 7983--7987.

Racusen, D., and Foote, M. (1980). A major soluble glycoprotein of potato tubers. *J. Food. Biochem*. **4**, 43--52.

Randall, J.C., Ambroso, J.L., Groutas, W.C., Brubaker, M.J., and Richardson, R.J. (1997). Inhibition of neurotoxic esterase in vitro by novel carbamates. *Toxicol. Appl. Pharmacol*. **143**, 173--178.

Rainier, S., Bui, M., Mark, E., Thomas, D., Tokarz, D., Ming, L., Delaney, C., Richardson, R.J., Albers, J.W., Matsunami, N., Stevens, J., Coon, H., Leppert, M., and Fink, J.K. (2008). Neuropathy target esterase gene mutations cause motor neuron disease. *Am. J. Hum. Genet*. **82,** 780--785.

Richardson, R.J. (2005). Neurotoxicity, delayed. In *Encyclopedia of Toxicology 2nd ed., Vol. 2* (P. Wexler, ed.), Academic Press, New York, pp. 302--306.

Richardson, R.J., Worden, R.M., and Makhaeva, G.F. (2009). Biomarkers and biosensors of delayed neuropathic agents. In *Handbook of Toxicology of Chemical Warfare Agents* (R. Gupta, Ed.), Academic Press, London, UK, pp. 859--876.

Rydel, T.J., Williams, J.M., Krieger, E., Moshiri, F., Stallings, W.C., Brown, S.M., Pershing, J.C., Purcell, J.P., and Alibhai, M.F. (2003). The crystal structure, mutagenesis, and activity studies reveal that patatin is a lipid acyl hydrolase with a Ser-Asp catalytic dyad. *Biochemistry*. **42**, 6696--6708.

Schuettelkopf, A.W., and van Aalten, D.M.F. (2004). PRODRG: a tool for high-throughput crystallography of protein-ligand complexes. *Acta Cryst*. **D60**, 1355--1363.

Senanayake, N., and Jeyaratnam, J. (1981). Toxic polyneuropathy due to gingili oil contaminated with tri-cresyl phosphate affecting adolescent girls in Sri Lanka. *Lancet*. **1**, 88--89.

Strickland, J.A., Orr, G.L., and Walsh, T.A. (1995). Inhibition of diabrotica larval growth by patatin, the lipid acyl hydrolase from potato tubers. *Plant Physiol*. **109**, 667--674.

van Tienhoven, M., Atkins, J., Li, Y., and Glynn, P. (2002). Human neuropathy target esterase catalyzes hydrolysis of membrane lipids. *J. Biol. Chem*. **277**, 20942--20948.

Wijeyesakere, S.J., Richardson, R.J., and Stuckey, J.A. (2007). Modeling the tertiary structure of the patatin domain of neuropathy target esterase. *Protein J*. **26**, 165--172.

Zhang, Y., Kua, J., and McCammon, J.A. (2002). Role of the catalytic triad and oxyanion hole in acetylcholinesterase catalysis: an ab initio QM/MM study. *J. Am. Chem. Soc*. **124**, 10572--10577.

Zhu, Y.C., Liu, X., Maddur, A.A., Oppert, B., and Chen, M.S. (2005). Cloning and characterization of chymotrypsin- and trypsin-like cDNAs from the gut of the Hessian fly [Mayetiola destructor (Say)]. *Insect Biochem. Mol. Biol.* 35, 22--32.

Chapter 5

Conclusions

While over half a century has elapsed since the infamous 'Ginger Jake' epidemic of the prohibition-era (Smith *et al.*, 1930; Richardson, 2005), the exact biochemical mechanism involved in the initiation and progression of organophosphorus compound (OP)-induced delayed neuropathy (OPIDN) remains a riddle that has yet to be explained. The current model for the initiation of this condition has it that once >70% of NTE is inhibited by a neuropathic OP, the covalently-bound NTE-OP adduct needs to undergo a post-inhibitory reaction termed 'aging' during which it gains a negative charge. The most common mechanism for accomplishing this is via the net loss of one of the OP adducts alkyl side chains. Once aged, the NTE conjugate cannot be reactivated and, given exposure to a sufficient dose of a neuropathic OP, the progression to OPIDN is inevitable (Fig 1.2) (Richardson, 2005).

Currently, the exact stage(s) through which the aging of NTE initiates the progression to OPIDN are unknown. However, it has been postulated that in the process of (or indeed, as a result of) gaining of its negative charge, OP-aged NTE also gains a new 'toxic' function that leads to axonal degradation and is ultimately detrimental to the survival of the axon (Glynn, 1999). On the other hand, given the axiom that form follows function, it is reasonable to hypothesize that if NTE were to gain a new function, it must also experience a concurrent change in its form (i.e. its structure). For this reason, investigating tertiary structural changes associated with inhibition and aging of NTE by OPs was used to test the validity of the 'toxic gain-of function' model. However, given the absence of an experimentally derived structure, I employed molecular modeling along with solving the OP-conjugated structures of NTE's catalytic (patatin-homology) domain (PNTE) homologue, patatin-17 (pat17) to test my hypothesis.

As stated earlier in the introduction, the primary aim of this endeavor was to test the hypothesis that the aging of an OP on NTE results in a conformational change in the protein's structure, leading to the initiation of OPIDN. The overall goals of this project were two-fold: a) to gain insight into the putative structure of NTE's catalytic domain, and b) to gain a fundamental

understanding of the expected conformational changes associated with the inhibition and aging of an OP on NTE, using NTE's catalytic-domain homologue, patatin, as the target protein. To this end, this body of work has shown that pat-17 could serve as a template for the structure of NTE's catalytic domain (PNTE) (Wijeyesakere *et al*., 2007) and that when considering the overall molecule, there is no significant conformational change seen in pat17's Cα backbone when it is inhibited and aged by a neuropathic OP relative to its native and inhibited states. Furthermore, this result is consistent with that seen in other serine esterases such as acetylcholinesterase (AChE) where no significant global conformational changes in the overall protein structures were seen following inhibition and aging, although the presence of localized conformational changes in AChE's acyl pocket were reported (Millard *et al.*, 1999).

My findings with patatin and PNTE, coupled with previously reported findings on global conformational changes in AChE serve to suggest that the previously mentioned 'toxic gain-of-function' hypothesis for the pathogenesis of OPIDN may not be correct and raise important questions as to the significance of the aging reaction in the initiation and progression of this condition. The fact that I failed to observe any significant conformational changes in both, the aged PNTE model and the aged pat17 crystal structure, indicate that a new model is needed to explain the biochemical processes that underlie OPIDN. On the other hand, until experimentally derived structures for full-length NTE in its native, inhibited and aged states are available; it would be unwise to rule out completely, regardless of how remote the possibility, the notion that there is a true conformational change associated with aging of an OP on NTE, resulting in NTE's toxic gain of function. However, given my recent findings, coupled with new results on NTE's biochemistry, it is prudent to explore an alternate hypothesis (dubbed the 'lipid hypothesis') to aid in developing a new model to explain the initiation and progression of OPIDN.

The lipid hypothesis: A new model for OPIDN

The first stage in developing this new model for OPIDN's pathogenesis would have to involve a thorough understanding NTE's physiological role. While there is still some uncertainty, recent papers by Paul Glynn and colleagues as well as by John Casida's research group have indicated that NTE could be a lysophospholipase, a protein that hydrolyses lysophospholipids (the lipid end-product of phospholipid hydrolysis by phospholipase A2 (PLA_2)) to yield free fatty acids and a glycerophosphate head (van Tienhoven *et al.*, 2002 and Quistad *et al.*, 2003). Work by Paul Glynn's research group has shown that NTE can act as both, a phospholipase as well as a lysophospholipase, with a preference towards the latter role (van Tienhoven *et al*., 2002), a result

confirmed recently by Mark Worden and colleagues at Michigan State University (personal communication). Incidentally, lysophospholipids such as lysophosphatidylcholine can also serve as the substrate for lysophospholipase D, resulting in the formation of lysophosphatidic acid (LPA), a molecule capable of eliciting a wide-range of biological responses including the ability to mimic the effect of growth factors (Moolenaar *et al*., 1997; Moolenaar, 2002; Wang and Dennis, 1999) and the ability to block caspase-8 (Kang *et al*., 2004).

In addition to the mitogenic effects of its derivative, LPA, the presence of a single hydrophobic fatty acid chain enables lysophospholipids to act as detergents, and as a result, their concentrations within lipid membranes are usually limited to 0.5-6% (by weight) of the membrane's total lipid content (Wang and Dennis, 1999; Stafford *et al*., 1989). Therefore, any loss of homeostasis with respect to a membrane's lysophospholipid levels could jeopardize the membrane's structure as a result of micelle formation and solubilization of membrane segments. If such a disruption were to take place in the membrane of the endoplasmic reticulum (ER) (where NTE is localized (Li *et al.*, 2003)), it would be expected to lead to a loss of calcium homeostasis in the cell, because the ER is the cell's primary calcium store (Verkhratsky, 2005). In fact, increased levels of intracellular calcium, along with indirect evidence indicating the associated activation of calpains (a class of calcium-activated cysteine proteases), was reported *in-vivo* via co-administration of the neuropathic OP phenyl saligenin phosphate along with the phenlalkylamine calcium-channel blocker Verapamil in adult hens (el-Fawal and Ehrich, 1993). Physiologically, the loss of calcium homeostasis in the cell, if not rectified in a timely manner, could result in the unregulated activation of calpains, which would begin the process of breaking down the cell's cytoskeleton, as well as result in the accumulation of calcium in the mitochondria, thereby initiating the formation of the mitochondrial permeability transition, the first step in apoptotic cell death. In the case of a neuron, a local-axonal self-destruct mechanism (analogous to an 'axonal apoptosis') has been postulated by Raff *et al*. (2002) and could be used to explain the axonopathy associated with OPIDN.

Based on these findings, and as depicted in figure 5.1, the lipid hypothesis postulates that a neuropathic OP induces OPIDN via the slow build-up of lysophospholipids in the ER membrane, resulting in its disruption via the formation of lysophospholipid micelles, which would solubilize regions of the membrane. If this damage were of sufficient severity, it would be expected to result ultimately in axonopathy (Figure 5.1). Therefore, if the proposed lipid hypothesis for the mechanism of OPIDN were correct, it would indicate that it is the act of inhibiting sufficient levels of a neuron's NTE, leading to a build-up of lysophospholipids and the

subsequent disruption of ER, that leads to the pathology seen in OPIDN as opposed to an aging-induced 'toxic gain-of-function' (or, by extension, a change of structure) in NTE.

Based on the proposed model for the lipid hypothesis (depicted in figure 5.1), it is predicted that neuropathic OPs should be more potent against NTE and/or the acyltransferases (enzymes that catalyze the acylation of lysophospholipids) than PLA_2 (given that a compound that is more potent against PLA_2 would inhibit the formation of these lysophospholipids to a greater degree than their hydrolysis by NTE or their re-acylation by acyltransferases). This finding is supported, in part, by results published by Casida and Quistad (2005) that indicate that neuropathic OPs such as chlorpyrifos oxon (CPO; the bio-transformed form of the pesticide chlorpyrifos that is neuropathic at supralethal doses) and ethyl octylphosphonofluoridate (EOPF) are more potent against NTE than PLA_2 with reported IC_{50} values for CPO and EOPF against PLA_2 in excess of 10,000 nM compared to values of 180 nM (Casida *et al*., 2008) and 0.05 nM, respectively, (Casida *et al*., 2008; Casida and Quistad, 2005) for these compounds against NTE. However, in order to gain a complete understanding of an OP's neuropathic potential, further research is needed to identify the acyltransferases involved in catalyzing the re-acylating lysophospholipids that serve as substrates for NTE along with the ability of neuropathic and non-neuropathic NTE inhibitors to inhibit these acyltransfereases.

On the other hand, non-neuropathic OPs should be more potent against PLA_2 than NTE, other lysophospholipases or the acyltransferases (see figure 5.1). Consequently, this would result in a slower rate of formation of lysophospholipids relative to its rate of clearance, taking into account the turnover rates for these enzymes. Therefore, in the absence of a build-up of lysophospholipids in the ER membrane, a disruption in calcium homeostasis and consequent pathology would not be expected. Thus, it follows that it is the differences in the relative inhibitory potentials of OPs against PLA_2, NTE, other lysophospholipases, and the acyltransferases that determine which OPs are neuropathic and which are not.

As a result of this new model for OPIDN, it is proposed that future research be directed at identifying conclusively, which lysophospholipids serve as NTE's substrates as well as in determining which acyltransferases are involved in re-acylating these lysophospholipids. In order to gain a more complete understanding of the sub-cellular pathways associated with NTE, it would also be important to identify lysophospholipases (other than NTE) that are able to catalyze the hydrolysis of the lysophospholipids that serve as physiological substrates for NTE. Furthermore, if the lipid hypothesis for OPIDN is correct, the current EPA guidelines for testing the neuropathic potential of OPs, which currently mandates testing an OP's *ex-vivo* inhibition of NTE (U.S. EPA, 1991), be revised to also include testing their inhibitory potentials against PLA_2

and the relevant acyltransferases. Alternatively, a metabalomic approach involving identifying the phospholipid:lysophospholipid ratios (at varying time intervals post-exposure) in cells treated with neuropathic and non-neuropathic OPs could be used as an *in vitro* technique to investigate the neuropathic potential of OPs.

An interesting finding of this new model is that while an OP's potential for aging may be an indicator of its neuropathic potential, it is not a causative event in the initiation of OPIDN. Therefore, there should be non-neuropathic NTE inhibitors (using the conventional definition of these compounds not being able to age) that could, in practice, inhibit NTE to a greater degree than PLA_2, thereby leading to OPIDN. While this arena has not been researched extensively, there have been published clinical case reports of delayed neurotoxicity allegedly arising from the ingestion of carbamates (Dickoff *et al*., 1987; Umehara *et al*., 1991). Then again, one must be cautious and not attribute too much significance to these reports, because they are not the result of controlled experiments and could simply represent cases where the ingested carbamates were contaminated with conventional neuropathic OPs. However, this represents an area where further research is needed before a conclusive statement can be made regarding the validity of these case-findings.

A potential complication faced by the proposed lipid hypothesis has to do with the issue of enzyme turnover, in particular, the turnover of NTE. Any model for OPIDN has to explain the post-exposure 1-4 week asymptomatic period, which is characteristic of this condition. Currently, it is known that the half-life for the turnover of OP-treated NTE is on the order of 5 days in the brain and approximately 7 days in the spinal cord (Meredith and Johnson, 1988). One possible explanation for this discrepancy between enzyme turnover and the appearance of OPIDN's signs and symptoms is that following the turnover of a sufficient quantity of inhibited NTE, there is a delay in the clearance of accumulated lysophospholipids during which unacceptably high levels of lysophosopholipids remain in the ER membrane. Furthermore, one must also consider the rates of turnover of other organophosphorylated enzymes (such as the phospholipases and the acyltransferases) that are predicted to play an important role in the phospholipid hydrolysis pathway that is the focus of the lipid hypothesis in order to gain a complete understanding of the timing of events that take place once a neuron is exposed to a neuropathic OP.

While the issue of enzyme turnover may present a challenge to the acceptance of the lipid hypothesis, it presents an even bigger stumbling block for the current aging-centric toxic gain-of-function model for OPIDN. This is due to the fact that the current model for OPIDN posits the involvement of a single enzyme (i.e. NTE) in the pathogenesis of OPIDN. Therefore, the rate of turnover of NTE is expected to play an event greater role since the turnover of OP-aged NTE (i.e.

the ‘toxic’ NTE) would be expected to halt the insult to the neuron, thereby allowing it to recover. On the other hand, there is always the possibility that the aged state of NTE presents a persistent form of the protein that is cleared (via protein turnover) at a slower rate than the native form of the enzyme (thus far, NTE turnover has been measured as the return of NTE activity (i.e. the production of new NTE molecules), not the removal of the OP-treated NTE form). This would allow the ‘toxic’ form of NTE to remain in the cell and could be used to explain the delay between exposure, enzyme turnover and the appearance of the signs and symptoms of OPIDN.

In conclusion, while the results of my research effort did not identify a definitive global conformational change associated with the aging of a neuropathic OP-protein conjugate via computational molecular modeling of PNTE and via x-ray crystallography using the PNTE homologue patatin, it has shed new light on the need to re-evaluate the importance of this reaction in the pathogenesis of OPIDN. In addition to this, using these findings, I have been able to devise a new hypothesis for the mechanism for OPIDN’s initiation and progression using recent biochemical insights into NTE’s putative physiological role.

Alternative models for OPIDN

While the lipid hypothesis provides an intriguing model for the initiation and progression of OPIDN, one must also consider other possibilities though which this condition can occur. One model that has been discussed extensively in the literature as well as throughout my dissertation, and whose validation was the initial goal of my thesis is the current aging-centric model for OPIDN’s pathogenesis. However, in discussing alternative models for OPIDN, it would be prudent to put aside the classical model for OPIDN as well as the new lipid hypothesis that is the focus of this chapter and instead focus on other, less well-known proposals for how this condition could occur.

When considering the notion that NTE can act as a phospholipase as well as a lysophospholipase (with a preference towards the latter role) (van Tienhoven *et al*., 2002), it could raise the question as to whether NTE plays a role in the release of arachidonic acid from phospholipids. If this were the case, it could be the case that OPIDN is the result of a disruption in the arachidonic signaling pathway and not a ‘toxic gain-of function’ or a lysophospholipid-mediated disruption of the ER membrane. However, given that the PLA_2 enzymes are known to play a central role in the release of arachidonic acid from phospholipids (Dessen *et al*., 1999), and given that current evidence points to neuropathic OPs such as CPO and EOPF being more potent against NTE than PLA_2 (IC_{50} values for CPO and EOPF against PLA_2 have been reported to be in

excess of 10,000 nM versus IC_{50} values of 180 nM and 0.05 nM, respectively for these compounds against NTE (Casida *et al*., 2008; Casida and Quistad, 2005)), it is unlikely that a significant disruption in arachidonic acid release could result from the exposure of NTE to a neuropathic OP.

An even more intriguing, and unique possibility for the pathogenesis of OPIDN that has been proposed by Rudy Richardson is that the act of organophosphorylation of NTE by a neuropathic OP could present a persistent form of an endogenous phosphorylation signal by mimicking the action of a protein kinase (Richardson, 1984). Therefore, interactions between NTE and an OP could result in the pathological regulation (via activation or inactivation) of some cellular activity that has yet to be identified, but which is under the control of the phosphorylated NTE state. Unfortunately, bioinformatic analyses of NTE's primary sequence have shown that its active site Ser966 residue (which is the target for organophosphorylation) does not lie in a consensus sequence for any known endogenous phosphorylation sites. Thus, based on the weight of current scientific evidence, this phosphorylation-mimicking model for OPIDN is probably not viable. Therefore, based on my recent findings with molecular modeling and crystallography, along with the relative improbability of alternative models, it is proposed that the lipid hypothesis be considered as an alternative model for the pathogenesis of OPIDN.

Future work: Testing the lipid hypothesis

The key characteristic of any scientific theory is that it must yield testable hypotheses. This applies to the proposed lipid hypothesis for the initiation of OPIDN, which, while having some disparate pre-published data in the scientific literature supporting it, needs to be verified in a thorough and consistent manner before its validity (or invalidity) is established. Unlike the previous aging-centric and aging-initiated model for OPIDN, one disadvantage faced by the lipid hypothesis is that it postulates the involvement of a more complex system, involving imbalances in the catalytic activities of multiple enzymes. This complexity, while making for a more intricate theory, is borne out of complexities seen in all biological systems. Because no single enzyme is an island that acts completely independently of other enzymes in a biological pathway, the complexity of the lipid hypothesis should not be rejected out of hand, based solely on the intricacy of the proposed system.

In order to thoroughly test the lipid hypothesis, we would first need to have a thorough understanding of NTE's preference for phospholipids and lysophospholipids (i.e. NTE's physiological substrates). Once these lipids and lysophospholipids have been identified, we

would need to establish which phospholipases, lysophospholipases, and acyltransferases are involved in catalyzing the hydrolysis and acylation of NTE's physiological substrates. After this complete list of enzymes has been assembled, the core predictions of the lipid hypothesis can be tested in a direct manner. These predictions state that neuropathic OPs (such as DFP) are expected be more potent (i.e. have a higher bimolecular rate constant of inhibition (k_i) or lower 20-minute IC_{50}) against NTE and the lysophospholipases and/or the acyltransferases, relative to their inhibitory potencies against the phospholipases, while the opposite is expected to be true of the non-neuropathic OPs.

An initial area of investigation could be to study the potency of the non-neuropathic NTE inhibitor phenylmethanesulphonylfluoride (PMSF) against a series of phospholipases, lysophospholipases and acyltransferases. If the lipid hypothesis, as stated in this chapter is correct, it is predicted that the 20-minute IC_{50}s for PMSF against the PLA_2 and acyltransferases would be higher than its 20-minute IC_{50} values against NTE and the lysophospholipases. Alternatively, a metabalomic approach involving identifying the presence of phospholipids and lysophospholipids (at varying time intervals post-exposure) in cells treated with neuropathic and non-neuropathic OPs could be used as a mechanism to investigate the validity of the proposed lipid hypothesis.

In the absence of a complete list of phospholipids and enzymes involved, the lipid hypothesis could be tested indirectly by measuring the levels of phospholipids and lysophospholipids at regular intervals over a month in neurons following exposure to neuropathic and non-neuropathic NTE inhibitors. This can be accomplished using either an *ex-vivo* animal model, or an *in-vitro* cell culture model. A recent study conducted by Y.J. Wu and colleagues reported no change in levels of phosphatidylcholine and lysophosphatidylcholine in the nervous systems of mice treated with TOCP versus those treated with either PMSF or the control group (Wu *et al*., 2009). While this report may suggest a repudiation of the proposed lipid hypothesis, there are several factors we must consider with respect to this study: the first issue with this work is that historically, mice have been shown to have a faster turnover of NTE ($t_{1/2}$ of approximately 2 days) (Glynn, 1999). Secondly, while the adult hen is the classical test animal in which OPIDN is studied, mice are not considered a suitable model in which to investigate OPIDN (Richardson *et al*., 2009), presumably due to their small size (leading to shorter axonal lengths) and rapid turnover of OPIDN. Finally, with respect to the methodology used (TOCP was administered as a single dose (900 mg/kg)), work by Mohamed Abou-Donia's research group has shown that in order to have a significant decrease *in vivo* of mouse brain NTE activity, daily dosing (po) with TOCP is needed, while administration of two single 1,000 mg/kg doses of TOCP was shown to

be insufficient to significantly decrease brain NTE activity (relative to control) (Lapadula *et al*., 1985). Therefore, given these issues with the research methodology used, the work by Hou *et al*. (2009) does not provide sufficient data to validate or invalidate the proposed lipid hypothesis. In conclusion, the central prediction of the lipid hypothesis, which predicts that higher levels of lysophospholipids would be seen in neurons exposed to neuropathic NTE inhibitors and not in those exposed to the non-neuropathic NTE inhibitors presents an area where further research is needed. Therefore, testing of the lipid hypothesis for the pathogenesis of OPIDN is expected to yield insight into the mechanism by which exogenous agents can induce a chemical transection of the axon.

Figure 5.1: Proposed mechanism for the lipid hypothesis. (a) The phospholipid hydrolysis pathway depicting the points at which and OP can act. Hydrolysis of a phospholipid at the *sn-2* position by PLA_2 results in the formation of a lysophospholipid. Under normal circumstances, the levels of lysophospholipids in the membrane is maintained at 0.5-6% (by weight) of the membrane's total lipid content, with acyltransferases catalyzing the re-acylation of lysophospholipids to phospholipids and lysophospholipases (such as NTE) catalyzing the hydrolysis of the remaining fatty acid ester bond resulting in the release of a fatty acid and the phospholipid's glycerophosphate head. OPs can inhibit PLA_2, acyltransferases, as well as NTE (and, presumably, other lysophospholipases). Thus, it is postulated that it is the differential rates of inhibition of these enzymes that determines the neuropathic potential of an OP. (b) In the case of a non-neuropathic OP, it is postulated that the OP's inhibitory potential against PLA_2 is greater than that against NTE, other lysophospholipases (LysoPLA) or the acyltransferases (the relative inhibitory potencies of the OP against PLA_2, acyltransferase, as well as NTE and other lysophospholipases are indicated by the length of the thick red lines with the longer lines indicating higher levels of inhibition). Thus, the rate of formation of lysophospholipids is lower than its clearance by acyltransferases and NTE. (c) On the other hand, a neuropathic OP is expected to be more potent against NTE/other lysophospholipases and/or the acyltransferases, relative to PLA_2, thus leading to a slow build-up of lysophospholipids (LysoPL) in the membrane. The unregulated build-up of these lysophospholipids (prior to physiological levels of the enzymes listed are restored via enzyme turnover), disrupts the stability of the ER membrane thereby compromising its structure. If this insult is sufficiently severe, is expected to lead to axonopathy. For this reason, it is proposed that it is the resulting disruption of lipid homeostasis in the cell, and not an aging-induced global toxic-gain-of-function by NTE (or, by extension, a change in NTE's structure), that leads to the pathology seen in OPIDN. LysoPLA: Lysophospholipase; LysoPL: Lysophospholipid; X: Polar head group; R: alkyl chain.

A. Phospholipid hydrolysis pathway showing the points at which OPs can act (bold red lines)

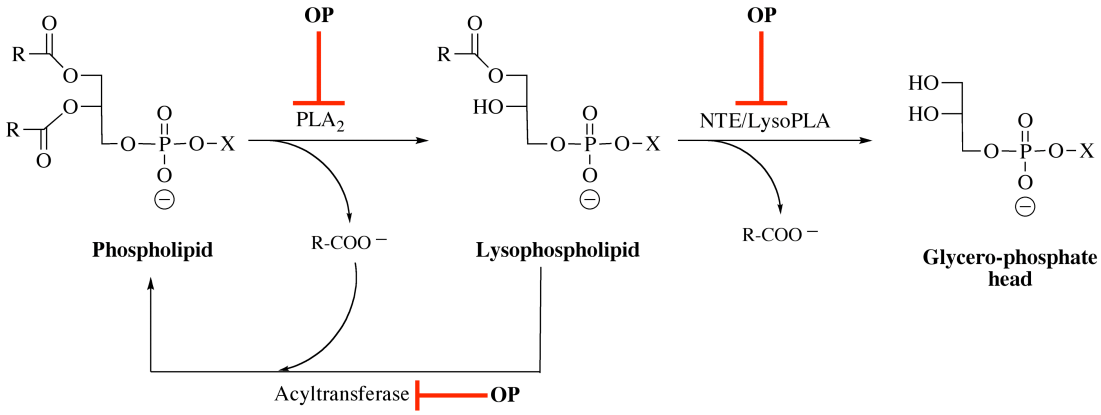

B. Proposed action of a non-neuropathic OP (longer red lines indicate higher levels of inhibition)

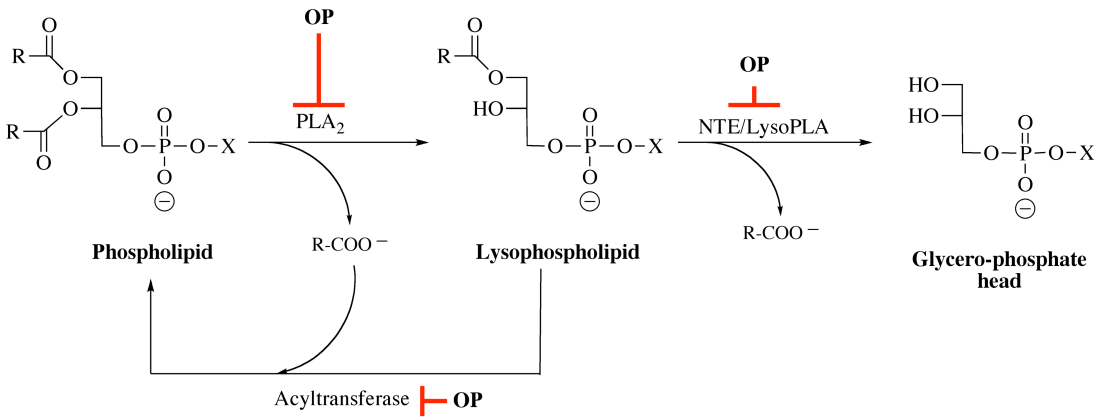

C. Proposed action of a neuropathic OP (longer red lines indicate higher levels of inhibition)

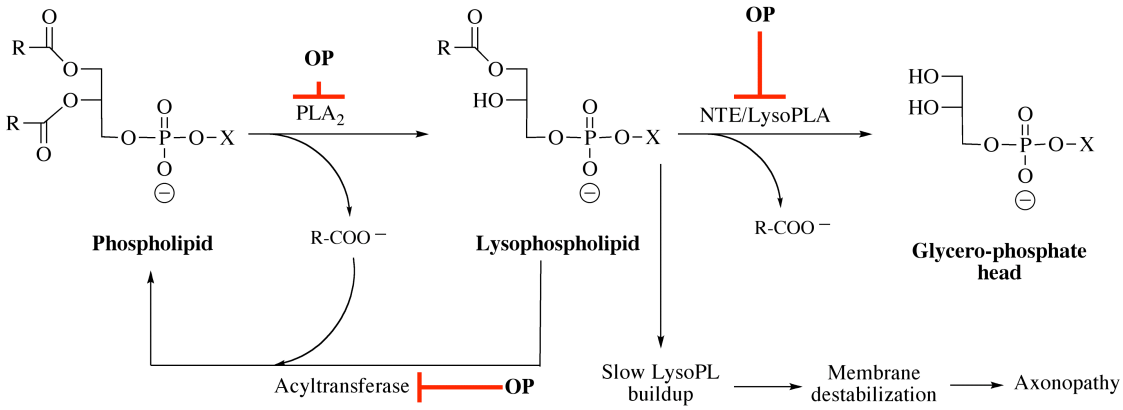

X: Polar head group (choline, inositol, glycerol, etc.)
R: Alkyl chain

References

Casida, J.E., and Quistad, G.B.(2005). Serine hydrolase targets of organophosphorus toxicants. *Chem. Biol. Interact*. **157-158,** 277--283.

Casida, J.E., Nomura, D.K., Vose, S.C., and Fujioka, K. (2008). Organophosphate-sensitive lipases modulate brain lysophospholipids, ether lipids and endocannabinoids. *Chem. Biol. Interact*. **175**, 355--364.

Dessen, A., Tang, J., Schmidt, H., Stahl, M., Clark, J.D., Seehra, J., and Somers, W.S. (1999). Crystal structure of human cytosolic phospholipase A2 reveals a novel topology and catalytic mechanism. *Cell*. **97**, 349--360.

Dickoff, D.J., Gerber, O., and Turovsky, Z. (1987). Delayed neurotoxicity after ingestion of carbamate pesticide. *Neurology*. **37**, 1229--1231.

el-Fawal, H.A., and Ehrich, M.F. (1993). Calpain activity in organophosphorus-induced delayed neuropathy (OPIDN): effects of a phenylalkylamine calcium channel blocker. *Ann. N. Y. Acad. Sci*. **28**, 325--329.

Glynn, P. (1999). Neuropathy target esterase. *Biochem. J*. **344**, 625--631.

Hou, W.Y., Long, D.X., and Wu, Y.J. (2009). The homeostasis of phosphatidylcholine and lysophosphatidylcholine in nervous tissues of mice was not disrupted after administration of tri-o-cresyl phosphate. *Toxicol. Sci*. Apr 6. (Epub ahead of print).

Kang, Y.C., Kim, K.M., Lee, K.S., Namkoong, S., Lee, S.J., Han, J.A., Jeoung, D., Ha, K.S., Kwon, Y.G., and Kim, Y.M. (2004). Serum bioactive lysophospholipids prevent TRAIL-induced apoptosis via PI3K/Akt-dependent cFLIP expression and Bad phosphorylation. *Cell Death Differ*. **11**, 1287--1298.

Lapadula, D.M., Patton, S.E., Campbell, G.A., and Abou-Donia, M.B. (1985). Characterization of delayed neurotoxicity in the mouse following chronic oral administration of tri-o-cresyl phosphate. *Toxicol. Appl. Pharmacol*. **79**, 83--90.

Li, Y., Dinsdale, D., and Glynn, P. (2003). Protein domains, catalytic activity, and subcellular distribution of neuropathy target esterase in Mammalian cells. *J. Biol. Chem*. **278**, 8820--8825.

Meredith, C., and Johnson, M. K. (1988). Neuropathy target esterase: Rates of turnover *in vivo* following covalent inhibition with phenyl di-*n*-pentylphosphinate. *J. Neurochem.* **51**, 1097--1101.

Millard, C.B., Kryger, G., Ordentlich, A., Greenblatt, H.M., Harel, M., Raves, M.L., Segall, Y., Barak, D., Shafferman, A., Silman, I., and Sussman, J.L. (1999). Crystal structures of

aged phosphonylated acetylcholinesterase: nerve agent reaction products at the atomic level. *Biochemistry*. **38**, 7032--7039.

Moolenaar, W.H. (2002). Lysophospholipids in the limelight: autotaxin takes center stage. *J. Cell Biol*. **158**, 197--199.

Moolenaar, W.H., Kranenburg, O., Postma, F.R., and Zondag, G.C. (1997). Lysophosphatidic acid: G-protein signalling and cellular responses. *Curr. Opin. Cell Biol*. **9**, 168--173.

Quistad, G.B., Barlow, C., Winrow, C.J., Sparks, S.E., and Casida, J.E. (2003). Evidence that mouse brain neuropathy target esterase is a lysophospholipase. Proc. Natl. Acad. Sci. U.S.A. 100, 7983--7987.

Raff, M.C., Whitmore, A.V., and Finn, J.T. (2002). Axonal self-destruction and neurodegeneration. *Science*. **296**, 868--871.

Richardson, R.J. (1984). Neurotoxic esterase: Normal and pathogenic roles. In *Cellular and Molecular Neurotoxicology* (T. Narahashi, Ed.), pp. 285--295, Raven Press, New York.

Richardson, R.J. (2005). Neurotoxicity, delayed. In *Encyclopedia of Toxicology 2nd ed., Vol. 2* (P. Wexler, Ed.), Academic Press, New York, pp. 302--306.

Richardson, R.J., Worden, R.M., and Makhaeva, G.F. (2009). Biomarkers and biosensors of delayed neuropathic agents. In *Handbook of Toxicology of Chemical Warfare Agents* (R. Gupta, Ed.), Academic Press, London, UK, pp. 859--876.

Smith, M.I., Elvove, E., and Frazier, W.H. (1930). The pharmacological action of certain phenol esters with special reference to the etiology of the so-called ginger paralysis. *Public Health Rep.* **45**, 2509--2524.

Stafford, R.E., Fanni, T., and Dennis, E.A. (1989). Interfacial properties and critical micelle concentration of lysophospholipids. *Biochemistry*. 28, 5113--5120.

Umehara, F., Izumo, S., Arimura, K., and Osame, M. (1991). Polyneuropathy induced by m-tolyl methyl carbamate intoxication. *J. Neurol*. **238**, 47--48.

U.S. Environmental Protection Agency (EPA) (1991). Pesticide Assessment Guidelines, Subdivision F; Hazard Evaluation: Human and Domestic Animals: Addendum 10, Neurotoxicity. Series 81, 82, and 83, pp. 3--12. EPA 540/09–91–123, PB 91-154617, Health Effects Division, Office of Pesticide Programs, U.S. Environmental Protection Agency, Washington, DC.

van Tienhoven, M., Atkins, J., and Glynn, P. (2002). Human neuropathy target esterase catalyzes hydrolysis of membrane lipids. *J. Biol. Chem.* **277**, 20942--20948.

Verkhratsky, A. (2005). Physiology and pathophysiology of the calcium store in the endoplasmic reticulum of neurons. *Physiol. Rev*. **85**, 201--279.

Wang, A., and Dennis, E.A. (1999). Mammalian lysophospholipases. *Biochim. Biophys. Acta*. **1439**, 1--16.

Wijeyesakere, S.J., Richardson, R.J., and Stuckey, J.A. (2007). Modeling the tertiary structure of the patatin domain of neuropathy target esterase. *Protein J*. **26**, 165--172.